



**Extra-Function of Ribosomal Protein L10a via
Insulin Signaling Pathway**

Netnapa Chaichanit

**A Thesis Submitted in Partial Fulfillment of the Requirements for the
Degree of Doctor of Philosophy in Molecular Biology and Bioinformatics
Prince of Songkla University
2021
Copyright of Prince of Songkla University**



**Extra-Function of Ribosomal Protein L10a via
Insulin Signaling Pathway**

Netnapa Chaichanit

**A Thesis Submitted in Partial Fulfillment of the Requirements for the
Degree of Doctor of Philosophy in Molecular Biology and Bioinformatics
Prince of Songkla University
2021
Copyright of Prince of Songkla University**

Thesis Title Extra–Function of Ribosomal Protein L10a via Insulin
 Signaling Pathway
 Author Miss Netnapa Chaichanit
 Major Program Molecular Biology and Bioinformatics

Major Advisor

Examining Committee :

.....
 (Assoc. Prof. Dr. Wilaiwan Chotigeat)

.....Chairperson
 (Prof. Dr. Kosum Chansiri)

.....Committee
 (Assoc. Prof. Dr. Wilaiwan Chotigeat)

.....Committee
 (Prof. Dr. Amornrat Phongdara)

The Graduate School, Prince of Songkla University, has approved this thesis as partial fulfillment of the requirements for the Doctor of Philosophy Degree in Molecular Biology and Bioinformatics

.....
 (Prof. Dr. Damrongsak Faroongsarng)
 Dean of Graduate School

This is to certify that the work here submitted is the result of the candidate's own investigations. Due acknowledgement has been made of any assistance received.

.....Signature
(Assoc. Prof. Dr. Wilaiwan Chotigeat)
Major Advisor

.....Signature
(Miss Netnapa Chaichanit)
Candidate

I hereby certify that this work has not been accepted in substance for any degree, and is not being currently submitted in candidature for any degree.

.....Signature

(Miss Netnapa Chaichanit)

Candidate

ชื่อวิทยานิพนธ์	Extra-Function of Ribosomal Protein L10a via Insulin Signaling Pathway
ผู้เขียน	นางสาวเนตรนภา ชัยชนิดีย์
สาขาวิชา	ชีววิทยาโมเลกุลและชีวสารสนเทศ
ปีการศึกษา	2563

บทคัดย่อ

Ribosomal protein L10a (RpL10a) เป็นหนึ่งในโปรตีนของไรโบโซมที่มีหน้าที่นอกเหนือจากการผลิตโปรตีนในไรโบโซม ปัจจุบันมีงานวิจัยหลายฉบับที่แสดงให้เห็นว่า RpL10a มีบทบาทหน้าที่ที่นอกเหนือจากหน้าที่ของไรโบโซมอลโปรตีน (extra-ribosomal function) ซึ่งได้แก่ บทบาทในการควบคุมการสร้างเซลล์สืบพันธุ์เพศเมีย (oogenesis), กระบวนการสร้างตัวอสุจิ (spermatogenesis), การพัฒนาของรังไข่ (ovarian development), การพัฒนาของอวัยวะ (organogenesis) และการพัฒนาของตัวอ่อน (embryogenesis) การแสดงออกของ RpL10a ที่มากเกินไปในแมลงหวี่ส่งผลให้จอตาของแมลงมีการเพิ่มจำนวนเซลล์ที่มากผิดปกติและมีการสูญเสียเม็ดสีที่กลางจอตา ความผิดปกติเหล่านี้แสดงให้เห็นว่า RpL10a มีบทบาทเกี่ยวข้องกับการแพร่ขยายหรือการเพิ่มจำนวนเซลล์ (cell proliferation) ในทางกลับกัน การขาด RpL10a ในรังไข่แมลงหวี่ส่งผลให้ฟอลลิเคิลเซลล์รอบๆ เซลล์ไข่ขาดหายไป ซึ่งลักษณะความผิดปกติดังกล่าวมีความคล้ายคลึงกับลักษณะความผิดปกติของรังไข่ที่ขาดตัวรับอินซูลิน (insulin receptor) ความผิดปกตินี้แสดงให้เห็นว่า RpL10a มีบทบาทเกี่ยวข้องกับการสร้างเซลล์สืบพันธุ์เพศเมีย ซึ่งโดยปกติ ตัวรับอินซูลินเป็นโปรตีนตัวรับใน insulin signaling pathway ที่มีบทบาทในการควบคุมการพัฒนาและการแบ่งตัวของเซลล์ ควบคุมอัตราการเผาผลาญโดยเฉพาะการควบคุมสถานะสมดุลของกลูโคส ดังนั้นอาจเป็นไปได้ว่า RpL10a มีความเกี่ยวข้องกับการควบคุมการทำงานของตัวรับอินซูลินเพื่อควบคุมการเผาผลาญและการพัฒนาของเซลล์ เพื่อศึกษาความเกี่ยวข้องของ RpL10a กับการควบคุมสถานะสมดุลของกลูโคส จึงทำการตรวจสอบปริมาณคาร์โบไฮเดรตในตาของแมลงหวี่ที่มีการแสดงออกของ RpL10a ที่มากเกินไป (RpL10a-overexpressed flies) เปรียบเทียบกับแมลงหวี่ในกลุ่มควบคุม โดยใช้ anthrone-sulfuric acid colorimetric assay

งานวิจัยนี้ทำการศึกษาการทำงานของ RpL10a ที่มีความเกี่ยวข้องกับการพัฒนาและการเผาผลาญคาร์โบไฮเดรต ซึ่งจากผลการทดลองโดยเทคนิค qPCR และ immunohistochemistry พบว่าในแมลงหวี่ที่มีการแสดงออกของ RpL10a ที่มากเกินไปมีการแสดงออกของตัวรับอินซูลินเพิ่มขึ้นทั้งในระดับ mRNA และระดับโปรตีน ตามลำดับ นอกจากนี้โปรตีนที่เป็นตัวกลางในการส่งสัญญาณของอินซูลิน ได้แก่ Akt และ dFOXO ในแมลงหวี่ที่มีการแสดงออกของ RpL10a ที่มากเกินไป มีการเพิ่มขึ้นของการเติมหมู่ฟอสเฟตซึ่ง

เป็นรูปแบบการส่งสัญญาณใน pathway ในขณะที่ปริมาณไกลโคเจนลดลงในแมลงหวี่ที่มีการแสดงออกของ RpL10a ที่มากเกินไป การค้นพบนี้แสดงให้เห็นว่า RpL10a มีความเกี่ยวข้องกับการแพร่ขยายหรือการเพิ่มจำนวนเซลล์และการสลายไกลโคเจน (Glycogenolysis) และเพื่อศึกษาปฏิสัมพันธ์ระหว่าง RpL10a กับ ตัวรับอินซูลิน จึงทำการตรวจสอบการจับกันของโปรตีนทั้ง 2 โดยใช้เทคนิคทางชีวสารสนเทศ (bioinformatics) โดยการทำนายการจับกันด้วยโปรแกรม (*In Silico*) ผลการจำลองจากโปรแกรม ClusPro แสดงให้เห็นว่า RpL10a จากกุ้งสามารถจับกับตัวรับอินซูลินจากมนุษย์ได้ในบริเวณที่ต่างจากการจับของอินซูลินบนตัวรับอินซูลินที่ fibronectin type III (FnIII) domain ทั้งนี้เพื่อลดระยะเวลาในการเพาะเลี้ยงสัตว์ทดลองและเพื่อควบคุมความแปรผันของสภาวะการเพาะเลี้ยงได้ง่ายขึ้น จึงทำการศึกษาการทำงานของ RpL10a ต่อใน Chinese hamster ovary (CHO-S) cell line โดยตรวจสอบผลการจับกันของโปรตีนทั้งสองที่ได้จากโปรแกรมในหลอดทดลอง (*in vitro*) โดยใช้โปรตีน RpL10a จากกุ้ง และใช้ตัวรับอินซูลินจาก CHO-S cells เป็นโปรตีนต้นแบบในการจำลองการจับกัน และสามารถยืนยันตำแหน่งการจับกันได้จากผลการตรวจสอบการจับกันของ RpL10a และตัวรับอินซูลินในตำแหน่งที่ทำนายจาก ClusPro ด้วย pull-down assay และ immunofluorescence assay การจับกันของโปรตีนทั้งสองทำให้ RpL10a สามารถกระตุ้น insulin signaling pathway ได้ และเห็ยวนำให้เกิดการใช้คาร์โบไฮเดรตเพิ่มขึ้น ในขณะที่ไม่ส่งผลกระทบต่อการผลิตไขมัน นอกจากนี้งานวิจัยนี้ยังได้ศึกษาผลของ RpL10a ต่อการผลิตกลูโคสในสภาวะที่ดื้อต่ออินซูลิน โดยการเห็ยวนำภายใต้สภาวะกลูโคสที่สูงเพื่อให้ CHO-S cells เข้าสู่สภาวะดื้อต่ออินซูลินก่อนที่จะกระตุ้นด้วย RpL10a หลังจากการกระตุ้นด้วย RpL10a พบว่า RpL10a สามารถกระตุ้นให้เซลล์นำกลูโคสเข้าสู่เซลล์ได้ดีในสภาวะที่ดื้อต่ออินซูลินเมื่อเทียบกับเซลล์ปกติ อีกทั้ง RpL10a ยังสามารถกระตุ้นการทำงานของเอนไซม์ hexokinase ใน กระบวนการสลายกลูโคส (glycolysis) และลดการทำงานของเอนไซม์ glucose-6-phosphatase ในกระบวนการสังเคราะห์กลูโคส (gluconeogenesis) การค้นพบเหล่านี้แสดงให้เห็นว่า RpL10a สามารถบรรเทาอาการดื้อต่ออินซูลิน โดยการกระตุ้นการใช้กลูโคสและยับยั้งกระบวนการผลิตกลูโคสของเซลล์ในสภาวะที่ดื้อต่ออินซูลินภายใต้การเห็ยวนำด้วยสภาวะความเข้มข้นกลูโคสสูง จากบทบาทที่นอกเหนือจากหน้าที่ของ ribosomal protein ที่กล่าวมานี้ เป็นไปได้ว่า RpL10a อาจทำหน้าที่เป็นตัวเลียนแบบอินซูลิน (insulin-mimetic) ตัวหนึ่งในการรักษาเบาหวานได้

Thesis Title	Extra–Function of Ribosomal Protein L10a via Insulin Signaling Pathway
Author	Miss Netnapa Chaichanit
Major Program	Molecular Biology and Bioinformatics
Academic Year	2020

ABSTRACT

Ribosomal protein L10a (RpL10a) is one of several ribosomal proteins which has functions besides protein synthesis in the ribosome. Many reports recently revealed the extra–ribosomal function of RpL10a, including a role in oogenesis, spermatogenesis, ovarian development, organogenesis, and embryogenesis. In *Drosophila melanogaster*, the overexpression of the shrimp RpL10a resulted in the loss of red pigment in the eye center. This finding suggests that RpL10a also plays a role in cell proliferation. In contrast, the lack of RpL10Ab (RpL10Ab^{-/-}) in the germline of fruit flies showed the disappearance of the follicle cells surrounding the egg chamber, similar to the insulin receptor mutants (InR^{-/-}), indicating that RpL10a plays a role in oogenesis. Normally, InR is the transmembrane receptor of the insulin signaling pathway that plays a key role in cell development, cell division, metabolism regulation especially the role in glucose homeostasis regulation. Therefore, RpL10a may be involved in the step of regulation of InR to regulate cell development and metabolism.

To determine whether RpL10a is involved in regulating glucose homeostasis, carbohydrate content was observed in the eyes of normal and overexpressed flies by using an anthrone-sulfuric acid colorimetric assay. In this study, the function of shrimp RpL10a involved in insulin receptor (InR) and carbohydrate metabolism were investigated. In the eyes of RpL10a–overexpressed flies, the expression of InR was extensively increased in mRNA level and protein level, determined by qPCR and immunohistochemistry, respectively. Moreover, In the RpL10a–overexpressed eyes of the mutant fly showed the highly phosphorylated insulin signaling mediators such as

Akt and dFOXO, whereas the mutant flies showed the reduction of the glycogen. This finding revealed that shrimp RpL10a affects cell proliferation and glycogenolysis through the insulin signaling pathway. Besides, The interaction between RpL10a and InR was performed both *in silico* and *in vitro* binding. The shrimp RpL10a protein and the human InR protein were obtained as a *silico* binding model. The ClusPro software indicated that RpL10a could interact with InR at the difference site on fibronectin type III (FnIII) domain of insulin bound to InR. Then, to reduce the culture time and to control the culture condition easily, the study of shrimp RpL10a function was performed in CHO-S cell line. The *in vitro* study results, including pull-down assay and immunofluorescence assay, confirmed the binding of the proteins. The binding of the two proteins could stimulate the insulin signaling pathway by binding at the FnIII domain of InR and increased the carbohydrate utilization while the lipid metabolism was unchanged. Also, the effect of RpL10a on glucose metabolism was investigated in insulin resistance conditions. The CHO-S cells were induced to insulin resistance under high glucose conditions before stimulating with RpL10a. After the healthy cells and insulin-resistant cells (IRCs) were incubated with RpL10a, RpL10a could induce glucose uptake by the IRCs better than healthy cells.

Moreover, RpL10a could induce the expression of hexokinase in glycolysis and decreased the expression of glucose-6-phosphatase in gluconeogenesis. These findings suggested that RpL10a could alleviate the insulin resistance by inducing the glucose uptake into the cells, activating glycolysis, and suppressing glucose synthesis in IRCs induced under high glucose conditions. From this important function, RpL10a may have a function as an insulin-mimetic for insulin-resistant diabetes treatment.

ACKNOWLEDGMENTS

I am extremely grateful to my supervisor, Prof. Dr. Wilaiwan Chotigeat, for giving me the opportunity, supporting and assisting me in developing my scientific skills and also providing valuable guidance throughout the duration of my degree. Many thanks to Asst.Prof.Dr. Monwadee Wonglapsuwan for assisting me in basic science skills, teaching and providing me in the usage of *Drosophila* model. And also thanks to Asst.Prof.Dr. Ponsit Sathapondecha for suggesting and assisting me in a study the protein binding and other scientific skills.

I appreciate all of the help from my friends, especially in BSc.1007 over the time we have shared, for all your friendly and constant encouragement rendered to me.

I am thankful to the molecular biotechnology and bioinformatics department to provide me the facilities to carry out my work until the completion of the thesis.

Many thanks to my scholarship from Prince of Songkla University, The PSU-Ph.D. Scholarship and Research Grant for Thesis for supporting me the thesis financial during the period of study. And many thanks to The Royal Golden Jubilee Ph.D. Program (RGJ-Ph.D. Program) from the Thailand Research Fund (TRF) (4.JP.PS/56/B.1) for supporting me during the period of study and providing me special experiences in Japan for a short period. I take this opportunity to give a sincere thanks to Prof. Dr. Naoya Kenmochi, Frontier Science Research Center, the University of Miyazaki, for providing me the laboratory space for studying the function of RpL10a in the zebrafish model. And especially thanks to Kenmochi lab' members who give me a warm welcome, taking good care of me, kind assistance, and suggesting the interesting point in my work and thanks to my friends who give me a warm welcome and taking care of me during study in Japan.

I am thankful to the examining committee: Prof. Dr. Amornrat Phongdara and Prof. Dr. Kosum Chansiri, for their valuable advice and for taking the time to review my thesis.

Finally, this work would not have been possible without the true love and ongoing moral support from my family.

Netnapa Chaichanit

CONTENTS

	Page
Contents	x
List of Figures	xi
List of Tables	xiv
List of Abbreviations and Symbols	xv
Chapter	
1. Introduction	1
2. Literature Reviews	3
3. Objectives	17
4. Materials and Methods	18
5. Results and Discussion	43
6. Conclusions	78
References	81
Appendix	95
Appendix A	96
Appendix B	99
Vitae	118

LIST OF FIGURES

Figure	Page
1. The nucleotide sequence and amino acid sequences of the <i>RpL10a</i>	5
2. The alignment of the amino acid sequence of RpL10a	6
3. The GAL4/UAS system in transgenic flies	8
4. The phylogenetic tree of RpL10a from <i>F. merguiensis</i> and other organisms	9
5. The amino acid sequence alignment of shrimp RpL10a and <i>Drosophila</i> RpL10Ab	9
6. The overexpression of shrimp RpL10a in the eyes of fruit flies	11
7. The eyes membrane morphology of RpL10a–overexpressed flies	11
8. The excess RpL10a increased the expression of <i>InR</i> gene and InR protein	12
9. The schematic and the structure of insulin receptor	13
10. The insulin signaling pathway	14
11. The excess of RpL10a increased the phosphorylation of Akt	44
12. The excess of RpL10a increased the phosphorylation of dFOXO	44
13. The excess RpL10a altered carbohydrate metabolism	46
14. The effect of RpL10a may unchanged the total lipid content in normal flies and the RpL10a–overexpressed flies.	47
15. The excess RpL10a induced mRNA expression of <i>Shc</i>	48
16. The Swiss-Model report of the RpL10a protein model 02	51
17. Ramachandran plot	52
18. The 3D structure of shrimp Ribosomal protein L10a (RpL10a) and human insulin receptor (InR)	54

LIST OF FIGURES (Continued)

Figure	Page
19. The the binding site of Ribosomal protein L10a (RpL10a) and the insulin receptor (InR)	55
20. The interaction of Ribosomal protein L10a (RpL10a) and the insulin receptor (InR).	56
21. The interaction of of InR protein (green) is bound to insulin (orange)	57
22. The diagram of shrimp Ribosomal protein L10a (RpL10a) protein sequence conserved domain.	58
23. The sequence of the insulin receptor (InR) target cloning site	60
24. The amino acid sequence of InR-FnIII	62
25. Expression and purification of the GST-InR-FnIII	64
26. Expression and purification of the His-RpL10a	65
27. The interaction between His-RpL10a (prey) and GST-InR-FnIII (bait)	66
28. The interaction between ribosomal protein L10a (RpL10a) and the insulin receptor (InR)	68
29. The binding of RpL10a and InR induced Akt phosphorylation in RpL10a treated cells	69
30. The binding of RpL10a and InR altered the sugar metabolism in RpL10a treated cells	70
31. RpL10a induced glucose uptake in CHO-S cells	71
32. Induction of the Insulin resistance in Chinese hamster ovary (CHO-S) cells	72

LIST OF FIGURES (Continued)

Figure	Page
33. The cells density after 24 h of each induction condition	73
34. The induction of insulin resistance in Chinese hamster ovary (CHO-S) cells with 50 mM glucose	74
35. His-RpL10a increase the glucose uptake by healthy cells and insulin-resistant cells (IRCs)	75
36. RpL10a changes the glucose metabolism-related genes expression	76

LIST OF TABLES

Table	Page
1. Primer list	19
2. Composition of the cDNA synthesis reaction	22
3. Composition of PCR reaction	23
4. Thermal cycling of PCR	24
5. Composition of Real-Time PCR reaction	25
6. Thermal cycling of Real-Time PCR	25
7. Composition of PCR reaction	31
8. Thermal cycling of PCR	31
9. The top of 15 protein models	50
10. The list of the amino acid residue of RpL10a protein model 02	53
11. Composition of 12% SDS-polyacrylamide gel	97
12. Code of amino acids	117

LIST OF ABBREVIATIONS AND SYMBOLS

2-DG	=	2-Deoxy-D-glucose
2-DG6P	=	2-deoxy-D-Glucose-6-phosphate
3D	=	Three Dimensional
Akt	=	Serine-Threonine Protein Kinase
AMV	=	Avian Myeloblastosis Virus
AP	=	Alkaline phosphatase
Arg	=	Arginine
AS160	=	Akt Substrate Of 160 KDa
ASN	=	Asparagine
ASP	=	Aspartic acid
BCIP	=	5-Bromo-4-chloro-3-indolyl phosphate
bp	=	Base pair
BSA	=	Bovine serum albumin
cDNA	=	Complementary DNA
CHO	=	Chinese hamster ovary
cm ²	=	Square Centimeter
Conc.	=	Concentration
CR	=	Cysteine-rich region
<i>D. Melanogaster</i>	=	<i>Drosophila melanogaster</i>
DAPI	=	4',6-diamidino-2-phenylindole
DCAD2	=	<i>Drosophila</i> E-cadherin
DI	=	Deionized
Dlnr	=	<i>Drosophila</i> insulin-like receptor
DMEM	=	Dulbecco's Modified Eagle Medium
DNA	=	Deoxyribonucleic Acid
dNTP	=	Deoxynucleotide triphosphate
DTNB	=	5,5'-dithiobis-(2-nitrobenzoic acid)
<i>E. coli</i>	=	<i>Escherichia coli</i>
EDTA	=	Ethylene diamine tetraacetic acid

LIST OF ABBREVIATIONS AND SYMBOLS (Continued)

Erk	=	Extracellular signal-regulated kinase
ERK1/2	=	Extracellular signal-regulated kinase 1/2
F1	=	Filial 1
FBS	=	Fetal bovine serum
FITC	=	Fluorescein isothiocyanate
FnIII	=	Fibronectin type III
FoxO	=	Forkhead box protein, O subfamily
FoxO1	=	Forkhead box protein O1
G6K	=	Glucose-6-phosphate
G6pc3	=	Glucose-6-phosphatase 3
GAL4	=	Regulatory protein GAL4
GAPDH	=	Glyceraldehyde-3-phosphate dehydrogenase
GDP	=	Guanosine diphosphate
Gln	=	Glutamine
Glu	=	Glutamic acid
GLUT4	=	Glucose transporter 4
GLY	=	Glycine
GMQE	=	Global Model Quality Estimation
Grb2	=	Growth factor receptor-bound protein 2
GSK3	=	Glycogen synthase kinase 3
GST	=	Glutathione S-transferase
GTP	=	Guanosine triphosphate
h	=	Hour (s)
HEPES	=	4-(2-hydroxyethyl)-1-piperazineethanesulfonic acid
His	=	Histidine
Hk1	=	Hexokinase 1
IgG	=	Immunoglobulin G
InR	=	Insulin receptor
IPTG	=	Isopropyl-1-thio- β -D-galactosidase

LIST OF ABBREVIATIONS AND SYMBOLS (Continued)

IRCs	=	Insulin-resistance cells
IRS	=	Insulin receptor substrates
kDa	=	kilodaltons
KRPH	=	Krebs-Ringer-Phosphate-HEPES
L1	=	Leucine-rich repeat
L2	=	Leucine-rich repeat
LB	=	Luria-Bertani
LYS	=	Lysine
mA	=	Milliamp
MAPK	=	Mitogen-activated protein kinase
MEK	=	MAPK/Erk kinase
Met	=	Methionine
mg	=	Milligram
min	=	Minute (s)
ml	=	Milliliter
mM	=	Millimolar
mRNA	=	Messenger ribonucleic acid
mSOS	=	Mammalian Son-of-sevenless
mTOR	=	Mammalian Target Of Rapamycin
N	=	Normality (concentration)
NADP	=	Nicotinamide adenine dinucleotide phosphate
NADPH	=	Nicotinamide adenine dinucleotide phosphate hydrogen
NBT	=	Nitro blue tetrazolium chloride
NCBI	=	National Center for Biotechnology Information
ng	=	Nanogram
nm	=	Nanometer
nM	=	Nanomolar
OD	=	Optical density
PAGE	=	Polyacrylamide gel electrophoresis

LIST OF ABBREVIATIONS AND SYMBOLS (Continued)

p-Akt	=	Phosphorylated Akt
PBAF	=	PBS, bovine serum albumin and fetal calf serum
PBS	=	Phosphate buffered saline
PBST	=	Phosphate buffered saline Tween-20
PCR	=	Polymerase chain reaction
PDB	=	Protein Data Bank
p-FOXO	=	Phosphorylated FOXO
pH	=	Potential of Hydrogen
Phe	=	Phenylalanine
pI	=	Isoelectric point
PI3K	=	Phosphoinositide 3-kinase
PIP3	=	Phosphatidylinositol (3,4,5)-trisphosphate
PKB	=	Protein kinase B
pmole	=	Picomole
PMSF	=	Phenylmethylsulfonyl fluoride
PRO	=	Proline
Pwop	=	Peas without pod
qPCR	=	Quantitative PCR
qRT-PCR	=	Quantitative Reverse Transcription PCR
RCSB	=	Research Collaboratory for Structural Bioinformatics
RNA	=	Ribonucleic acid
RNase	=	Ribonuclease
RpL10a	=	Ribosomal protein L10a
RpL10Aa	=	Ribosomal protein L10Aa
RpL10Ab	=	Ribosomal protein L10Ab
RpL22	=	Ribosomal protein L22
RpL9	=	Ribosomal protein L9
rpm	=	Revolutions per minute
RpS19	=	Ribosomal protein S19

LIST OF ABBREVIATIONS AND SYMBOLS (Continued)

RpS26	=	Ribosomal protein S26
S6K1	=	Ribosomal protein S6 kinase 1
SD.	=	Standard Deviation
SDS	=	Sodium dodecyl sulfate
Sec	=	Second
SER	=	Serine
Shc	=	Sh2-containing collagen-related protein
SPSS	=	Statistical Product and Service Solutions
T1DM	=	Type 1 diabetes mellitus
T2DM	=	Type 2 diabetes mellitus
Taq	=	Thermus aquaticus
TBS	=	Tris-buffered saline
TBST	=	Tris-buffered saline Tween-20
Thr	=	Threonine
Tris-HCl	=	Tris(hydroxymethyl)aminomethane hydrochloride
U	=	Unit
UAS	=	Upstream activation sequence
V/V	=	Volume per volume
W	=	Watt
W/V	=	Weight per Volume
Å	=	Angstrom
µl	=	Microliter
µg	=	Microgram
µM	=	Micromolar

CHAPTER 1

INTRODUCTION

Ribosomal proteins are important in the step of ribosome biogenesis and protein synthesis. Recently, many publications revealed that ribosomal proteins can perform extra-ribosomal functions that influence cellular processes. For example, Ribosomal Protein L22 (RpL22) controlled morphogenesis by regulating the pre-mRNA splicing (Zhang et al., 2017), Ribosomal protein S19 (RpS19) mutation increased the grooming behaviors in mice (Chen et al., 2016) and, Ribosomal protein L9 (RpL9) deficiency inhibited the growth of colorectal carcinoma (Baik et al., 2016). In addition, many ribosomal proteins have the extra-ribosomal functions associated with insulin pathways. The ribosomal protein S6 kinase 1 (S6K1), relate to the insulin resistance that induced by the nutrient overload, regulated the insulin receptor substrate 1 (IRS1) (Tremblay et al., 2005; Um et al., 2004; Yoon, 2017). S6K1 deficiency induced mild glucose intolerance and decreased the levels of circulating insulin (Pende et al., 2000). Ribosomal protein S26 (RpS26) linked to many diabetes genes (Schadt et al., 2008) and the high expression of RpS26 was found in the pancreas and islets of Langerhans.

Ribosomal protein L10a (RpL10a); a constitutive protein of the large subunit ribosomes, has the extra-ribosomal functions in controlling organogenesis, embryogenesis, cell proliferation (Balcer-Kubiczek et al., 1997; Fusicaro et al., 1995), and ovarian maturation (Palasin et al., 2014; Wonglapsuwan et al., 2011, 2010). In addition, the relationship between RpL10a and insulin receptor (InR) was reported in a previous publication. Saetan et al. (2016) reported that both *RpL10a* and *InR* showed up-regulation expression during ovarian maturation. RpL10Ab deficiency in *Drosophila* egg chambers showed the peas without pods (Pwop) phenotype as well as in InR mutation (Pritchett and McCall, 2012; Wonglapsuwan et al., 2011). Moreover, a recent study indicated that the overexpression of shrimp RpL10a could activate the *Drosophila* InR expression to stimulate cell proliferation (Chaichanit et al., 2018). All the evidence suggests that RpL10a may have a special function in controlling InR expression.

InR is the transmembrane receptor of the insulin signaling pathway that plays a key role in controlling the glucose metabolism. The binding between InR and insulin or other ligands initiate the signal transduction throughout the cell by autophosphorylation to regulate the cellular process. Mutation of InR or abnormality of the signal transduction results in insulin resistance, abnormal glucose metabolism, and diabetes mellitus (Campbell, 2009). Thus, insulin replacement therapy has required for the treatment of diabetic patients. Several publications have reported the use of recombinant insulin, insulin analogs, and insulin-mimetic as the diabetic patient treatment (Babu et al., 2020; Moura et al., 2020; Qiang et al., 2014; Xie et al., 2020).

Therefore, the effect of shrimp RpL10a overexpression involved in insulin pathway was investigated in the eyes of RpL10a-overexpressed flies. The relationship between shrimp RpL10a and InR was explained by studying the interaction between RpL10a and InR both *in silico* and *in vitro* study and demonstrating the effects of the protein-protein binding on the insulin pathway in CHO-S cell line to make it easier to control the culture conditions. Moreover, shrimp RpL10a which acts as an insulin-mimetic was also investigated by using insulin resistance CHO-S cells as a model.

CHAPTER 2

LITERATURE REVIEWS

1. Extra-ribosomal functions

Ribosomal proteins (PRs), the RNA-binding proteins, have the essential function in ribosome biogenesis and protein synthesis (de la Cruz et al., 2015). The defect of ribosome biogenesis are known as ribosomopathies, has been linked to many clinical syndromes (Narla and Ebert, 2010). In Diamond-Blackfan anemia (DBA), the mutations of *RpS19* and *RpS24* genes resulted in ribosome biogenesis disorder (Choismel et al., 2008, 2007; Flygare et al., 2007). The expression of several ribosomal protein genes, including *RpL29*, *RpL23*, *RpL22*, *RpL15*, *RpL6*, *RpS20*, and *RpS9* was decreased in Schwachman-Diamond syndrome (SDS) (Rujkijyanont et al., 2009). Moreover, loss of PRs in DBA and SDS models relate to the insulin signaling pathway. Deficiency of Ribosomal protein in these models promoted activation of S6 kinase phosphorylation leading to inhibition of the insulin pathway through insulin resistance mechanism (Heijnen et al., 2014). Besides, many reports suggest that several ribosomal proteins also present an additional extra-ribosomal function (Lu et al., 2015; Warner and McIntosh, 2009; Wool, 1996). *RpS20* and *RpL6* affect the RNA Polymerase III transcription level in *S. cerevisiae* (Dieci et al., 2009; Hermann-Le Denmat et al., 1994). Yeast ribosomal protein S3 (*RpS3p*) has an endonuclease activity that cleaves variously damaged DNA (Jung et al., 2001; Seong et al., 2012), and knockdown of *RpS3* resulted in an early embryonic developmental arrest in mice (Peng et al., 2019). In addition, the extra-ribosomal function of some RPs also involved in insulin resistance and insulin signaling pathway. *RpS26*, which may play an extra-ribosomal function, is expressed highly in the pancreas and islets of Langerhans, and involved in many genes in Type 1 diabetes mellitus (T1DM). (Schadt et al., 2008). *S6K1*, an insulin signaling mediator, negatively regulates *IRS1* (Zick, 2004). Studies in mice have shown that lacked *S6K* caused mildly glucose intolerant and decreased the circulating insulin level (Pende et al., 2000). Indicating that *S6K1* may be associated with the insulin resistance induced

by nutrient overload condition (Patti and Kahn, 2004; Tremblay et al., 2005; Um et al., 2004).

2. Ribosomal protein L10a (RpL10a)

RpL10a, which belonged to the L1P family of ribosomal proteins, is a component protein of a large subunit of the ribosome. It is located in the cytoplasm. RpL10a protein encoded by the *rpl10a* gene. This gene expression is downregulated in the thymus by cyclosporin-A (CsA) which is an immunosuppressive drug. Previously, this gene was referred as NEDD6 (neural precursor cell expressed, developmentally downregulated 6) and it was then renamed as RpL10a. During development in mice showed that the *rpl10a* gene expression is downregulated in neural precursor cells. RpL10a is ubiquitously expressed in all tissues but It highly expression in the organs of female, pancreas, kidney, muscle, and so on. RpL10a has the function of combining 60S and 40S ribosomes to form the 80S ribosomes (Turtoi et al., 2008). RpL10a enhances the expression of Insulin-Like Growth Factor2 (IGF2), Early Growth Response 1 (EGR1), and Pleiotrophin (PTN) (Shi et al., 2017). Moreover, many previous publications reported that RpL10a had been shown additional extra-ribosomal functions. RpL10a may be related to the cell proliferation such as the roles in organogenesis, embryogenesis, (Balcer-Kubiczek et al., 1997; Fisticaro et al., 1995), spermatogenesis regulation, development control in zebrafish's embryos (Palasin et al., 2019), and maturation in shrimp's ovaries (Palasin et al., 2014; Wonglapsuwan et al., 2011, 2010). Moreover, many pieces of evidence showed the relation between RpL10a and InR. This relationship had been found during ovarian maturation in shrimp's ovary, which shows up-regulation of *rpl10a* and *InR* (Saetan et al., 2016). In the *Drosophila*'s ovary, InR mutation resulting in disappearing of the somatic follicle cells in the egg chambers. This phenotype is called "Pwop" (Pritchett and McCall, 2012), It is similar to the deficiency of RpL10Ab (RpL10Ab^{-/-}) in germline clone which lack of follicle cells surrounding the egg chamber (Wonglapsuwan et al., 2011). Moreover, the RpL10Ab^{-/-} flies could survive by using the shrimp (*Fenneropenaeus merguensis*) RpL10a protein to rescue the fruit flies. It indicated that Shrimp RpL10a has a functional conservation with the RpL10Ab of *Drosophila* (Wonglapsuwan et al., 2011).

shrimp *rpl10a* gene comprised of 669 bp and encoded to 217 amino acids (Figure 1). It has the Ribosomal L1 superfamily domain at amino acid residue 2–217 (NCBI Conserved Domain Database (CDD)). This domain functions as a ribosomal protein bound to rRNA and it functions as a translation repressor by binding to its own mRNA. The RpL10a also has the nuclear localization signal and eight phosphorylation sites including Ser2, Ser50, Ser86, Ser141, Thr9, Thr52, Thr139, and Tyr11. The molecular weight and pI of this protein were 25.7 kDa and 10.06, respectively.

```

CGGACAAGGAGCACCATGTCGAGCAAGGTGACGAGGGACACCCTCTACGAG 51
1      M  S  S  K  V  T  R  D  T  L  Y  E
TGCATCAACGGCGTGCTTCAGGGCGCCAAGGACAAGAAGCGCAACTTCCGC 102
13     C  I  N  G  V  L  Q  G  A  K  D  K  K  R  N  F  R
GAGACGGTCGAGCTCCAGATCGGCCTCAAGAACTATGACCCCCAAAAGGAT 153
30     E  T  V  E  L  Q  I  G  L  K  N  Y  D  P  Q  K  D
AAGCGTTTCAGTGGCACAGTGAAGTTGAAGCACATCCCCAAGCCCAACATG 204
47     K  R  F  S  T  G  V  K  L  K  H  I  P  K  P  N  M
AAGATCTGTGTCCTTGGTGACCAGATGCACATTGATGAGGCTAAGGAGAAC 255
64     K  I  C  V  L  G  D  Q  M  H  I  D  E  A  K  E  N
AACATTCCTGCATGTCTGCCGATGACCTCAAGAAGCTGAACAAGGACAAG 306
81     N  I  P  C  M  S  A  D  D  L  K  K  L  N  K  D  K
AAGCTTGTCAAGAAGCTGGCAAAGAAGTATGATGCCTTCATTGCCTCTGAT 357
98     K  L  V  K  K  L  A  K  K  Y  D  A  F  I  A  S  D
GCCCTTATCAAGCAGATTCCCCGTCTGTTGGGCCCTGGTCTCAACAAGGTT 408
115    A  L  I  K  Q  I  P  R  L  L  G  P  G  L  N  K  V
GGCAAGTTCCTACCATGTGCACTCACTCTGAGAAGTTGACAGACAAGTGC 459
132    G  K  F  P  T  M  C  T  H  S  E  K  L  T  D  K  C
AATGAGATCAAGGCCACCATCAAGTTCAGATGAAGAAGGTGTTGTGCCTG 510
149    N  E  I  K  A  T  I  K  F  Q  M  K  K  V  L  C  L
TCTGTTGCCATTGGCCACGTTGAGATGGCTTCGGATGAACTAGTGCAGAAC 561
166    S  V  A  I  G  H  V  E  M  A  S  D  E  L  V  Q  N
GTTTACCTGGCCATGAACTTCTTGTTTCGCTGTTGAAGAAGCATTGGCAG 612
183    V  Y  L  A  M  N  F  L  V  S  L  L  K  K  H  W  Q
AACGTGCGATCCCTGCATATTAAGTCTACCATGGGAAGGCCCCAACGCCTG 663
200    N  V  R  S  L  H  I  K  S  T  M  G  R  P  Q  R  L
TACTAG 669
217    Y  *

```

Figure 1. The nucleotide sequence and amino acid sequences of the *RpL10a*. The asterisk indicates the stop codon. Red letter with underline indicates the nuclear localization signal. The circles indicate the phosphorylation sites including four sites of serine (Ser/S) (blue), three sites of threonine (Thr/T) (green), and one site of tyrosine residues (Tyr/Y) (yellow) (Wonglapsuwan et al., 2010).

Shrimp RpL10a has homologs in with other organisms, both vertebrates and invertebrates (Figure 2) and all organisms have the POKDKRF amino acid, a highly conserved sequence.

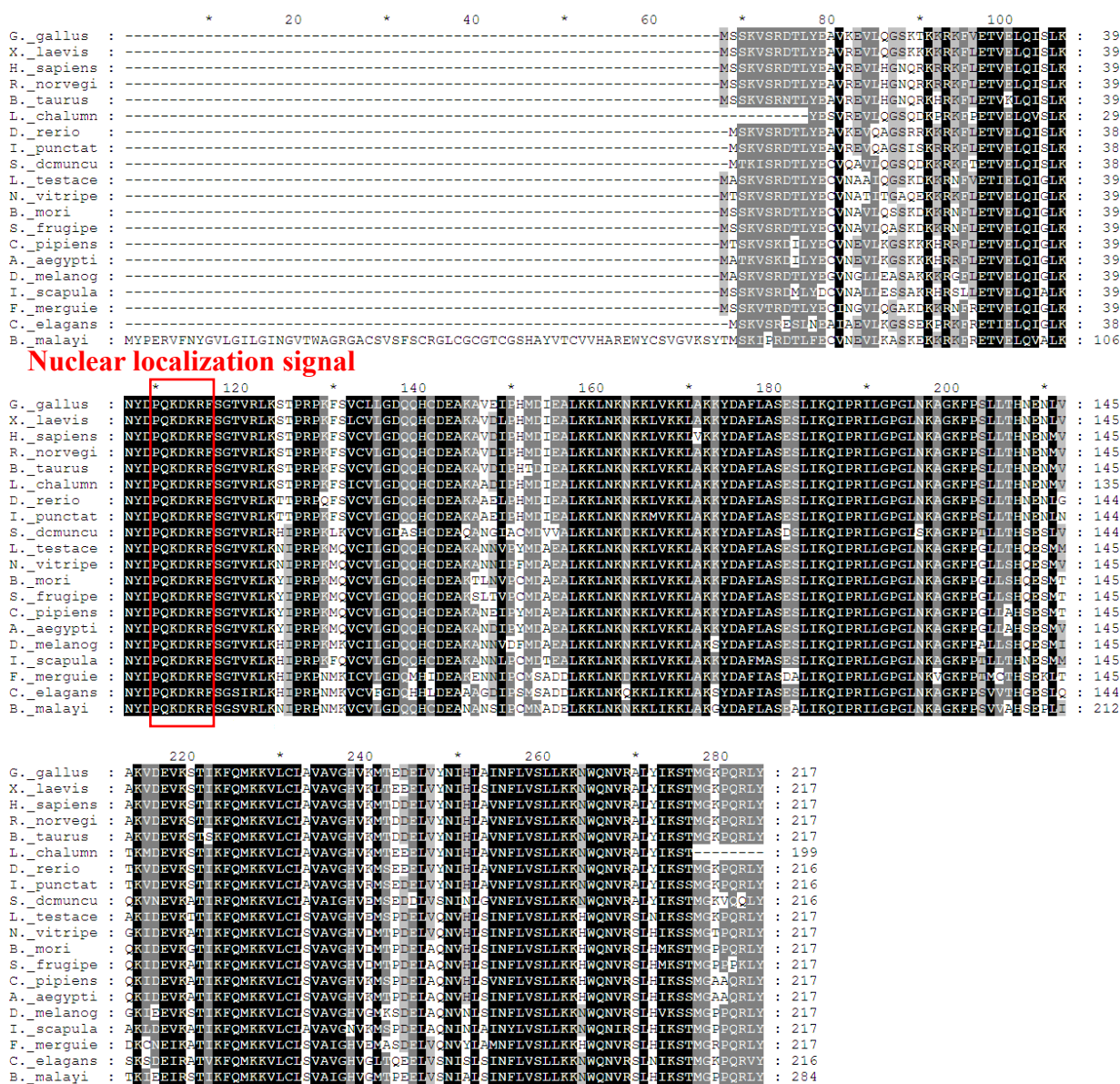


Figure 2. The alignment of the amino acid sequence of RpL10a (GenBank accession number FJ623402) from *F. merguensis* with other homologous RpL10a. The red square indicates the nuclear localization signal (Wonglapsuan et al., 2010).

3. *Drosophila melanogaster*

3.1. General biology of *Drosophila melanogaster*

The *Drosophila melanogaster* (fruit fly) is a popular model organism used to study human diseases, such as human cancer (Mirzoyan et al., 2019). 60% of the *Drosophila* genome homologous to the humans genome and shares approximately 75% homologous to disease-causing genes of human, and the genome less redundancy than in humans (Chien et al., 2002; Pandey and Nichols, 2011; Ugur et al., 2016; Yamamoto et al., 2014). And other advantages indicate that *D. melanogaster* is a powerful genetic tool such as small size, short life cycle, easy cultivation, a large number of offspring per generation, low raising cost (Millburn et al., 2016; Sang, 2001).

3.2. The GAL4/UAS system in transgenic flies

The GAL4/UAS system is a developed method commonly used in *Drosophila* to study the expression of an interesting gene (Brand and Perrimon, 1993). The system of GAL4/UAS consists of two parts, including the GAL4 protein, derived from yeast, which serves as a DNA binding transcription factor, and the upstream activation sequence (UAS), an enhancer specific to the GAL4 protein. GAL4 is a yeast protein not ordinarily express in *Drosophila* but expressed in transgenic GAL4 flies to drive the transcription of the interesting gene, constructed by link with the UAS sequences (Fischer et al., 1988). Therefore, this system is widely used to drive tissue-specific expression of interesting genes in the fruit fly (Brand and Perrimon, 1993). The target gene is constructed by inserting next to the UAS sequence and keep in a transgenic line, which the target gene remains silent in the absence of its activator. The GAL4 with a tissue-specific promoter is kept in another line in which activation protein is expressed without target genes to activate. When the two transgenic lines are crossed together to produce F1 flies, the GAL4 protein will bind to the UAS and activate the expression of the tissue-specific gene which is set by the promoter (Figure 3). The phenotype of the target tissue can then be observed in the progeny (Cho et al., 2014; Duffy, 2002; Fischer et al., 1988; Kelly et al., 2017; Xu et al., 2017).

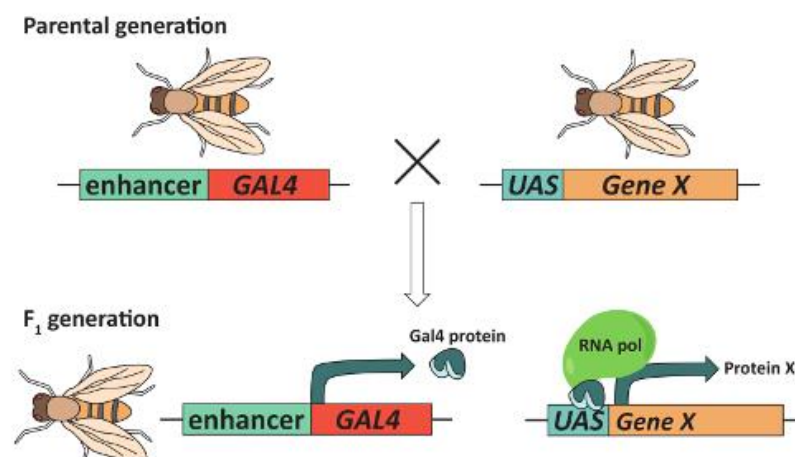


Figure 3. The GAL4/UAS system in transgenic flies (Kelly et al., 2017)

3.3. Ribosomal protein L10a in *D. Melanogaster*

In *Drosophila*, there are two *RpL10a* genes that reported in the FlyBase database (<https://flybase.org/>). *RpL10Aa* lacks an intron while another, *RpL10Ab*, has an intron between exon. They indicated that *RpL10Aa* might be a consequence of *RpL10Ab* retrotransposition (Marygold et al., 2007). *RpL10Aa* has a limited expression pattern in cells and less expressive than the *RpL10Ab* gene, whereas the *RpL10Ab* gene plays a role in producing most of the RpL10a protein in most cells (Marygold et al., 2007). Therefore, the *RpL10Ab* is an interesting gene in the study of *RpL10a* function in *Drosophila*. The previous publication reported that *RpL10Ab* is an important gene during oogenesis in *Drosophila* (Wonglapsuwan et al., 2011). The *Drosophila* *RpL10Ab* gene is closely correlated with the shrimp *RpL10a* (Figure 4) by showing the conserved function with the *Drosophila* *RpL10Ab* in the rescue experiment (Wonglapsuwan et al., 2011). RpL10a from *F. merguensis* shares 86% similarity with *Drosophila* RpL10Ab (Figure 5).

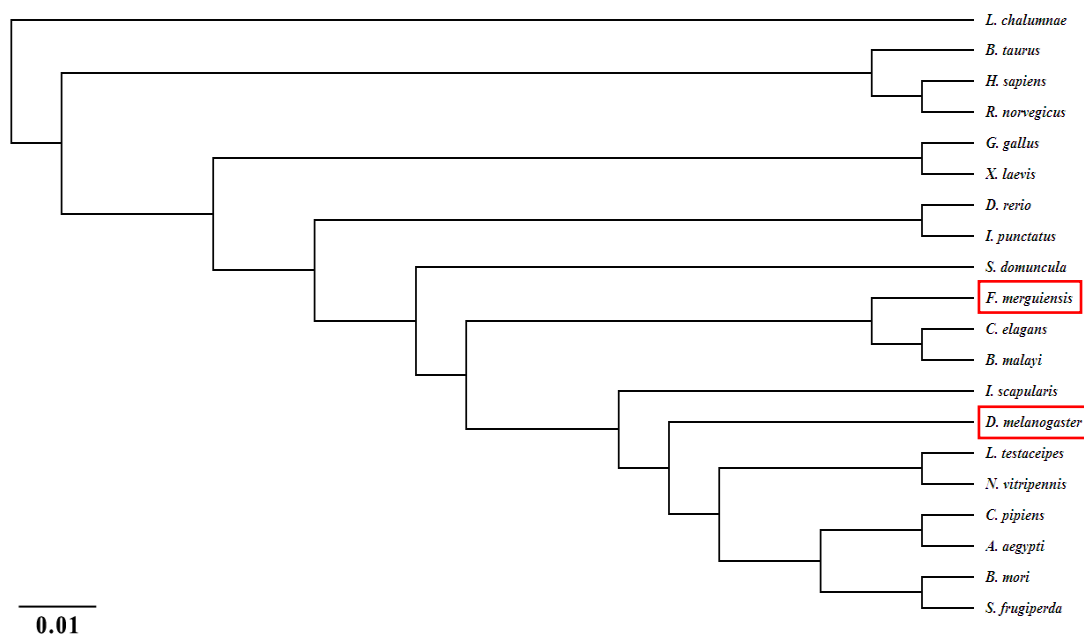


Figure 4. The phylogenetic tree of RpL10a from *F. merguiensis* and other organisms. The phylogenetic tree was created based on the amino acid sequence comparisons that are shown in Figure 2 (Wonglapsuwan et al., 2010).



Figure 5. The amino acid sequence alignment of shrimp RpL10a and *Drosophila* RpL10Ab.

Some pieces of evidence indicated the correlation between RpL10a and InR. In *Drosophila*, lack of *RpL10Ab* (*RpL10Ab^{-/-}*) in germline showed a complete failure to progress into mid-oogenesis and showed disappearance of the follicle cells surrounding the *Drosophila* egg chamber but showed the normal nurse cells. This result is called a Pwop phenotype, which is reminiscent of *InR* mutants (*InR^{-/-}*) that the somatic follicle cells disappeared in the egg chambers but the germline persisted (Pritchett and McCall, 2012). This phenotype is also found in the *insulin-receptor substrate (IRS)-like chico* mutants (Drummond-Barbosa and Spradling, 2001). Many reports showed that insulin also regulates the oogenesis in many organisms such as *Drosophila*, mosquito, and shrimp (Brown et al., 2008; McCall, 2004; Sun et al., 2010; Wonglapsuwan et al., 2011). In *D. melanogaster*, the overexpression of shrimp RpL10a under the GMR promoter resulted in the abnormality of ommatidia in which a decreasing of the red pigment in the eyes center (Wonglapsuwan et al., 2011) and RpL10a could control the trehalose metabolism and stimulate cell proliferation in RpL10a–overexpressed flies by inducing the expression of InR and Shc (Chaichanit et al., 2018). These evidence revealed that RpL10a might have another extra–ribosomal function involved in cell proliferation and metabolism regulation through the insulin pathway.

3.4. InR in RpL10a–overexpressed eyes.

Overexpression of shrimp RpL10a under the eye-specific promoter, GMR, in the *Drosophila*, resulted in increasing the roughness of ommatidia and losing a red pigment in the center area of the eyes. whereas, the GMR-Gal4 control flies showed normal red eyes (Wonglapsuwan et al., 2011). They were indicating that the excess of RpL10a Affect the death of pigment cells in the eyes of *Drosophila* (Figure 6).

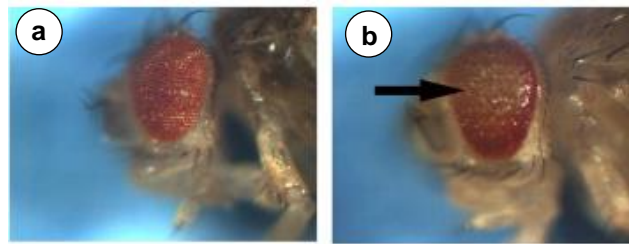


Figure 6. The overexpression of shrimp RpL10a in the eyes of *Drosophila*. (a) Control (*GMR-GAL4/+*) shows normal red eyes. (b) The RpL10a–overexpressed flies (*GMR-Gal4/+; UAS-RpL10a*) show abnormal eyes with rough ommatidia and a loss of the red color in the center of the eye (arrow) (Wonglapsuwan et al., 2011).

The excess of RpL10a causes disappearance of the eyes membranes (Figure 7) (Chaichanit et al., 2018), as well as in the lack of *RpL10Ab* resulted in the membrane organization in the follicle cells of fruit flies (Wonglapsuwan et al., 2011). These characters were similar to *Dlnr* (*Drosophila insulin-like receptor*) overexpression in *Drosophila's* eye that showed a large ommatidial with unusual pattern (Brogiolo et al., 2001).

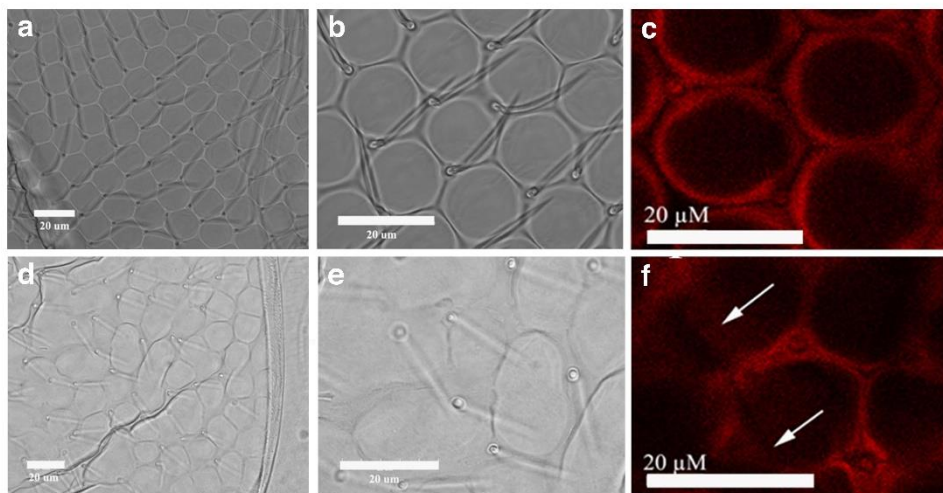


Figure 7. The eyes membrane morphology of RpL10a–overexpressed flies. (a, b, d, and e) the unstained ommatidia are represented in phase contrast, (c and f) the ommatidia were stained with *Drosophila* E-cadherin (DCAD2), an adherens junctions specific (red). (a-c) the eyes of *GMR-GAL4/+* flies. (d-f) the eyes of *GMR-Gal4/+; UAS-RpL10a* flies. The arrows indicate the loss of the eyes membrane. The scale bars represent 20 μm (Chaichanit et al., 2018).

The excess of RpL10a also induces the expression of InR in both mRNA level and protein level (Figure 8). This effect indicated a correlation between RpL10a and InR. Generally, InR is a tyrosine kinase receptor that plays critical regulatory roles in cell division, cell development and metabolism.

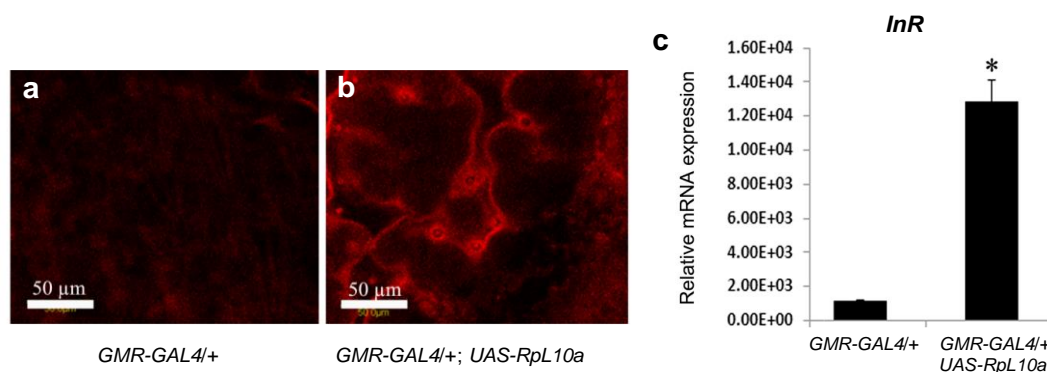


Figure 8. The excess of RpL10a increased the expression of *InR* gene and InR protein. (a–b) The eyes of (a) *GMR-GAL4/+* and (b) *GMR Gal4/+; UAS-RpL10a* were stained with anti-insulin receptor (Red). The scale bars represent 50 μm . (c) The InR mRNA expression level was measured by real-time PCR. Histogram shows the InR relative mRNA expression which normalized by GAPDH gene. The asterisk indicated a significant difference in each group. ($p < 0.05$) (Chaichanit et al., 2018).

4. Insulin signaling pathway

The insulin signaling pathway controls many biological processes such as cell proliferation, glucose metabolism, and lipid metabolism. After the InR is activated by interacting with the insulin or other specific ligands, the signal was generated by the autophosphorylation mechanism (De Meyts, 2000; Ward and Lawrence, 2009).

The InR consists of two alpha subunits and two beta subunits which connected together via a disulfide bond. the insulin bind to the alpha subunits located on the outside of the membrane whereas the two beta subunits are the transmembrane proteins that act as a signal transducer. (Belfiore et al., 2009; GOLDFINE, 1987; Seino and Bell, 1989). The InR structure consists of 8 domains including a leucine-rich repeat domain

(L1 domain), a cysteine-rich region (CR, domain), an additional leucine-rich repeat domain (L2, domain), three fibronectin type III domains (FnIII-1, FnIII-2, and FnIII-3), and two insert domains (ID α and ID β) that lie on the FnIII-2 domain. The downstream of the FnIII-3 domain contains a transmembrane helix (TH), intracellular juxtamembrane (JM) region, and the intracellular tyrosine kinase (TK) catalytic domain that involved in the intracellular signaling (Smith et al., 2010) (Figure 9). The InR consists of 2 ligand binding sites, which are site 1, consisting of L1 and α CT domains and site 2, consisting of fibronectin type III 1 (FnIII1) and FnIII2 domains (Ward and Lawrence, 2009).

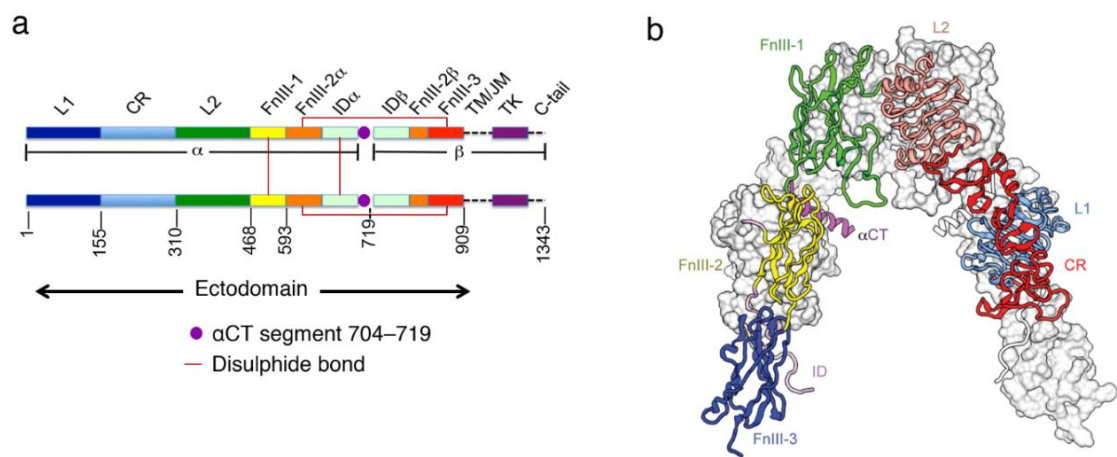


Figure 9. The schematic (a) and the structure of insulin receptor (b). (Croll et al., 2016; Menting et al., 2013)

Insulin binds to the alpha subunit of the InR and changes the beta subunit's conformation for inducing the tyrosine kinase. The auto-phosphorylation of this beta subunit leads phosphorylation of IRS. Then, the phosphorylated IRS activates PI3K/Akt signaling pathway and MAPK Signaling Pathway (Figure 10) (Poloz and Stambolic, 2015).

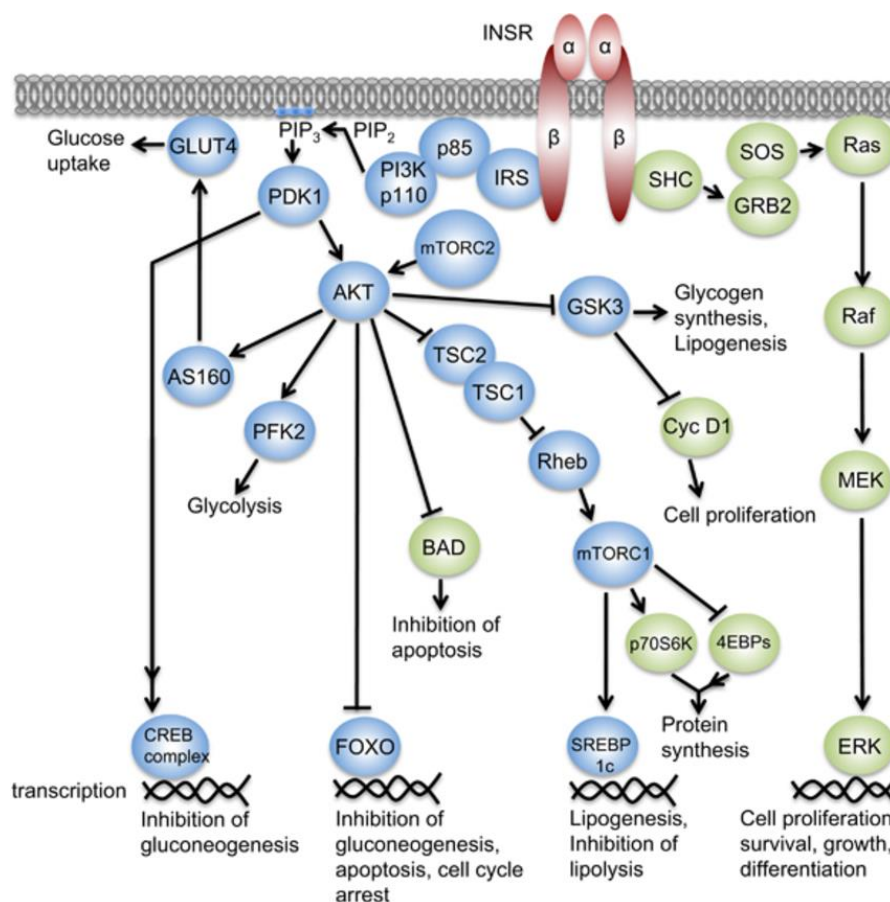


Figure 10. The insulin signaling pathway (Poloz and Stambolic, 2015)

The PI3K/Akt Signaling is the pathway regulated by insulin mainly through the PI3K (phosphoinositol 3 kinase) to control the metabolism. After activation of PI3K by activated IRS1, the activated PI3K then activates phosphatidylinositol phosphorylation to generate the 3, 4, 5-phosphatidylinositol-3, 4, 5-triphosphate (PIP₃). Then the activated PIP₃ activates the Akt at serine/threonine-protein kinase. The phosphorylated Akt can activate many substrates and act as a mediator of the insulin effect. For example, Akt phosphorylates GSK3 (glycogen synthase kinase 3), involved in glycogen synthesis regulation. GSK3, a serine/ threonine-protein kinase, inhibits glycogen synthase when it was phosphorylated by AKT/PKB (Cohen and Frame, 2001). Akt phosphorylates FoxO (forkhead box-containing protein, O subfamily) transcription factors, to inhibit their translocation to the nucleus to stimulate the expression of gluconeogenesis genes. (Accili and Arden, 2004; Taniguchi et al., 2006). Akt also phosphorylates AS160, a glucose transporter 4 (GLUT4) to translocate to the cell

membrane to uptake glucose. And Akt also phosphorylates mTOR, a mammalian target of rapamycin, to regulate the synthesis of protein and cell growth (Harris and Lawrence, 2003).

The MAPK Signaling Pathway is mainly controlling cell growth and protein synthesis. This pathway is initiated when Grb2 (growth factor receptor-bound protein 2) binds to tyrosine-phosphorylated Shc (Sh2-containing collagen-related protein). After Grb2 links to the mammalian nucleotide exchange factor mSOS, this complex then activates Ras. The activated Ras activates Raf and then Raf activates MAPK/Erk kinase (MEK) to regulates transcription factors involved in cell proliferation, cancer gene, and protein synthesis.

In insulin resistance, because the mutation of InR or abnormality of signal transduction results in an abnormality of glucose metabolism and leads to type 2 diabetes mellitus (Keith Campbell, 2009). On the other hand, type 1 diabetes is caused by autoimmune responses that destroy the beta cells resulting in abnormal insulin production in the pancreas. (Bluestone et al., 2010). Thus, insulin replacement therapy has required for the treatment of diabetic patients such as recombinant insulin, insulin analogs, and insulin-mimetic (Babu et al., 2020; Moura et al., 2020; Qiang et al., 2014; Xie et al., 2020). For example, a chaetochromin derivative 4548-G05 that has the function as an insulin-mimetic, could activate InR and its downstream pathways by binding to the InR on on different site of the insulin binding (Qiang et al., 2014). Several alternative insulin analogs will be useful for the patient.

5. Insulin resistance model

Type 2 diabetes, the major cause of death worldwide, is characterized by insulin resistance. It occurs when the insulin-responsive tissues such as liver, adipose tissue, and skeletal muscle are unable to respond to insulin properly (Chang et al., 2015). Insulin resistance is closely correlated with over-nutrition and obesity and other factors such as chronic inflammation and stress responses. (Johnson and Olefsky, 2013; Olefsky and Glass, 2009). Since there are several pieces of research that aim to study the mechanism of insulin resistance and try to find a new therapeutic drug for insulin resistance. Thus, several animal models of insulin resistance have been developed to facilitate opportunities to explore the impact of insulin resistance. There are multiple important effects of insulin resistance, many approaches to developing insulin-resistance cells. According to the previous study, the high-glucose (50 and 75 mM) was used to induce insulin resistance in gingival fibroblasts cells (Buranasin et al., 2018). High levels of insulin can cause insulin resistance (Shanik et al., 2008). High glucose/insulin also induced cell to insulin resistance condition which was observed in the 3T3-L1 adipocyte cells induced by the combination of 25 mM glucose and 5 nM insulin for 24 h. (Ross et al., 2000). Oxidative stress is accepted as a factor in insulin resistance development (Bloch-Damti and Bashan, 2005). The hepatocyte cell line BRL-3A was induced to insulin resistance cells by using Glucose oxidase, an oxidoreductase catalyzing the conversion of glucose to gluconolactone, which is further converted to glucuronic acid and H₂O₂. (Wang et al., 2012). A combination of TNF- α , a proinflammatory cytokine, and hypoxia are able to induce insulin resistance in 3T3-L1 adipocytes cells (Lo et al., 2013). (Chang et al., 2015). TNF- α can induce insulin resistance in FL83B liver cells (Chang et al., 2014, 2011). In addition, there are many other agents are also can cause insulin resistance, such as free fatty acids (Nguyen et al., 2005; Samuel and Shulman, 2012), interleukin-1 (IL-1) (Jager et al., 2007), IL-6 (Rotter et al., 2003), dexamethasone (Sakoda et al., 2000), growth hormone (Smith et al., 1997), glucosamine (Nelson et al., 2000), hypoxia (Regazzetti et al., 2009), and so on.

OBJECTIVES

This research focused on the correlation between ribosomal protein L10a (RpL10a) and insulin receptor (InR) and the extra-ribosomal function of RpL10a that acts as insulin-mimetic in insulin resistance condition. The objectives of this research are as follows:

1. To investigate the effect of excess RpL10a on the insulin pathway in RpL10a-overexpressed flies.
2. To study the correlation between RpL10a and InR by *in silico* binding and *in vitro* binding and investigate their binding effects on CHO-S cells' insulin pathway.
3. To characterize extra-the ribosomal function of RpL10a that acts as insulin-mimetic in both healthy and insulin-resistant conditions.

CHAPTER 3

MATERIALS AND METHODS

I. Materials

1. Plasmid vector

pGEM[®]-T Easy Vector was purchased from Promega (Madison, WI, USA) and pGEX-4T-1 Vector was purchased from GE Healthcare (Chicago, IL, USA).

2. Bacterial strains

Escherichia coli BL21 (DE3) and Top10 strain were provided from Chotigeat's lab.

3. Chemicals

Chemicals and solvents (analytical grade) were purchased from Amersham, Biosciences; Fluka, Switzerland; Life Technologies, USA; Sigma, USA; PIERCE, USA; Roche, Germany; BIO-RAD, USA; Clontech, USA.

4. Primers

The oligo primer for qPCR in *Drosophila melanogaster* and for cloning into pGEX-4T-1 expression vector was synthesized from Sigma (Germany). The oligo primer for qPCR in IRCs was synthesized from Wardmedic (Singapore), as shown in Table 1.

Table 1. Primer list

Primer name	Primer sequences (5'→ 3')
CHOInR:F (qPCR)	CGAGTCGTCCAGTGAATGCT
CHOInR:R (qPCR)	CACATTCCCCACCTCGTCAA
β-actin:F (qPCR)	GACTCAACACGGGGAAAC
β-actin:R (qPCR)	ATGAAGTGYGACGTGGACATC
DmShc:F (qPCR)	TCACAGCGGAGGTGTGGTTCCA
DmShc:R (qPCR)	CGTGTGCCCAGTGGTAGTTGAT
CHOInR-FnIII:F	TTAGTCGACTGCACCTGTACCCCGGAGAG
CHOInR-FnIII:R	CATGCGGCCGCTCAGACAGAAGGGTTAGTGGCATC
CHOHk1:F (qPCR)	GGAGTGGATGGGACGCTCTA
CHOHk1:R (qPCR)	CTTGCCACTGCCATCTTCAG
CHOG6pc3:F (qPCR)	TCTTCTCAGGTGGCATCTCG
CHOG6pc3:R (qPCR)	ACCTGGTGAGGGAAATGTGC

II. Methods

Part I: The effect of RpL10a on *Drosophila* eyes

1. *GMR-GAL4; UAS-RpL10a* flies

RpL10a-overexpressed flies were provided from the previous publication (Wonglapsuwan et al., 2011). Briefly, the *GMR-GAL4* was used to overexpress the RpL10a in the eye. First, the *GMR-GAL4/+* flies were crossed to *CyO; TM2/T (2; 3) ap^{xa}*. Then, *GMR-GAL4/CyO; +/TM2* was then crossed to the *+/CyO; UAS-RpL10a*. The males and virgin females of *GMR-GAL4/CyO; UAS-RpL10a/TM2* flies were mated to produce the *GMR-GAL4/+; UAS-RpL10a* flies. The *GMR-GAL4/+* flies were used as a control group.

2. Immunohistochemistry of Akt and dFOXO phosphorylation in the eyes of RpL10a-overexpressed flies

The eyes of *GMR-GAL4/+; UAS-RpL10a* flies and control *GMR-GAL4/+* flies were dissected in phosphate-buffered saline (PBS) (137 mM NaCl, 2.7 mM KCl, 8 mM Na₂HPO₄ and 1.46 mM KH₂PO₄, pH 7.4) and fixed in a fixative buffer (300 µl Graces medium, 100 µl of 16% formaldehyde and 200 µl heptane) at room temperature for 20 min. The fixed ommatidia were then washed three times with PBST (PBS, 0.5% tween 20) before blocking in PBAF (PBS, 0.5% bovine serum albumin and 5% fetal calf serum) for 1 h. To detect the phosphorylation level of the insulin signaling mediators ,Akt and dFOXO proteins, the ommatidia were incubated for 2 h at 4°C in primary antibody, including 1:250 dilution of Rabbit polyclonal anti-p-Akt (CST, Massachusetts, USA) and 1:250 dilution of anti-p-FOXO antibodies (CST, Massachusetts, USA). Then, the ommatidia were washed 4 times with PBST before blocking again with PBAF. After 1 h of blocking, the ommatidia were incubated with 1:500 dilution Goat anti-rabbit IgG conjugated with rhodamine (Santa Cruz, CA) for 1 h at room temperature. And then, the ommatidia were washed 4 times with PBST within 2 h before mounting in mounting media with DAPI to label the nuclei (Vector Labs, Burlingame, CA). The signal of the phosphorylation level was observed on an Olympus FV10i confocal microscope.

3. Semi-Quantitation of Akt and dFOXO phosphorylation in RpL10a-overexpressed flies by western blot analysis

Two hundred of the eyes of *GMR-GAL4/+; UAS-RpL10a* and *GMR-GAL4/+* were dissected in 50 µl lysis buffer (187.5 mM Tris-HCl, 6% W/V SDS, 1mM EDTA and 1mM PMSF). Then, the eyes sample was crushed to extract the proteins. The protein solution was separated by centrifugation at 10,000 ×g for 20 min under 4°C. The concentration of the protein solution was quantified by Lowry's method before use. Then, 80 µg proteins of the RpL10a overexpressed, and control *GMR-GAL4/+* flies were separated on 12% SDS PAGE gel and transferred to the nitrocellulose membranes with current 2mA/cm² for 4 h. The transferred membranes were washed with Tris-

Buffered Saline (TBS) (25 mM Tris-HCl, 2.5 mM KCl, and 140 mM NaCl) for 5 min at room temperature before blocking in TBST (TBS and 0.1% Tween 20) with 5% W/V of BSA for 2 h at room temperature. Then, the blocked membranes were then washed 3 times with TBST before probing with the primary antibody. the membranes were incubated with 1:1,000 dilution of a rabbit polyclonal anti-p-Akt and rabbit polyclonal anti-p-FOXO (CST, Massachusetts, USA) overnight under 4°C. After primary antibody incubation, the membranes were then washed 3 times with TBST and followed by incubating with 1:5,000 dilution of goat-anti-rabbit-alkaline phosphatase (Promega, Wisconsin, USA) for 1 h at room temperature. After secondary antibody incubation, the membranes were washed again 3 times with TBST and equilibrated with alkaline phosphatase buffer (100 mM NaCl, 50 mM MgCl₂ and 100 mM Tris-HCl pH 9.5) for 5 min at room temperature. The color was then developed by the NBT-BCIP (Nitro blue tetrazolium chloride/5-Bromo-4-chloro-3-indolyl phosphate, toluidine salt) (Roche, Germany) alkaline phosphatase buffer. Until the positive band was detected, then the reaction was stopped by 1% v/v acetic acid.

4. *Shc* expression in the eyes of RpL10a-overexpressed flies

4.1. RNA isolation

The eyes of *GMR-GAL4/+; UAS-RpL10a* flies and *GMR-GAL4/+* flies were dissected, and the total RNA of these eyes was isolated with TRIzol[®] Reagent (GIBCO BRL, USA). First, the eyes were homogenized in the TRIzol[®] Reagent. Then, chloroform was added to the homogenous and mixed well. The aqueous phase of the eyes homogenous was separated by centrifugation at 12,000 ×g for 15 min under 4°C and transferred to the new tube. The isopropyl alcohol was added to the aqueous phase tube to precipitate RNA and incubated at -80°C for 30 min before centrifugation at 12,000 ×g for 10 min under 4°C. The RNA pellet was cleaned with 75% ethanol, followed by centrifugation at 7,500 ×g for 5 min under 4°C. Then, the RNA pellet was dried before resuspension in RNase free water.

4.2. cDNA synthesis

Two micrograms of RNA were synthesized to cDNA using AMV Reverse Transcriptase (Promega, Wisconsin, USA). First, The RNA was incubated with random primer at 70°C for 5 min before placing it on ice immediately for 5 min to denaturation of RNA. Then, the other reagent was added to the denatured RNA tube, as shown in Table 2. Then, the RNA and reverse transcription reagent mix in this tube was synthesized to cDNA by incubating at 48°C for 2 h. The cDNA quality was checked by detecting the beta-actin (β -actin) housekeeping gene with PCR.

Table 2. Composition of the cDNA synthesis reaction

Reagent	volume per reaction (μ l)
Random primer (100 ng/ μ l)	2.00
dNTP Mix (10mM)	1.25
Reverse Transcription 10 \times Buffer	1.25
AMV Reverse Transcriptase (10 unit/ μ l)	1.00
RNase free water	To 12.5
Total volume	12.50

4.3. Amplification and purification of *Shc* gene for creating a standard curve in real-time PCR

One hundred nanogram of cDNA template was amplified using Taq DNA polymerase from Invitrogen, Life Technologies (USA) and a primer specific to *Shc* (Table 1). The reagents and thermal cycling for amplifying are shown in Tables 3 and 4, respectively. Then, The PCR product was detected via 1.5% agarose gel electrophoresis. After that, the PCR product was purified using NucleoSpin[®] Gel and PCR Clean-up (Takara, USA). The target DNA fragment was cut from the agarose gel and placed in 1.5 ml microcentrifuge tube. Then, 200 μ l of Buffer NTI was added into the DNA fragment tube to solubilize the gel slice. DNA fragment tube was incubated at 50°C for 5–10 min to dissolve the gel slice. After completely dissolve, the DNA

solution was transferred to the NucleoSpin® Gel and PCR Clean-up Column that was placed in the collection tube to bind the DNA fragment with the column. The DNA fragment was separated from the solution by centrifugation at 11,000 ×g (11,100 rpm) for 30 sec. The washing step was performed 2 times by adding 700 µl of Buffer NT3 to the column and spinning at 11,000 ×g (11,100 rpm) for 30 sec to wash the membrane. After that, the column was spun again to remove Buffer NT3 and dry the membrane completely. The column was placed into the new microcentrifuge tube, and 20 µl deionized water was added to the column. And finally, the column was incubated at room temperature for 1 min and spun to elute DNA.

Table 3. Composition of PCR reaction

Reagent	volume per reaction (µl)
cDNA template (100 ng/µl)	1.0
10× PCR buffer	2.5
25 mM MgCl ₂	2.5
<i>DmShc</i> :F primer (20 µM)	2.5
<i>DmShc</i> :R primer (20 µM)	2.5
10 mM dNTP Mix	1.0
Taq DNA polymerase (5 unit/µl)	1.0
Deionized water	12.0
Total volume	25.0

Table 4. Thermal cycling of PCR

Cycles	Temperature	Time
1	94°C	5 min
30	94°C	30 sec
	56°C	30 sec
	72°C	30 sec
1	72°C	10 min
1	4°C	∞

4.4. Real-Time PCR

Two hundred nanogram of cDNA was used as the template to determine the expression level of *Shc* gene. The Real-Time PCR was performed using 2× FastStart Universal SYBR Green Master (Rox) (Roch, Mannheim, Germany) in 12.5 µl of Real-Time PCR reaction. The cycle and fluorescence detection were performed by using the Mx3000P® qPCR System (Stratagene, La Jolla, CA, USA) as shown in Table 5 and Table 6. The primer specific to *Shc* gene, as shown in Table 1. The β -*actin* was used as an internal standard. All samples were performed in triplicate. The 10-fold serial dilutions of purified *Shc* gene in the range of 10^7 to 10^3 copies were prepared to create the standard curve. The copy number of each dilution was calculated by using the formula: a number of copies = [amount of DNA (ng) \times 6.022×10^{23}] / [length of DNA (bp) \times $1 \times 10^9 \times$ mass of DNA bp]. The ratio of *Shc* copy number to β -*actin* copy number in each sample was computed, and these ratios were compared between *GMR-GAL4/+*, and *GMR-GAL4/+; UAS-RpL10a* flies.

Table 5. Composition of Real-Time PCR reaction

Reagent	volume per reaction (μ l)
2 \times FastStart Universal SYBR Green Master (Rox)	6.25
<i>DmShc</i> :F Primer (20 μ M)	0.125 (Final Conc. 200 nM)
<i>DmShc</i> :R Primer (20 μ M)	0.125 (Final Conc. 200 nM)
Deionized water	To 12.5
Total volume	12.50

Table 6. Thermal cycling of Real-Time PCR

Cycles	Temperature	Time
1	95°C	5 min
40	94°C	30 sec
	59°C	30 sec
	72°C	30 sec

5. Determination of carbohydrate content in RpL10a–overexpressed flies

The carbohydrate content was determined as described previously with modification (Van Handel, 1985a).

5.1. Calibration

The sugar and glycogen content was calculated directly from the glucose standard curve. The standard curve was prepared using 1 mg/ml in 25% ethanol of glucose stock. The stock was diluted to a concentration of 12.5, 25, 50, 100, and 200 μ g/ml. Each concentration of glucose was prepared in triplicates in a final volume of 0.2 ml. Then, the anthrone reagent (530 ml of anthrone reagent: 150 ml of DI water, 380 ml of concentrate H₂SO₄, and 750 mg of anthrone) was added into each standard tube to a final volume of 5 ml. The colorimetric reaction was initiated by heating the glucose-anthrone mixture tubes at 90–92°C for 17 min. The glucose-anthrone mixture

tubes were then cooled, mixed, and measured the optical density at 625 nm. When the optical density of the standard tube is higher than 1, it should be diluted with the anthrone reagent, mixed, and measured the optical density at 625 nm until the standard tube's optical density is lower than 1.

The trehalose standard curve was prepared for the determination of the trehalose content in the flies. Similarly, the trehalose standard curve was prepared using 1 mg/ml in 25% ethanol of trehalose. The trehalose stock was diluted to a concentration of 12.5, 25, 50, 100, and 200 µg/ml. Each concentration of trehalose was prepared in triplicates in a final volume of 0.2 ml, and the colorimetric reaction was performed as above.

5.2. Determination of sugar

The *GMR-GAL4/+; UAS-RpL10a* flies and the control *GMR-GAL4/+* flies were aged for 2 days old before collecting to determine the sugar content. Ten flies were placed in 200 µl of 2% sodium sulfate solution and crushed with a micro pestle, and 1 ml of methanol was added into the homogenous, then mixed well and spun at 12,000 ×g for 1 min. The supernatant containing sugar was transferred to the glass tube. The distilled water of 200 µl was added into the pellet tube and mixed well to collect the residual sugar fraction. Then, 1 ml of methanol was added into the pellet tube. The pellet tube was mixed well and spun at 12,000 ×g for 1 min. Then, the second sugar fraction was combined with the first sugar fraction tube and evaporated at 90–92°C to 1 ml volume. The sugar concentration was determined by transferring 0.2 ml of sugar sample (20% of total sugar) to a new glass tube and by adding the anthrone reagent into the sugar sample tube to a final volume of 5 ml. The sugar-anthrone mixture tubes were mixed and heated at 92°C for 17 min. Then, the sugar-anthrone mixture tubes were cooled, mixed, and measured the optical density at 625 nm. The sugar content could be calculated directly from the standard curve of glucose. The experiment was performed in triplicate.

5.3. Determination of trehalose

First, The sugar was separated from ten flies, as described in method 5.2. After evaporation, 0.2 ml of evaporated sugar sample was transferred to a new glass tube. Trehalose was determined so the other type of sugar in the sample should be destroyed. 0.05 ml of 1N HCl was added into the sugar sample tube and incubated at 90°C for 7 min to hydrolyze sucrose into glucose and fructose form but leaves trehalose intact. To destroy the anthrone reactivity of glucose and fructose but leaves trehalose intact, 0.15 ml of 1N NaOH was added into the HCl hydrolyzed-sugar sample tube and incubated at 90°C for 7 min. Then, the colorimetric reaction was performed as above.

5.4. Determination of glycogen

After transfer, the residual sugar fraction in the pellet tube, the pellet tube containing glycogen, was dissolved in 1 ml of distilled water and mixed well. Then, 0.2 ml of glycogen solution was transferred to 3 new glass tubes, and the colorimetric reaction was performed as above.

6. Determination of lipid content in RpL10a-overexpressed flies

Lipid content was examined as described previously (Van Handel, 1985b). Mix sex and the virgin female of the *GMR-GAL4/+; UAS-RpL10a* flies and the control *GMR-GAL4/+* flies were aged for 2 days before use. Ten flies were placed in a microcentrifuge tube containing 0.5 ml of Chloroform: methanol (1:1) solution. Then, the sample was crushed with a micro pestle and mixed vigorously. Each group performed in triplicates. The homogeneous solution was carefully transferred to a new tube. This sample solution was evaporated at 92°C for 5–7 min. Then, 0.2 ml of sulfuric acid was added to the sample and heated at 92°C for 10 min. After cooling, vanillin reagent was added into the sample tube to a final volume of 5 ml, mixed, and determined the optical density at 525 nm. The lipid content was calculated directly from the lipid standard curve. The standard curve was created using 1 mg/ml of commercial vegetable

oil in chloroform. The standard lipid assay was performed in three sets of 50, 100, 200, and 400 μ l of 1mg/ml of the vegetable oil with a final volume of 0.5 ml.

7. Statistical analysis

Three separate samples were used for all experiments. The statistical analysis was performed on SPSS version 15.0 software (SPSS Inc., Chicago, IL, USA). The data are presented as the mean \pm SD. The results between groups were compared statistically using the independent-samples *t*-test with a significance level of $p < 0.05$.

Part II: RpL10a and InR interaction and the effect after binding

1. *In silico* binding

The sequence of RpL10a protein from *F. merguensis* was downloaded from the NCBI database with accession number ACU52718. The predicted 3D structure of RpL10a protein was modeled on Swiss-Model server (<https://swissmodel.expasy.org/>) and the three-dimensional structural accuracy of the predicted model was validated through RAMPAGE server (<http://mordred.bioc.cam.ac.uk/~rapper/rampage.php>) (Lovell et al., 2003) before docking. At the same time, 3D structure of human InR protein was downloaded from the RCSB Protein Data Bank (PDB). Then, the three-dimensional structure of RpL10a and InR were elucidated through the PyMol program. The RpL10a protein was used as a ligand, and the human InR was used as a receptor. The binding model with the largest cluster and lowest energy scores was selected. The scores of the interaction, including balanced, electrostatic-favored, hydrophobic-favored and van der Waals interactions, were determined by PIPER program on the ClusPro 2.0 server (<https://cluspro.bu.edu/login.php>). Then, the selected binding model was elucidated using the PyMol program. The insulin model was retrieved from the PDB entry 3e7y produced from X-ray diffraction with a resolution of 1.6 Å to compare the pattern of binding to InR protein between RpL10a and insulin. The protein-protein docking of insulin and InR was performed and elucidated through the PIPER program and PyMol program, respectively.

2. *In vitro* binding

2.1. Cloning and expression of the recombinant GST-InR-FnIII (InR binding site)

2.1.1. CHO's RNA isolation and cDNA synthesis

Chinese hamster ovary (CHO-S) cells (Gibco, USA) were maintained in Dulbecco's Modified Eagle Medium (DMEM) (Gibco, USA), supplemented with 10% heat-inactivated fetal bovine serum (Gibco, USA) and 1% of antibiotic–antimycotic (Gibco, USA) for 18 h at 37°C under 5% CO₂. The cells were grown until 80% confluence before harvesting to isolate total RNA. Total RNA was extracted using TRIzol[®] as described in method 4.1 (in part I). Two micrograms of total RNA were synthesized to cDNA by using AMV reverse transcriptase. Briefly, the RNA was incubated with 200 ng random primer at 70°C for 5 min before placing it on ice immediately for 5 min to denature the RNA. Then, the reverse transcription reaction mix was added to the 12.5 µl denatured RNA tube, as shown in Table 2. After that, the reverse transcription reaction mix synthesized cDNA by incubating at 48°C for 2 h. The quality of cDNAs synthesis was checked by amplification β-actin cDNA before using the cDNAs for amplification the target InR binding site.

2.1.2. Amplification and purification of the *InR-FnIII* gene

The target binding site (*InR* FnIII domain) was amplified from cDNA of CHO-S cell and ligated into pGEM[®]-T Easy cloning vector. One hundred ng of cDNA template was amplified using Taq DNA polymerase and *CHOInR-FnIII* forward primer carrying a *SalI* restriction site and *CHOInR-FnIII* reverse primer with *NotI* restriction site (Table 1). The reagents and thermal cycling for amplifying are shown in table 7 and 8, respectively. Then the PCR product was purified as described in method 4.3 (In part I).

Table 7. Composition of PCR reaction

Reagent	volume per reaction (μ l)
cDNA template (100 ng/ μ l)	1.0
10 \times PCR buffer	2.5
25 mM MgCl ₂	1.5
<i>CHOInR-FnIII</i> :F primer (20 μ M)	0.5
<i>CHOInR-FnIII</i> :R primer (20 μ M)	0.5
10 mM dNTP Mix	0.5
Taq DNA polymerase (5 unit/ μ l)	0.25
Deionized water	18.25
Total volume	25.0

Table 8. Thermal cycling of PCR

Cycles	Temperature	Time
1	94°C	3 min
35	94°C	30 sec
	55°C	30 sec
	72°C	30 sec
1	72°C	5 min
1	4°C	∞

2.1.3. Ligation of *InR-FnIII* to the pGEM[®]-T Easy cloning vector and transformation

The purified *InR-FnIII* gene was ligated to the pGEM[®]-T Easy vector. The ligation reaction including 10 ng of *InR-FnIII* gene, 30 ng of pGEM[®]-T Easy vector, 1 μ l of 10 \times ligase Buffer, 2 unit of T4 DNA Ligase (Promega, Madison, USA), and deionized water was added to the final of 10 μ l. The ligation reaction was incubated overnight at 4°C.

After that, 5 μ l of the ligation reaction was transformed into *E. coli* Top 10 F' competent cells. Briefly, a 100 μ l volume of the competent cells were thawed on ice before mixing with 5 μ l of the ligation reaction. Then, the transformation mixture was placed on ice for 30 min and incubated at 42°C for 90 sec and immediately place on ice for 5 min. Then, 900 μ l of LB broth was added to the transformed cells and stirred, 180 rpm at 37°C for 45 min. Finally, 200 μ l of transformed culture was spread on an LB plate containing 80 μ g/ml of ampicillin and incubated at 37°C for 16–18 h. After that, the single colonies of transformed cells were randomly collected and cultured into 1 ml of LB broth containing 80 μ g/ml ampicillin and cultured overnight at 37°C with shaking at 180 rpm before detecting the pGEM-*InR-FnIII*.

2.1.4. Detection of the pGEM-*InR-FnIII* from the positive clone

The bacterial culture of *E. coli* Top 10 F' in 1 ml of LB broth (from 2.1.3) was extracted as described in a previous study (Birnboim and Doly, 1979). The bacterial pellet was harvested by centrifugation at 12,000 \times g for 5 min at room temperature. Then, the pellet was collected and dissolved in 100 μ l of Solution I (50mM Glucose, 25 mM Tris-HCl pH8.0, 10 mM EDTA, 1 μ g/ml RNase A, stored at 4°C). The dissolved pellet tubes were placed at room temperature before adding 200 μ l of Solution II (0.2 N NaOH, 1% SDS) for bacterial lysis. The bacterial lysate was mixed and placed on ice for 5 min. Then, 300 μ l of Solution III (29.45% w/v of potassium acetate, 11.8% v/v of glacial acetic acid) was added and incubated on ice for 30 min. The bacterial lysate was precipitated by centrifugation at 12,000 \times g for 15 min under 4°C and the supernatant was carefully transferred to a new microcentrifuge tube. 1 ml of isopropanol was added into the supernatant and incubated at -80°C for 10 min before centrifugation at 12,000 \times g for 15 min under 4°C to precipitate the plasmid DNA. The plasmid DNA was washed with 70% ethanol and spun at 12,000 \times g for 15 min under 4°C. Then, the supernatant was discarded, and the plasmid DNA pellet was dried for 20–30 min. Finally, plasmid DNA was suspended in 20 μ l of deionized water and stored at -20°C. The recombinant plasmid was separated on 1% agarose gel compared with pGEM®-T Easy control plasmid. The recombinant plasmid, larger than the control plasmid, which expected to contain pGEM-*InR-FnIII* was selected to check the

sequence. Besides, the recombinant plasmid, which is expected to contain pGEM-*InR-FnIII* was checked by digestion with *SalI* and *NotI* (Promega) restriction enzymes. The 30 µl reaction of *SalI* and *NotI* digestion consisted of 1µg of plasmid DNA, 3 µl of Restriction Enzyme 10× Buffer D, 15 unit of each restriction enzyme, and deionized water was added to the final of 30 µl. The digestion reaction was incubated overnight at 37°C. Then, the digestion reaction was detected via 1.2% agarose electrophoresis. The clone containing 2 sizes of the nucleotide fragment was then selected for sequencing analysis.

2.1.5. Sub-cloning of the *InR-FnIII* from the pGEM[®]-T Easy cloning vector to the pGEX-4T-1 expression vector

The recombinant pGEM-*InR-FnIII* and the pGEX-4T-1 expression vector were digested using *SalI* and *NotI* restriction enzymes as described in method 2.1.4. The digestion reaction was separated via 1.2% agarose electrophoresis. The digested pGEX-4T-1 and digested *InR-FnIII* were purified as described in method 4.3 (In part I). The purified *InR-FnIII* gene was ligated to the purified pGEX-4T-1 vector at the *SalI* and *NotI* restriction site. The ligation reaction contained 2 ng of CHO *InR-FnIII* gene, 8 ng of pGEX-4T-1 vector, 1 µl of 10× ligase Buffer, 1 unit of T4 DNA Ligase (Promega, Madison, USA), and deionized water was added to the final of 10 µl and the reaction was incubated overnight at 4°C. Then, 5 µl of the ligation reaction was transformed to *E. coli* BL21 (DE3) competent cells as described in method 2.1.3.

2.1.6. Expression and purification of GST-InR-FnIII protein

A single colony of *E. coli* BL21 (DE3) containing the pGEX-*InR-FnIII* plasmid (from 2.1.5.) was inoculated into 1 ml of LB broth with 100 µg/ml of ampicillin and cultured at 37°C overnight with shaking at 180 rpm. Then, 100 µl of the bacterial culture was inoculated into 10 ml of LB broth with 100 µg/ml ampicillin and cultured at 37°C with shaking at 180 rpm until the optical density (OD) 600 nm was reached 0.5–0.8. The recombinant GST-InR-FnIII protein expression was induced with 0.1 mM

isopropyl-1-thio- β -D-galactosidase (IPTG) to the bacterial culture and incubated at 37°C with shaking at 180 rpm for 4 h. After 4 h of induction, the cells were collected by centrifugation at 7,700 \times g for 10 min at 4°C and suspended in 0.5 ml of ice-cool phosphate-buffered saline (PBS, 140 mM NaCl, 2.7 mM KCl, 10 mM Na₂HPO₄, 1.8 mM KH₂PO₄, pH 7.3). The cell suspension was sonicated on ice with a sonicator and using a 200–300 W microtip. The sonication condition was performed in 6 cycles of 10 sec sonicate and 10 sec cooling period. Then, the cell suspension was centrifuged at 12,000 \times g for 10 min at 4°C and collected as a fraction of soluble protein. Then, the soluble GST-InR-FnIII protein was purified by incubating with Glutathione Sepharose[®] 4 Fast Flow (GE Healthcare) in 1.5 ml microcentrifuge tube overnight at 4°C. The sample tube was spun at 500 \times g for 5 min, and the unbound protein was discarded. The sample tube was then washed five times by ice-cool PBS to eliminate the unbound protein. Then, the GST-InR-FnIII protein was eluted by elution buffer (50 mM Tris-HCl, 10 mM reduced glutathione, pH 8.0). The purity of GST-InR-FnIII protein was finally checked via 12% SDS-PAGE.

2.1.7. Expression and purification of histidine tag-RpL10a (His-RpL10a) protein

The recombinant His-RpL10a was obtained from the previous study (Wonglapsuwan et al., 2010). An *E. coli* BL 21 (DE3) single colony including the *pET-RpL10a* plasmid was inoculated in 30 ml of LB broth with 30 μ g/ml of kanamycin and cultured overnight at 37°C with shaking at 180 rpm. Then, the bacterial culture was inoculated into 300 ml of LB broth with 30 μ g/ml of kanamycin and incubated at 28°C with shaking at 180 rpm until the OD at 600 nm reached 0.5–0.7. Then, the expression of the recombinant His-RpL10a protein was induced by 1.0 mM IPTG and the cells were cultured at 18°C with shaking at 120 rpm for 16–18 h. The bacterial pellet was harvested by centrifugation at 4,000 \times g for 20 min at 4°C, and the cell pellet was suspended in 10 ml of lysis buffer (50 mM NaH₂PO₄, 300 mM NaCl, 10 mM Tris-HCl, pH 8.0). Then, 1 mg/ml of lysozyme was added into the cell suspension and incubated at room temperature for 30 min before sonication. The cell suspension was sonicated

on ice using a sonicator with 200–300 W microtip. The sonication condition was performed in 14 cycles of 10 sec sonicate and 20 sec cooling period within 7 min. The supernatant was harvested by centrifugation at 10,000 ×g for 20 min at 4°C and filtered through a 0.2-µm filter before applying to a His-Trap FF column (GE Healthcare Bio-Sciences, Sweden), and purified using the ÄKTA prime chromatography system following the manufacturer's instructions (GE Healthcare Bio-Sciences). The purity of the His-RpL10a protein was determined by 1.2% of SDS-PAGE. Finally, the purified His-RpL10a protein was dialyzed against the dialysis buffer (350 mM NaCl, 50 mM NaH₂PO₄, pH 7.4) to eliminate imidazole.

2.1.8. Western blot analysis of the recombinant protein His-RpL10a and GST-InR-FnIII proteins

The purified His-RpL10a protein (from method 2.1.7) was confirmed by western blot analysis. The 15 µg of purified His-RpL10a was separated on 12% SDS-PAGE gel and transferred to a nitrocellulose membrane with current 2mA/cm² for 2 h. The transferred membrane was washed with PBS for 5 min before blocking in PBST (PBS and 0.1% Tween 20) with 5% W/V of skim milk for 4 h at room temperature. The membrane was incubated with 1:3000 dilution of a mouse monoclonal 6X His tag[®] antibody (Abcam, Cambridge, UK) for 2 h at room temperature after blocking. Then, the membranes were cleaned three times with PBST and then incubated with a 1:5000 dilution of rabbit anti-mouse AP (Santa Cruz, CA) antibodies for 2 h at room temperature. The membranes were then washed three times with PBST and equilibrated with alkaline phosphatase buffer for 5 min at room temperature. The color was developed by the NBT-BCIP in alkaline phosphatase buffer. Until the positive band was detected, the reaction was stopped by 1% v/v acetic acid.

The purified GST-InR-FnIII protein (from method 2.1.6) was also confirmed by western blot as previously described above while it was detected with a goat polyclonal GST antibody (GE Healthcare Bio-Sciences, Sweden) and rabbit anti-goat AP (Invitrogen, Carlsbad, CA, USA) respectively.

2.2. GST pull-down

The interaction between RpL10a and InR was performed by the GST pull-down assay. The GST-InR-FnIII protein of 10 μ g in 200 μ l of binding buffer (350 mM NaCl, 50 mM NaH₂PO₄, pH 7.4) was incubated with 20 μ l of a 50% slurry of Glutathione Sepharose 4 Fast Flow overnight at 4°C with shaking. The mixture of protein was spun at 500 \times g for 5 min, and the supernatant was discarded to remove the excess GST-InR-FnIII protein. The pellet of Glutathione Sepharose bead was then washed four times with binding buffer to remove the unbound protein. Then, 10 μ g of the recombinant His-RpL10a protein in 200 μ l of the binding buffer were added to the pre-incubated GST-InR-FnIII with Glutathione Sepharose 4 Fast Flow beads and then incubated at 4°C overnight with shaking. The mixture was spun at 500 \times g for 5 min, the supernatant was removed, and the mixture was washed four times with binding buffer. Then, SDS sample loading dye of 20 μ l was added into the protein-protein complex and boiled for 5 min before spinning 10 min at 13,000 \times g to breakdown the Glutathione Sepharose beads. Then, the protein-protein interaction complex solution was separated on a 12% SDS-PAGE gel and transferred to the nitrocellulose membranes. The transferred membranes were blocked with PBST containing 5% w/v BSA for 4 h before probing with 1:3000 of A mouse monoclonal RpL10a antibody (Abcam, Cambridge, UK) and a goat polyclonal GST antibody (GE Healthcare Bio-Sciences, Sweden) for 2 h to detect RpL10a and GST-InR-FnIII, respectively. The membranes were then cleaned three times with PBST and incubated with a 1:5000 dilution of rabbit anti-mouse AP (Santa Cruz, CA) and rabbit anti-goat AP (Invitrogen, Carlsbad, CA, USA) antibodies for 2 h. Then, the membranes were washed with PBST, and the color was developed by the NBT-BCIP in alkaline phosphatase buffer until the positive band was detected. The reaction was stopped by 1% v/v acetic acid. GST incubated with His-RpL10a and GST-InR-FnIII was used as a control.

2.3. Immunofluorescence assay

CHO-S cells were cultured on the glass coverslips in a 6-well plate which contains the DMEM medium for 18 h at 37°C with 5% CO₂. After 18 h of culture, the medium was changed to the new DMEM with 3 µg/ml His-RpL10a, and cells were then incubated at 37°C for 6 h with 5% CO₂. The incubated cells were then cleaned three times with PBS before fixing with cool methanol for 5 min at room temperature and then carefully washed three times with PBS before blocking the fixed cells with blocking buffer (PBS containing 0.1% Triton X-100, 1% BSA, and 22.52 mg/ml glycine) for 30 min and were then incubated with a 1:1000 dilution of rabbit polyclonal anti-insulin R β antibody (Santa Cruz, CA, USA) and mouse monoclonal anti-6X His tag[®] antibody at room temperature for 3 h. Then, the primary antibody was discarded, and the cells were cleaned three times with PBS. Cells were then incubated with 1:5000 dilution of goat anti-rabbit IgG conjugated with rhodamine and goat anti-mouse IgG conjugated with FITC (Santa Cruz, CA, USA) in the dark for 1 h. After that, the cells were then washed with PBS before staining with DAPI solution (Thermo Fisher Scientific, MA, USA) and incubate for 5 min in the dark. Then the cells was washed with PBS before mounting. The signal of RpL10a and InR protein were observed on an Olympus BX51 microscope.

3. The effect of RpL10a and InR binding in CHO-S cells

3.1. RpL10a stimulation in CHO-S cells

CHO-S cells was maintained in DMEM supplemented with 10% heat-inactivated fetal bovine serum and 1% antibiotic–antimycotic for 18 h at 37°C with 5% CO₂. The cells were grown until 80% confluence before seeding 4×10⁵ cells into a 12-well plate and incubating for 18 h at 37°C with 5% CO₂. The cells were changed to the new DMEM containing 0.5 µM of His-RpL10a or 1 µM of insulin and incubate for 24 h. The cells incubated in new DMEM medium was used as a control.

3.2. Determination of Akt phosphorylation level in RpL10a incubated cells

After incubation of the cells with His-RpL10a for 24 h (From 3.1), the incubated cell was harvested for protein extraction. The cells was removed to the new microcentrifuge tube and the remaining medium was separated by centrifugation at $12,000 \times g$ for 1 min under 4°C . Then, the pellet cells were washed 3 times with PBS before dissolving in 50 μl of lysis buffer. The cell solution was homogenized and centrifuged at $10,000 \times g$ for 10 min under 4°C , and then the supernatant contains soluble protein was carefully transferred to the new tube. The protein solution was determined the total protein concentration by Lowry's method, as described in appendix A. After that, 40 μg of proteins from each group were separated on 12% SDS PAGE gel and transferred to thr membranes with the current of $2\text{mA}/\text{cm}^2$ for 2 h. The transferred membranes were blocked in TBST with 5% W/V of BSA at room temperature for 2 h. Then, the blocked membranes were incubated with 1:1,000 dilution of a rabbit polyclonal anti-p-Akt overnight under 4°C . The membranes were then washed 3 times with TBST before incubating with 1:5,000 dilution of goat-anti-rabbit-alkaline phosphatase at room temperature for 1 h. The membranes were then washed 3 times with TBST, and the color was developed as described in method 3 (in part I).

3.3. Glucose consumption determination

CHO-S cells were incubated as described in method 3.1, with various concentrations of His-RpL10a, and 0.5 μM of insulin was used as a positive control. During incubating the cells with His-RpL10a, the culture medium was collected every hour from 6–12 h of His-RpL10a incubation time. The glucose levels in the culture medium were calculated at the indicated time points by using the anthrone colorimetric assay as described above (Van Handel, 1985a). The collected medium was centrifuged at 13,000 rpm for 10 min to eliminate the remaining cells, and 2 μl of the medium were carefully transferred to the glass tube containing 198 μl distilled water to dilute into 1:100 dilution. The diluted medium was then mixed with 1 ml anthrone reagent and heated for 17 min at $90\text{--}92^{\circ}\text{C}$. Then, cool the sample tubes before measuring intensity of the green color at OD 625 nm. The glucose content was calculated from the glucose

standard curve. The standard glucose was prepared from 1 mg/ml glucose in 25% ethanol. The glucose stock was diluted to 25, 50, 100, and 200 $\mu\text{g/ml}$ and Two hundred microliters of each standard glucose dilution were mixed with anthrone reagent and analyzed as described above.

3.4. Glucose uptake assay

3.4.1. 2-DG6P standard solution preparation

The stock 2-DG6P standard solution was diluted to 0.1 mM (100 pmole/ μl) by adding 990 μl of Assay Buffer to 10 μl of 10mM the 2-DG6P solution. Then, 0.1 mM 2-DG6P solution was diluted to 0.01 mM working 2-DG6P solution by adding 450 μl of Assay Buffer to 5 μl of DG6P solution before use. The working solution including 0 (blank), 20, 40, 60, 80, and 100 pmole/well of 2-DG6P standard were added to 96-well plate, and the Assay Buffer was added into each standard well to the final volume of 50 μl . The standard was prepared in triplicate.

3.4.2. Sample preparation

CHO-S cells were grown as described in method 3.1 before seeding 3,000 cells into each well of the 96-well plate. The seeded cells were grown overnight at 37°C with 5% CO₂. Then, the cells were washed 2 times with PBS before starving in 100 μl of serum-free medium overnight. After that, the starved cells were washed 3 times with PBS before glucose starving for 40 min in 100 μl of Krebs-Ringer-Phosphate-HEPES (KRPH) buffer (20 mM HEPES, 5 mM KH₂PO₄, 1 mM MgSO₄, 1 mM CaCl₂, 136 mM NaCl, and 4.7 mM KCl, pH 7.4) containing 2% BSA. Then, the glucose starved cells were stimulated for 20 min with 0.5 μM His-RpL10a and with or without 1 μM insulin. After stimulation, the stimulated cells were mixed with 10 μl of 10 mM 2-DG and incubated for 20 min. And then, the cells were washed 3 times with PBS before lysis cells with 80 μl of Extraction Buffer by freeze/thaw in liquid nitrogen and then heat at 85°C for 40 min. Then the cells lysate was cooled on ice for 5 min before neutralizing

cells with 10 μ l of Neutralization Buffer. The neutralized cells were then spun at 13,000 \times g to precipitate the insoluble substance, and 5 μ l of soluble lysate was carefully transferred to a 96-well plate. The transferred soluble lysate was diluted to 10-fold by adding 45 μ l of Assay Buffer to each well of soluble lysate. All samples were prepared in triplicate.

3.4.3. Assay reaction

A Reaction Mix A (8 μ l of Assay Buffer and 2 μ l of Enzyme Mix) was added into each well of sample and standard and mixed by pipetting to generate the NADPH in sample and standard well. The reaction was protected from light and incubated at 37°C for 1 h, Extraction Buffer of 90 μ l was added into each well and sealed the well plate before incubating at 90°C for 40 min to degrade the NADP. And the cells were then cooled on ice for 5 min followed by adding 12 μ l of Neutralization Buffer. After that, the recycling reaction amplification was performed by adding 38 μ l of Reaction Mix B (20 μ l of Glutathione Reductase, 16 μ l of Substrate-DTNB, and 2 μ l of Recycling Mix) to each well, and the cells plate was mixed well by pipetting. Finally, the cell plate was measured the absorbance by a microplate reader (Thermo Scientific, Waltham, MA, USA) at 412 nm every 5 min until the absorbance value of 100 pmole standard reaches OD. 1.5–2.0.

3.4.4. Calculation

The absorbance value of the blank (0 pmole of 2-DG6P standard tube) was used as a background for this assay. The background value was subtracted from all absorbance values of sample tubes and standard tubes. After background subtraction, the subtracted value of standard generated a standard curve. Also the absorbance of sample was subtracted with the negative control, then corrected absorbance was determined the amount of accumulated 2-DG6P from the standard curve. The obtained amount of 2-DG6P is directly proportional to 2-DG.

Part III: The effect of RpL10a in insulin resistance cells

1. Insulin resistance cells induction

CHO-S cells were maintained 3.5×10^5 cells/well in DMEM medium (25 mM glucose) supplemented with 10% heat-inactivated fetal bovine serum and 1% antibiotic–antimycotic for 18 h at 37°C with 5% CO₂. The IRCs were induced under three induction conditions, including high glucose (50 mM), high insulin (100 nM), and high glucose plus insulin (250 mM glucose and 100 nM insulin). Briefly, the seeded cells were changed in fresh serum-free DMEM, which supplemented 25 mM glucose (final glucose concentration 50 mM) for high glucose induction condition, supplemented 100 nM insulin for high insulin induction condition, and supplemented both 100 nM insulin and 25 mM additional glucose for high glucose plus insulin induction condition. The cells in three induction conditions were cultured at 37°C with 5% CO₂ for 24 h. During 24 h of induction, the level of insulin resistance was determined by collecting the culture medium at 3 or 5 times point containing 0, 12, 24, 36, and 48 h of induction to measure the glucose consumption rate.

2. RpL10a stimulation in IRCs for glucose uptake

After 48 h of induction to the insulin resistance condition, The IRCs were incubated with fresh serum-free DMEM which containing 1, 5 or 15 µg/ml of His-RpL10a protein at 37°C with 5% CO₂ for 24 h. The IRCs incubated with 0.5 µM of insulin were used as a control group. During stimulation, the medium was collected to determine the glucose consumption rate. The medium was collected at 0, 12 and 24 h of His-RpL10a stimulation. The glucose levels in the medium were then measured at the indicated time points by using the anthrone colorimetric assay as described in the method 3.3. While, the 24 h stimulated cells were used for real-time PCR, whereas the untreated cells were used as a control.

3. qRT-PCR of glucose metabolism-related gene

The total RNA was isolated from IRCs and 1 µg/ml RpL10a-treated IRCs using TRIzol[®] Reagent as described in method 4.1 (in part I). Two micrograms of total RNA was reverse transcribed into cDNA by using AMV transcriptase as described in method 4.2 (in part I). Then, the Real-time PCR was performed in a 12.5 µl which containing 6.25 µl of 2× FastStart SYBR Green Master Mix (ABI, CA, USA), 300 nM of specific primers, and 10 ng of cDNA template. All samples were analyzed in triplicate. The fold change expressions of the glucose metabolism-related gene were calculated by using the $2^{-\Delta\Delta CT}$ method. The gene expression was normalized with β -actin gene. The primer sequences for qRT-PCR are shown in the Table 1.

CHAPTER 4

RESULTS AND DISCUSSION

Part I: The effect of RpL10a on *Drosophila*

1. RpL10a induced phosphorylation of Akt and dFOXO

The previous study in RpL10a-overexpressed flies revealed that RpL10a could induce the expression of InR both in mRNA and protein level (Figure 8) (Chaichanit et al., 2018). In this study, the downstream pathway of insulin signaling pathway was investigated in RpL10a-overexpressed flies. Usually, several insulin signaling mediators were activated by phosphorylation after InR activation. To investigate the excess RpL10a in RpL10a-overexpressed flies also induced the insulin signaling mediators phosphorylation, the phosphorylation level of Akt and dFOXO proteins which members of mediators in the insulin signaling pathway, were quantified. The eyes cell membrane of RpL10a-overexpressed flies were dissected and detected with phosphorylated-Akt and phosphorylated-FOXO antibodies to observe the phosphorylation level. The results showed the increase of the phosphorylated Akt (Figure 11b) and phosphorylated dFOXO (Figure 12b) in RpL10a-overexpressed flies compared with *GMR-GAL4/+* control flies (Figure 11a, 12a). Besides, the phosphorylation level of Akt and dFOXO proteins in RpL10a-overexpressed flies were also confirmed by western blot analysis. The western blot results showed a higher phosphorylation level of Akt (Figure 11c) and dFOXO (Figure 12c) in RpL10a-overexpressed flies than in control flies. These results suggest that RpL10a could activate the expression of InR and its downstream pathway.

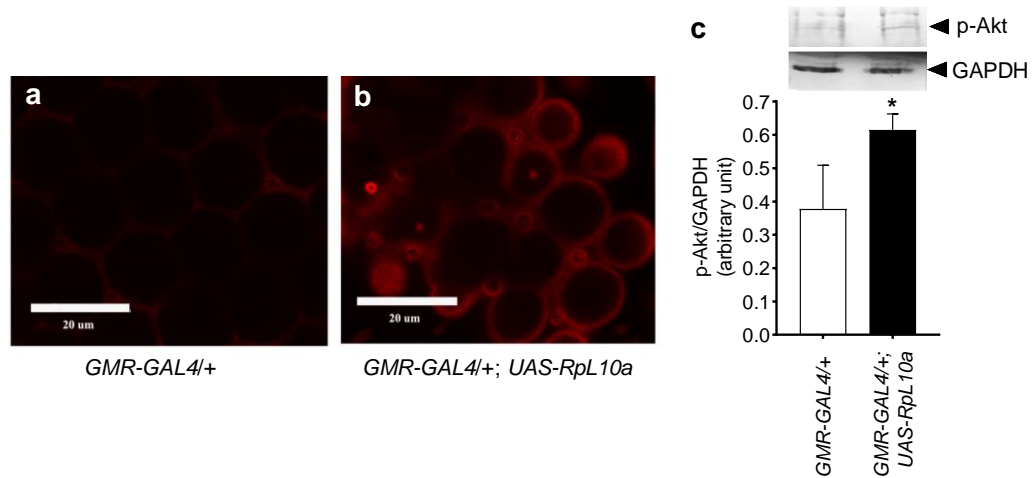


Figure 11. The excess of *RpL10a* increased the phosphorylation of Akt. The eyes of (a) Control *GMR-GAL4/+* and (b) *GMR-Gal4/+; UAS-RpL10a* were stained with an anti-p-FOXO antibody (Red). The scale bars represent 20 μm . (c) The phosphorylation level of p-Akt was detected by western blot analysis and the histogram shows the p-Akt level. The asterisk indicated a significant difference during each group. ($p < 0.05$).

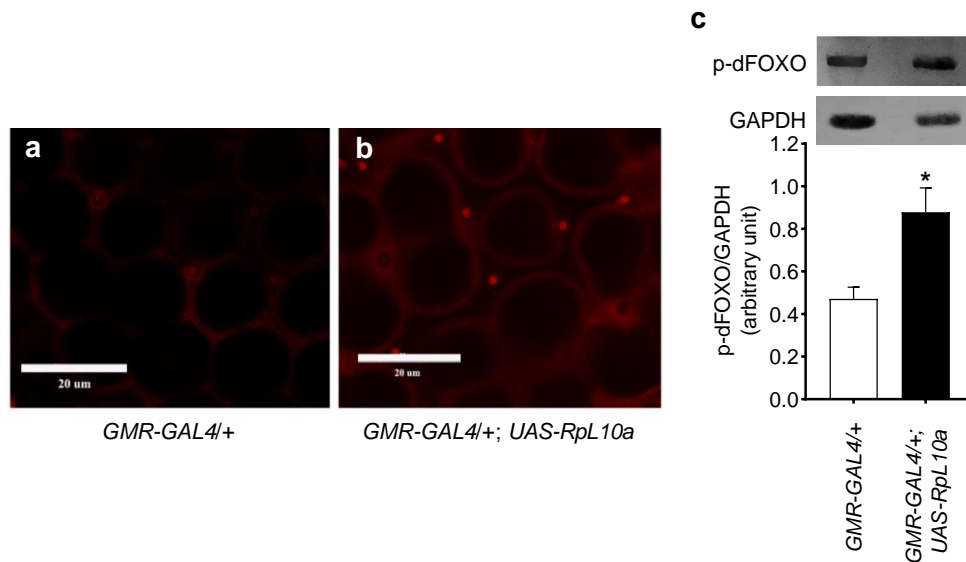


Figure 12. The excess of *RpL10a* increased the phosphorylation of dFOXO. The eyes of (a) Control *GMR-GAL4/+* and (b) *GMR-Gal4/+; UAS-RpL10a* were stained with an anti-p-FOXO antibody (Red). The scale bars represent 20 μm . (c) The phosphorylation level of p-dFOXO was detected by western blot and the histogram shows the p-dFOXO level. The asterisk indicated a significant difference during each group ($p < 0.05$).

2. Overexpression of RpL10a changed the carbohydrate metabolism

The carbohydrate metabolism was compared between normal flies and the RpL10a-overexpressed flies. The sugar, glycogen, and trehalose content showed a significant decrease in RpL10a-overexpressed flies compared with the normal flies (Figure 13). They were indicating that the total sugar and trehalose content was more used by the RpL10a-overexpressed flies (Figure 13a, 13c). RpL10a might induce the expression of InR then the receptor triggered the phosphorylation of insulin signaling mediators such as Akt and dFOXO to control glucose transport into the cell. Also, the phosphorylation of dFOXO promotes cell growth by using sugar to increase the cell number in *Drosophila* (Jünger et al., 2003). This study indicated that RpL10a induced InR stimulated the phosphorylation of Akt, which led to the activation of the phosphorylation of dFOXO by Akt, and this phosphorylated activation increased carbohydrate utilization. This finding might be explained how RpL10a stimulated cell proliferation in many previous reports (Fisicaro et al., 1995; Koga et al., 2003; Wonglapsuwan et al., 2011). Moreover, the influence of RpL10a via the insulin signaling pathway was observed not only in cell proliferation but also in glycogenesis. Glycogenesis was suppressed in the RpL10a-overexpressed flies through Akt phosphorylation. This study showed that the p-Akt content was higher in the RpL10a-overexpressed eyes than in the normal eyes, while the levels of glycogen were lower than in the normal flies (Figure 13b). Therefore, RpL10a might induce the expression of InR and then trigger the expression of PI3K (Phosphatidylinositol-4, 5-bisphosphate 3-kinase) to phosphorylate Akt, and control glycogenesis.

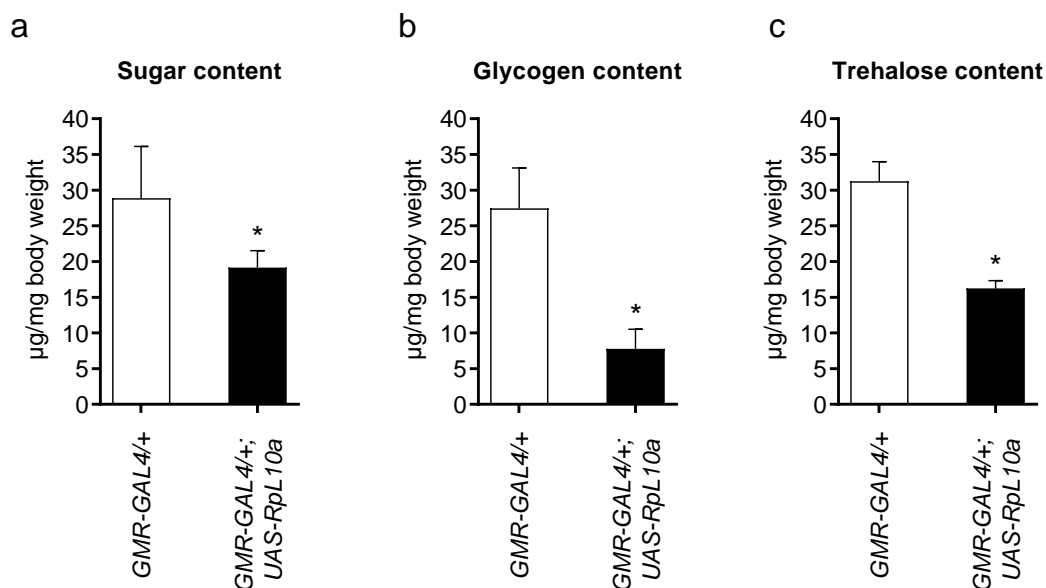


Figure 13. The excess RpL10a altered the carbohydrate metabolism in RpL10a-overexpressed flies. After hatching, the flies were aged for two days before carbohydrate determination. (a) Sugar, (b) glycogen, and (c) trehalose content was determined. Asterisk indicated a significant difference during each group ($p < 0.05$).

3. Lipid metabolism did not change in RpL10a-overexpressed flies

However, the level of lipid contents in RpL10a-overexpressed eyes was not significantly different compared to the control groups, as showed in Figure 14. Generally, lipid homeostasis needs many and more complex pathways, so the activation of InR by RpL10a might not be enough to affect homeostasis. In this study, the lipid metabolism was investigated in RpL10a-overexpressed flies. The flies of the normal group and the RpL10a-overexpressed flies were collected to determine the lipid content. The results showed no difference in lipid content between the two groups (Figure 14a). Due to the lipid content difference in the female and male flies. Therefore, the virgin female flies were used for lipid determination again to confirm the result. The virgin female flies were separated and raised until two days old before lipid determination. The graph also showed no difference in female lipid content between the two groups (Figure 14b).

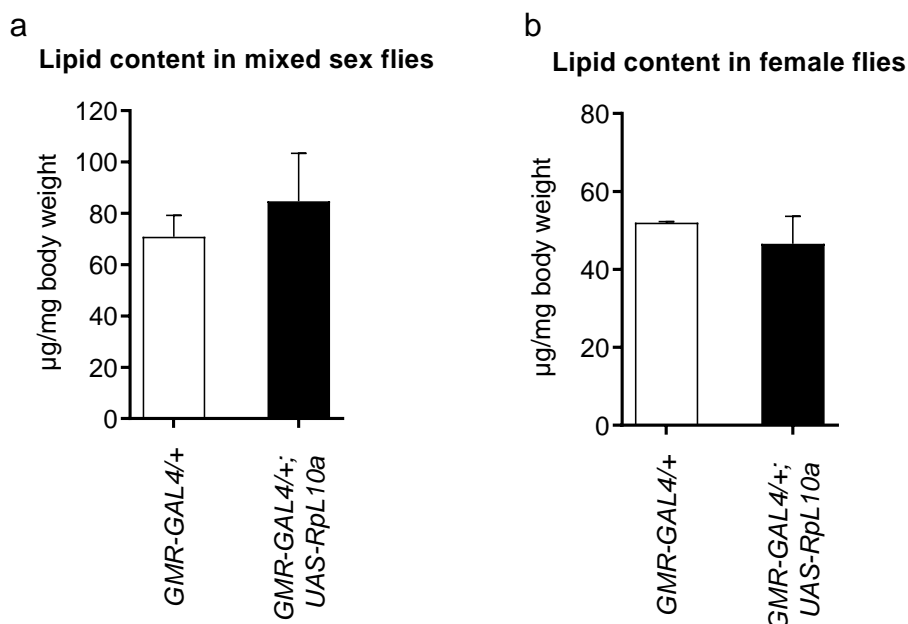


Figure 14. The effect of RpL10a may unchanged the total lipid content in normal flies and the RpL10a-overexpressed flies. The lipid of (a) mixed-sex flies and (b) virgin female flies was determined. The asterisk indicated a significant difference during each group ($p < 0.05$).

4. RpL10a altered the expression of the *Shc* gene

The previous publication demonstrated that RpL10a could stimulate cell proliferation. In this study, the effect of RpL10a on cell proliferation via the Ras pathway was investigated. Proliferation through the Ras pathway was observed by investigating *Shc* expression. The mRNA expression of *Shc*, a mediator of this pathway, was determined in the RpL10a-overexpressed eyes by real-time PCR with a primer specific to the *Shc* gene. The RpL10a-overexpressed flies showed significantly higher *Shc* mRNA expression than the normal flies (Figure 15). The high level of *Shc* in RpL10a-overexpressed eyes indicated that RpL10a affects cell proliferation via the insulin signaling pathway. This result could explain the role of RpL10a in cell proliferation in the processes of organogenesis, embryogenesis, and ovarian maturation (Balcer-Kubiczek et al., 1997; Wonglapsuwan et al., 2010).

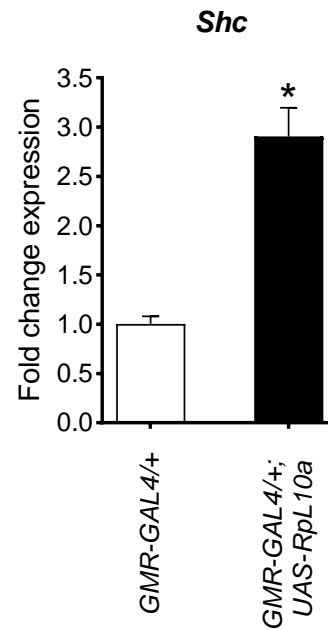


Figure 15. The excess RpL10a induced mRNA expression of *Shc*. The mRNA expression of the *Shc* gene was detected by real-time PCR. The relative mRNA expression level of the *Shc* gene normalized with the β -actin gene. The asterisk indicated a significant difference between each group ($p < 0.05$).

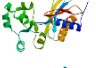
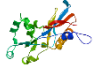
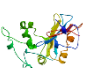
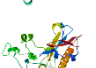
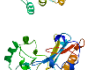
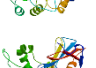
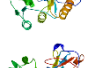

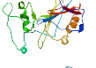
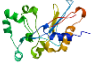

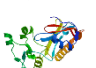

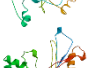
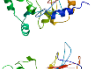
Part II: RpL10a and InR interaction and the effect after binding

1. The *In silico* binding

1.1. The structure of shrimp RpL10a protein

217 amino acid of RpL10a protein was built into a 3D structure through the SWISS-MODEL database. After modeling, the 43 templates were filtered and found matching with the target sequence. Then, 15 first models with the highest Global Model Quality Estimation (GMQE) scores were selected, as shown in table 9. GMQE is an assessment of the accuracy of the model built by that alignment, template, and target coverage (Waterhouse et al., 2018). GMQE scores are displayed as numbers between 0 and 1. Higher numbers indicate higher reliability.

Table 9. The top of 15 protein models with the highest Global Model Quality Estimation (GMQE) scores

Model	Id	Template	GMQE	QMEAN	
	02	6gz3.76.A	0.82	-1.94	👍
	13	4v8m.35.A	0.77	-4.40	👎
	03	6hcq.77.A	0.77	-5.54	👎
	01	4v6w.36.A	0.78	-6.05	👎
	14	4v7e.37.A	0.74	-7.50	👎
	05	3j7r.43.A	0.75	-7.52	👎
	10	4v7e.37.A	0.76	-7.55	👎
	04	5t2c.38.A	0.74	-7.72	👎
	11	5it7.42.A	0.76	-7.79	👎
	15	4v3p.30.A	0.74	-7.68	👎
	09	4v3p.30.A	0.76	-7.92	👎
	07	6ip5.43.A	0.74	-8.41	👎
	12	6uz7.42.A	0.75	-8.54	👎
	06	6ek0.43.A	0.74	-9.04	👎
	08	5lks.43.A	0.74	-9.29	👎

In table 9 shows the QMEAN Z-score of each model. QMEAN Z-score provides an estimate of the "degree of nativeness" of the structural features observed in the model on a global (Benkert et al., 2011). The scores around zero indicate good agreement between the model structure and experimental structures of similar size. This is also highlighted by the "thumbs-up" symbol next to the score. In contrast, the scores of -4.0 or below with a "thumbs-down" symbol indicate the models with low quality. In this

study, the protein model ID 02, which has the best QMEAN Z-score, was selected. 3D structure of RpL10a protein model 02 was modeled base on the template ID 6gz3.76.A with 71.43% identity (Figure 16).

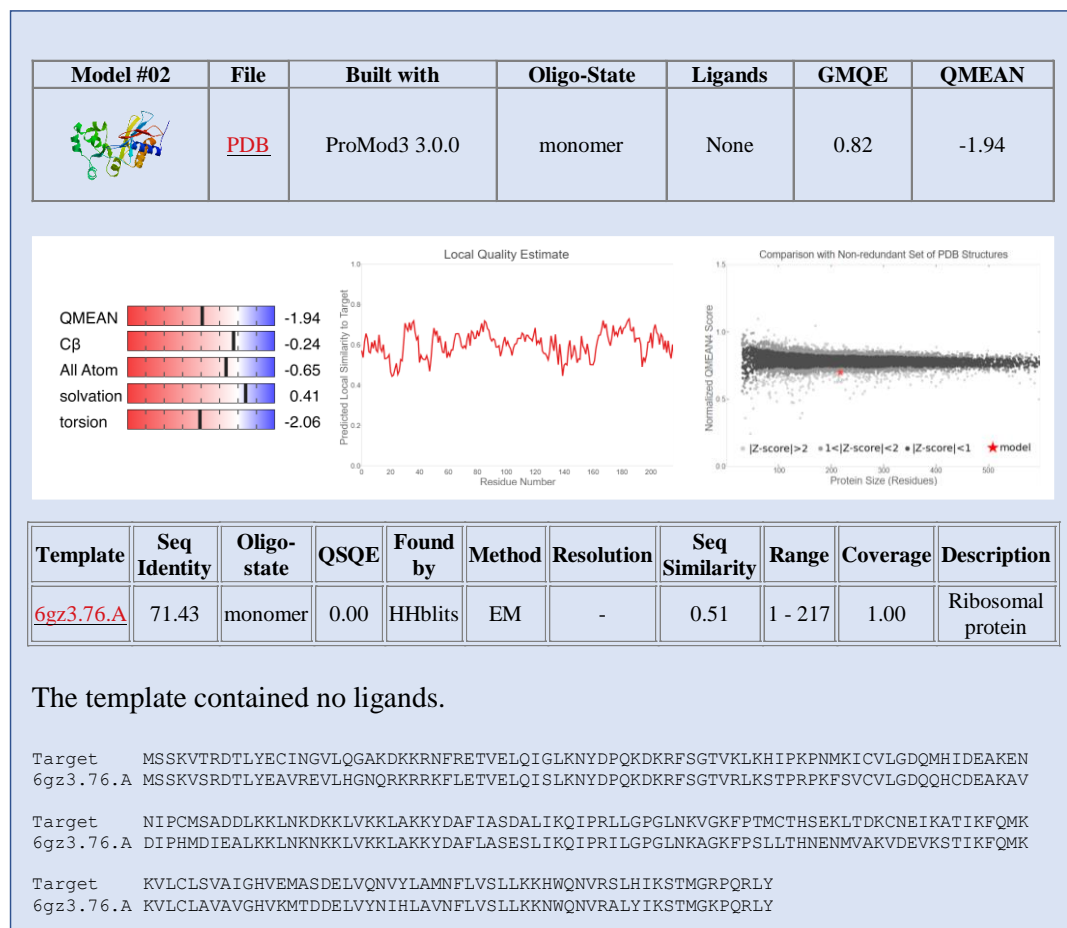


Figure 16. The Swiss-Model report of the RpL10a protein model 02 with the highest of GMQE score and the best QMEAN Z-score

The stereochemical quality of the selected model was evaluated. The Ramachandran plot showed dihedral angles ψ (Psi) and ϕ (Phi) of amino acid residues in a structure of RpL10a protein model 02 (Figure 17). The plot showed 203 (94.4%) of amino acid residues presented in the favorable region (dark green area), 11 (5.1%) of amino acid residues presented in the allowed region (green area). The residues

located in the allowed region were shown in Table 10. And only one (0.5%) of methionine residue 159 presented in the outlier region (light green area).

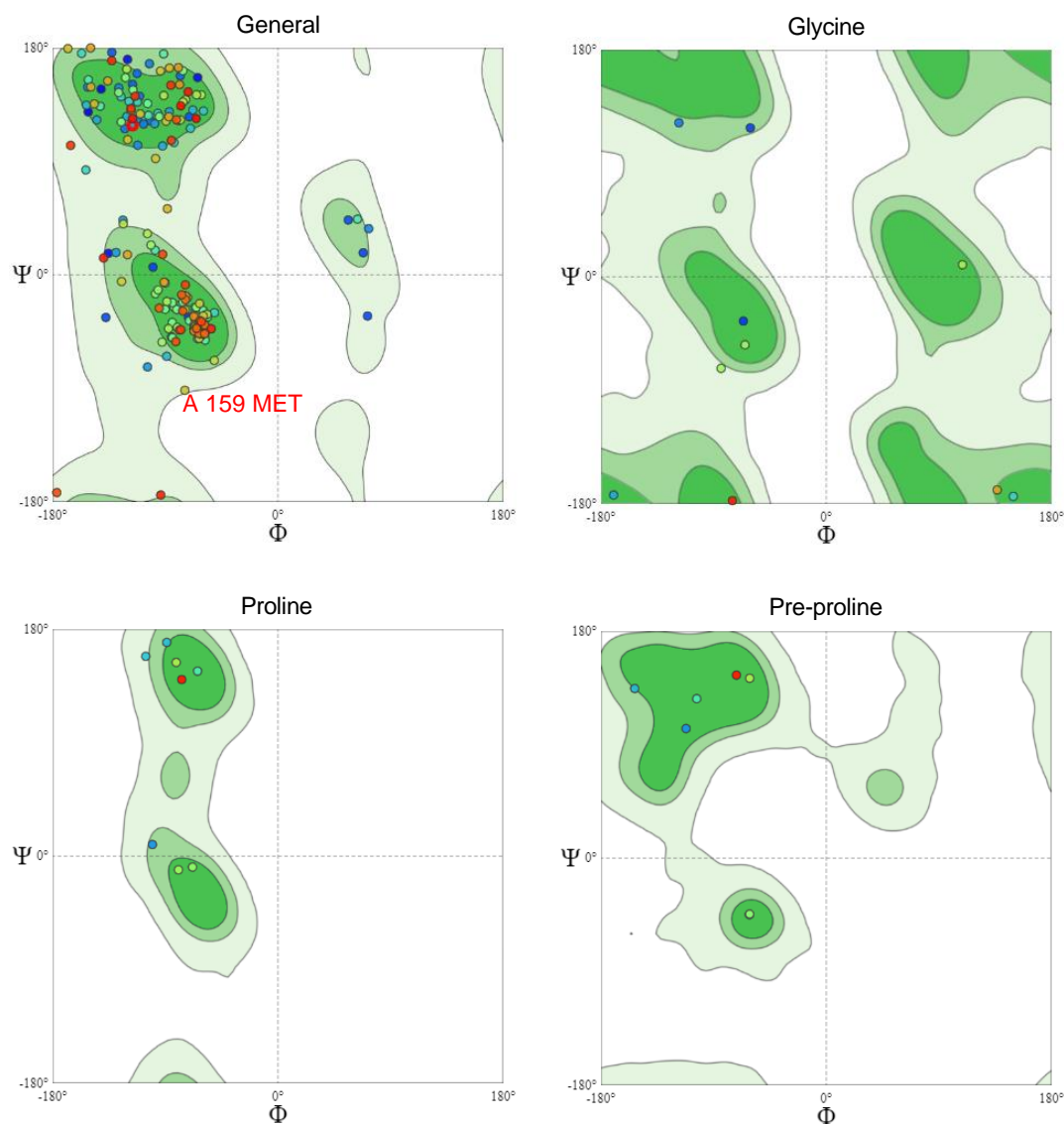


Figure 17. Ramachandran plot represents the dihedral angles of 217 amino acid residues of RpL10a protein model 02. The plot consists of the favorable region (dark green area), the allowed region (green area), and the outlier region (light green area).

Table 10. The list of the amino acid residue of RpL10a protein model 02 presented in allowed and outlier regions

Residue	(Psi(Ψ), Phi(Φ))	Region
A 22: LYS	(71.63, -32.67)	in Allowed region
A 23: ASP	(-137.47, -33.78)	in Allowed region
A 40: ASN	(72.60, 36.60)	in Allowed region
A 45: LYS	(-104.17, -73.03)	in Allowed region
A 57: HIS	(-88.83, -64.61)	in Allowed region
A 61: PRO	(-105.56, 158.51)	in Allowed region
A 70: ASP	(-153.42, 83.17)	in Allowed region
A 127: GLY	(-84.05, -72.58)	in Allowed region
A 145: THR	(-50.80, -67.91)	in Allowed region
A 197: HIS	(-176.67, -172.68)	in Allowed region
A 203: SER	(-165.57, 102.68)	in Allowed region
A 159: MET	(-74.29, -91.55)	in Outlier region
Number of residues in favored region	(~98.0% expected)	: 203 (94.4%)
Number of residues in allowed region	(~2.0% expected)	: 11 (5.1%)
Number of residues in the outlier region		: 1 (0.5%)

The 3D structure of the human InR protein was downloaded from PDB. The human InR ID is 3LOH from X-ray diffraction with a resolution of 3.8 Å. The structure of RpL10a and InR were elucidated through the PyMol program (Figure 18).

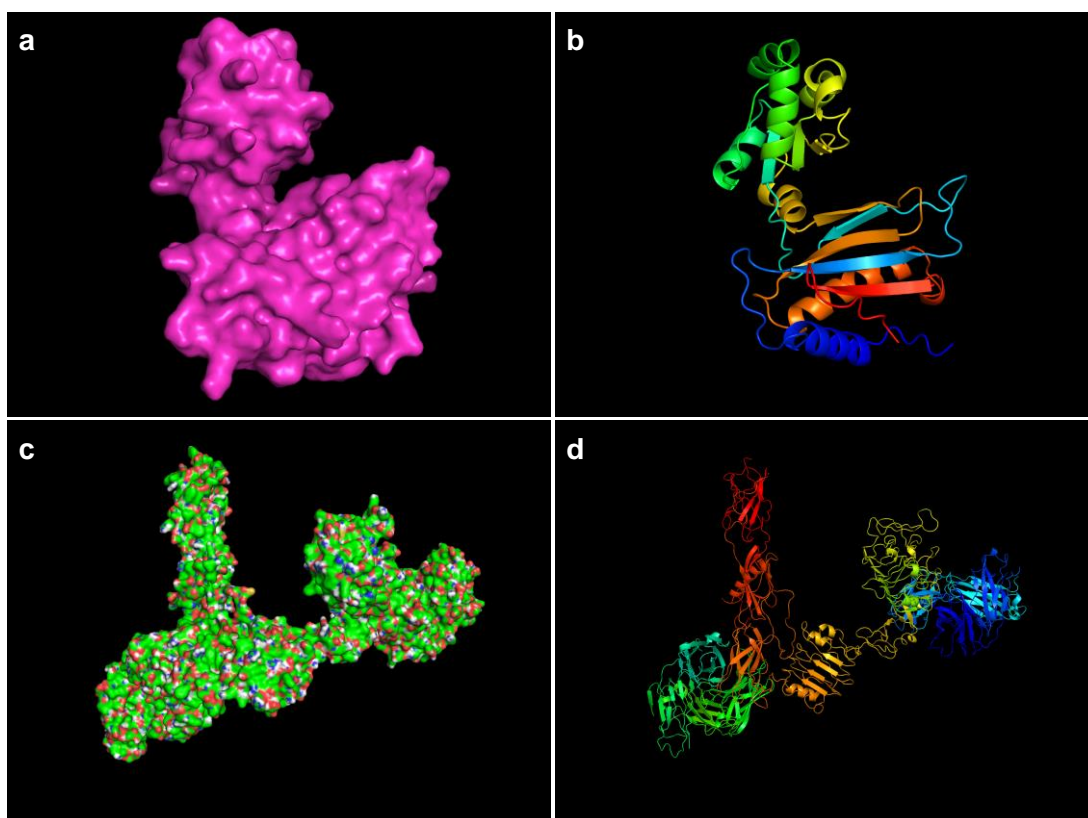


Figure 18. The 3D structure of shrimp Ribosomal protein L10a (RpL10a) and human insulin receptor (InR) were elucidated using the PyMol program. The 3D structure of RpL10a was presented in (a) surface form and (b) cartoon form. And the 3D structure of InR was presented in (c) surface form and (d) cartoon form.

1.2. The binding of RpL10a and InR from the PIPER program on ClusPro 2.0 server (*In silico*)

The interaction of RpL10a and InR was elucidated to study the mechanism by which RpL10a affects the insulin signaling pathway. First, the ClusPro server was used to predict the interaction between these two proteins, taking advantage offered by *in silico* experiments to ascertain the position of the interaction. The protein–protein docking of RpL10a and InR was performed through ClusPro 2.0. The software predicted that RpL10a could bind to InR with high scores (Figure 19a). The lowest energies of balanced, electrostatic-favored, hydrophobic-favored, and van der Waals

interactions were -958.1 , -1010.7 , -1174.8 , and -361.3 , respectively. Their binding may permit RpL10a to initiate insulin activity. Moreover, the binding site of RpL10a on InR was also observed. The site in which RpL10a bound to InR was different from the binding site of insulin on InR (Figure 19b).

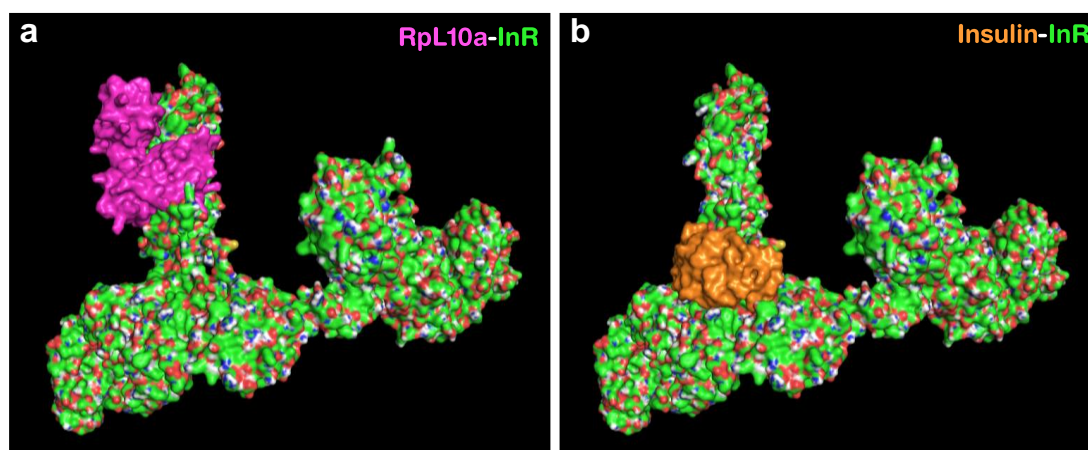


Figure 19. The the binding site of Ribosomal protein L10a (RpL10a) and the insulin receptor (InR) was different from the binding site of insulin on InR. The interaction was predicted through the PIPER program on the ClusPro 2.0 server. (a) The binding of InR (green) with RpL10a protein (pink). (b) The 3D structure of InR protein (green) is bound to insulin (orange).

RpL10a interacts with human InR at a part of the FnIII domain, which is located on residues 635–640 (Gln635, Asp638, Ser639, and Glu640 residues) and 697–702 (Glu697, Phe701, and Arg702 residues) of InR (Figure 20a–b).

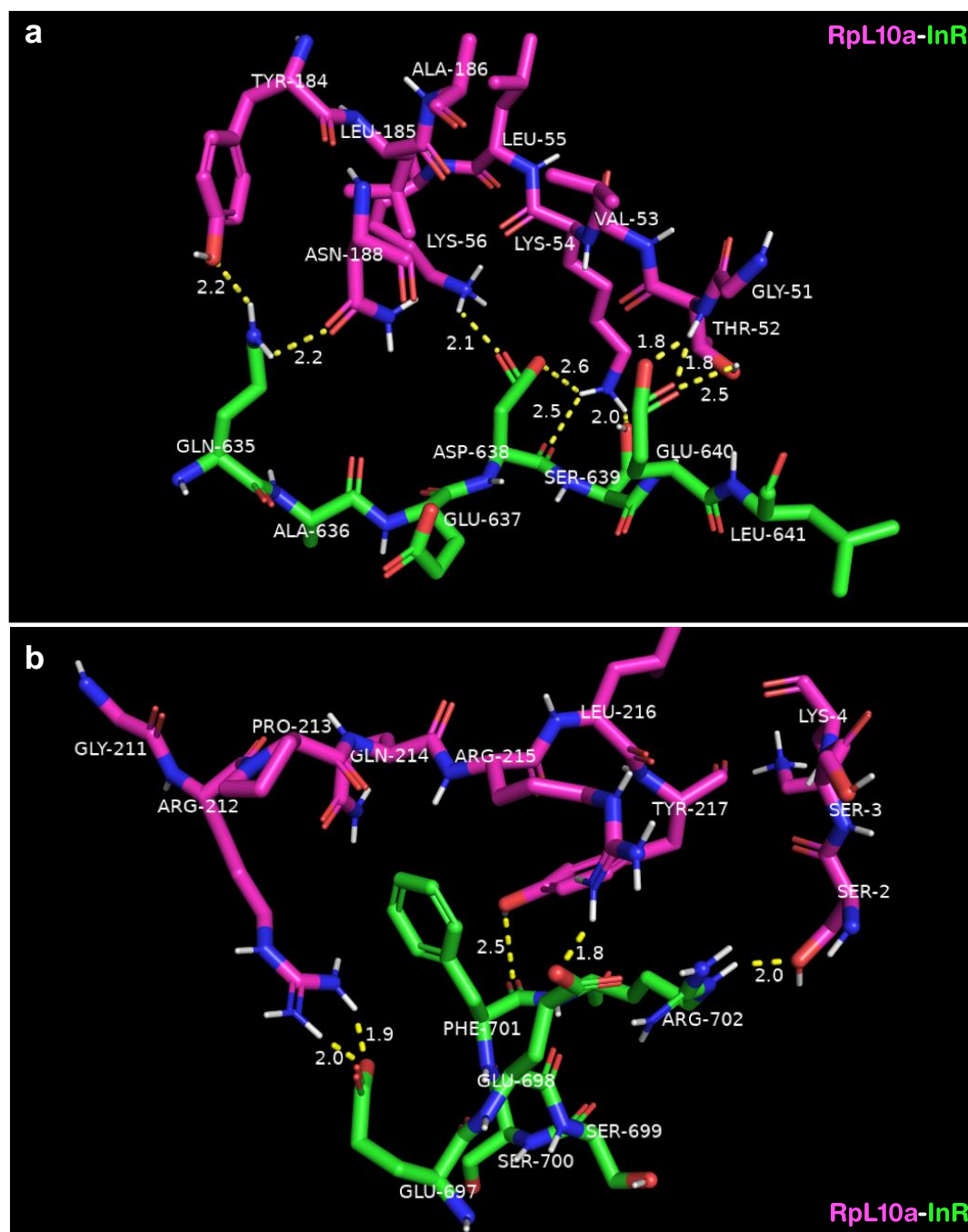


Figure 20. The interaction of Ribosomal protein L10a (RpL10a) and the insulin receptor (InR). The interaction was predicted through the PIPER program on the ClusPro 2.0 server. (a) The binding site between InR (green) and RpL10a (pink) at residues 635–640 of InR (Gln635, Asp638, Ser639, and Glu640). (b) and residues 697–702 of InR (Glu697, Phe701, and Arg702).

Whereas insulin binds to the InR at residues 704–710 (Thr704, Asp707, and His710) with the lowest energies of balanced, electrostatic-favored, hydrophobic-favored and van der Waals interactions were -1079.5 , -1045.2 , -1481.3 , and -192.8 , respectively (Figure 21). This insulin–InR binding result was similar to the previous study that reported the InR bound to the Ins at His710 and His714 residues in the binding region of the high-affinity site 2 (Menting et al., 2013). Normally, the binding sites of InR α -subunit bound to the insulin consist of two sites, including a low-affinity site1 located on L1 and CR domain and a high-affinity site2 on L2 and FnIII2 domain (De Meyts, 2008; Ward and Lawrence, 2009). The previous study reported some molecules activated the InR by interacting at the insulin–InR binding site (Li et al., 2005), while some insulin-mimetic molecules activated the InR by binding at other InR binding sites (Qiang et al., 2014). In addition, the activation of the InR and lowering blood glucose levels not only via α subunit but also via InR β -subunit such as a non-peptidyl fungal metabolite L-783,281 (Zhang et al., 1999) and LK16998 (Manchem et al., 2001). Therefore, the *in silico* binding suggests that RpL10a could bind to the InR on the region different from the InS binding site.

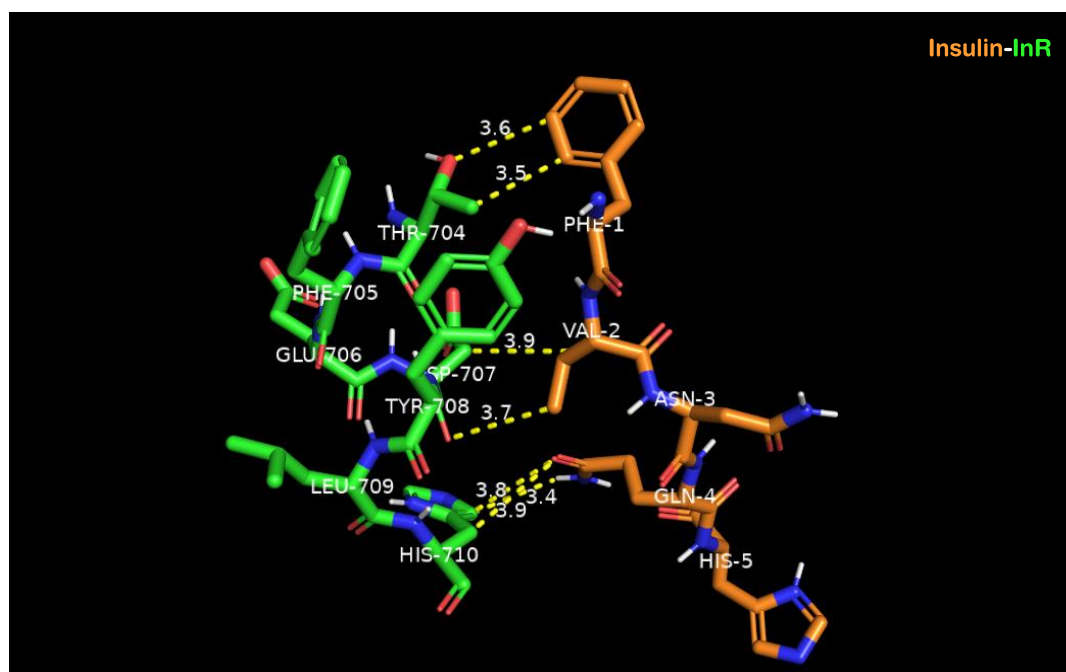


Figure 21. The interaction of of InR protein (green) is bound to insulin (orange). The binding site between InR (green) and insulin (orange) at residues 704–710 (Thr704, Asp707, and His710).

Moreover, most of the amino acid residues of shrimp RpL10a that bound to InR were located on the RpL10a conserve domain (Figure 22). RpL10a amino acid residues 51–56 and 184–188 (Gly51, Thr52, Lys54, Lys56, Tyr184, and Asn188) bound to residues 635–640 of InR and RpL10a amino acid residues 2 and 212–217 (Ser2, Arg212, Arg215, and Tyr217) bound to residues 697–702 of InR.



Figure 22. The diagram of shrimp Ribosomal protein L10a (RpL10a) protein sequence conserved domain. The black bar and the gray bar indicate the highly conserve domain and conserve domain, respectively. The binding site of RpL10a bound to InR showed in the square. The red square indicated the position of RpL10a amino acid bound to residues 635–640 of InR. The blue square indicated the position of RpL10a amino acid bound to residues 697–702 of InR. Red and blue asterisk indicated the RpL10a amino acid that bound to InR. The diagram was created base on the amino acid sequence alignment shown in Figure 2.

2. The *in vitro* binding

2.1. The nucleotide sequence of InR FnIII domain (*InR-FnIII*)

The GST pull-down assay was performed to confirm whether RpL10a could interact with InR (*in vitro*). First, the FnIII domain containing residues 635–640 and 697–702 of InR was amplified from CHO-S cells cDNA with a specific primer containing *SalI* and *NotI* restriction site (Figure 23a). The *InR-FnIII* fragment consisted of 442 bp (Figure 23b) was ligated into pGEM[®]-T Easy vector and checked the clone by restriction enzyme digestion. The selected clone showed the InR-FnIII insert fragment (Figure 23c). Then, the InR-FnIII fragment was subcloned from *pGEM-InR-FnIII* plasmid into pGEX-4T-1 expression vector (Figure 23d), and the selected clones were then checked by sequencing, and the sequence result showed 100% identity compared with the template (Figure 23e).

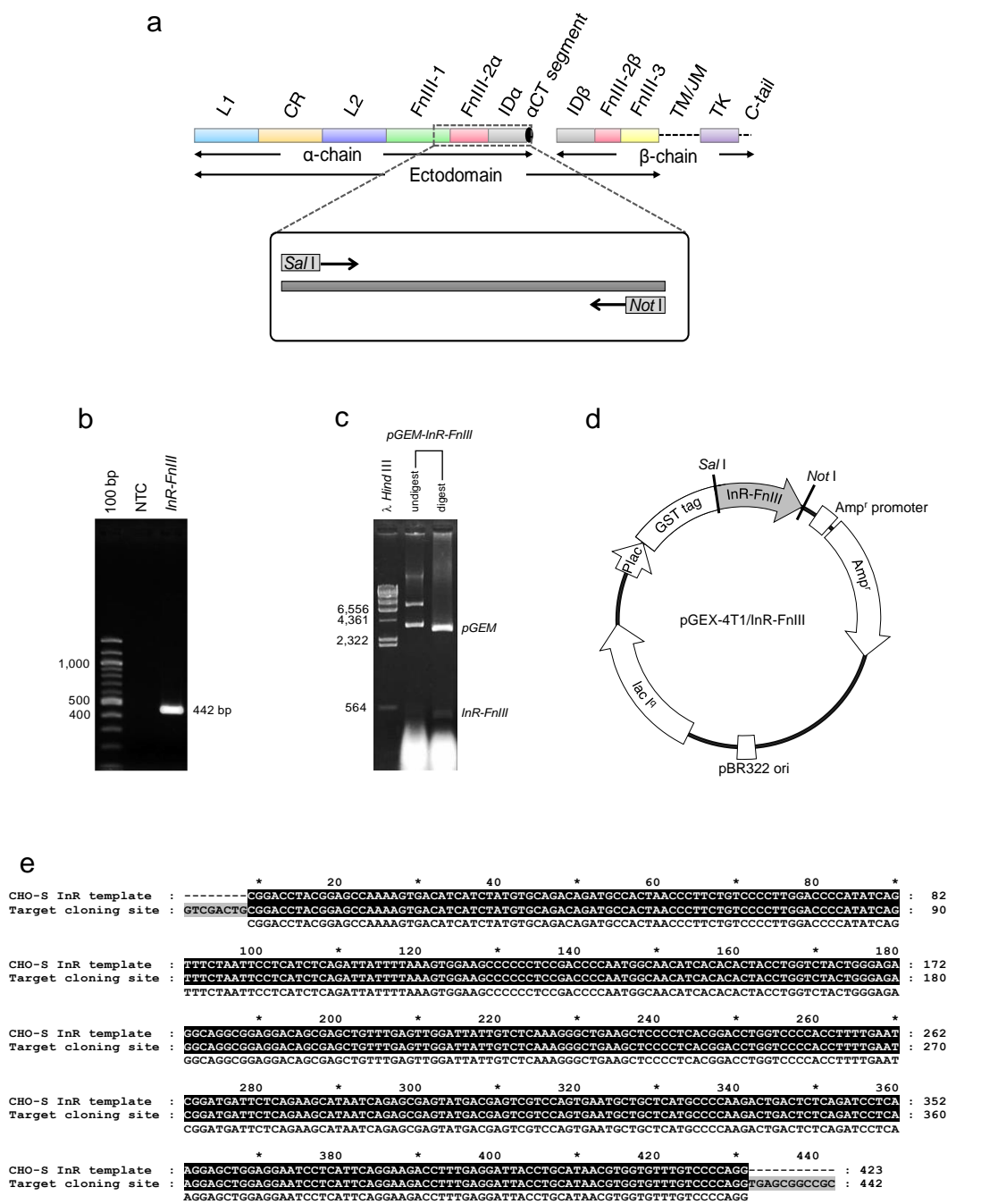


Figure 23. The sequence of the insulin receptor (InR) target cloning site was derived from CHO-S cells cDNA. (a) The PCR fragment was amplified from the FnIII domain of InR and (b) separated on gel electrophoresis. The size of the InR-FnIII fragment was 442 bp. The recombinant *pGEM-InR-FnIII* was constructed and (c) determined by restriction enzyme digestion. (d) The diagram of InR-FnIII ligated into *pGEX-4T1* vector at *SalI* and *NotI* restriction site. (e) The sequence of InR-FnIII fragment displayed 100% homology compared with CHO-S cells InR template.

2.2. Amino acid analysis of InR-FnIII protein

The nucleotide sequence of the *InR-FnIII* gene was translated into 141 amino acid residues with a predicted molecular mass of 16.20 kDa and pI 4.72. From the *in silico* binding result indicated that the RpL10a-binding site was located at residues 635–640 and 697–702 of the InR-FnIII protein. In comparison, the insulin binding site was located at residues 704–710 of the InR-FnIII protein (Figure 24a). The InR-FnIII protein clone shares 100% similarity with InR of *C. griseus* and 98.8% similarity with InR of *H. sapiens* (Figure 24b). Although this comparison showed some amino acid differences between Chinese hamsters and humans, the amino acid sequence at the binding site shares 100% identical (Figure 24b).

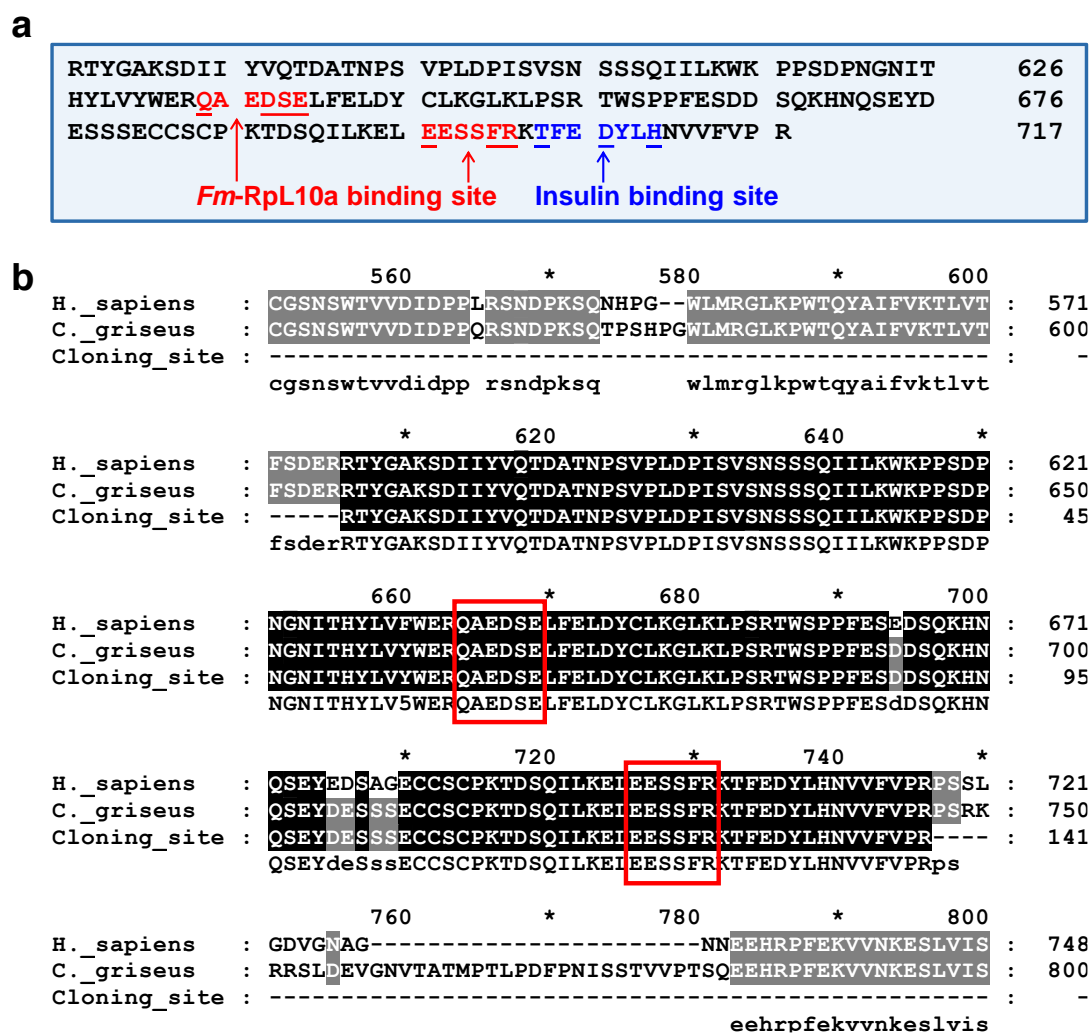


Figure 24. The amino acid sequence of InR-FnIII, (a) A diagram of the ribosomal protein L10a (RpL10a) and insulin binding sites in the insulin receptor (InR) domain. The RpL10a and insulin binding sites are located at a different area of the InR FnIII domain. (b) The protein sequence alignment among the InR target cloning site of *C. griseus*, full-length InR of *C. griseus*, and full-length InR of *H. sapiens*. Red squares indicate the amino acid sequence at the RpL10a binding site. The RpL10a and insulin binding sites of the InR target cloning site of *C. griseus* displayed 100% homology compared with full-length InR of *C. griseus*.

2.3. Expression, Purification, and Confirmation of the GST-InR-FnIII protein

The FnIII domain of InR was cloned and expressed in a pGEX-4T1 expression vector. The cell lysate was analyzed via SDS-PAGE (Figure 25a). The molecular mass of the recombinant GST-InR-FnIII protein is around 44 kDa which is close to the sum of the *in silico* predicted InR-FnIII molecular weight (16.2 kDa) and GST-tag molecular mass (28 kDa). The GST and GST-InR-FnIII proteins were purified with affinity purification and checked the purification quality via SDS-PAGE (Figure 25b–c). The expressed GST, and GST-InR-FnIII proteins were confirmed by Western blotting probing with anti-GST antibody (Figure 25d). The Western blotting result showed the expressed GST and GST-InR-FnIII with a molecular mass around 28 and 44 kDa, respectively.

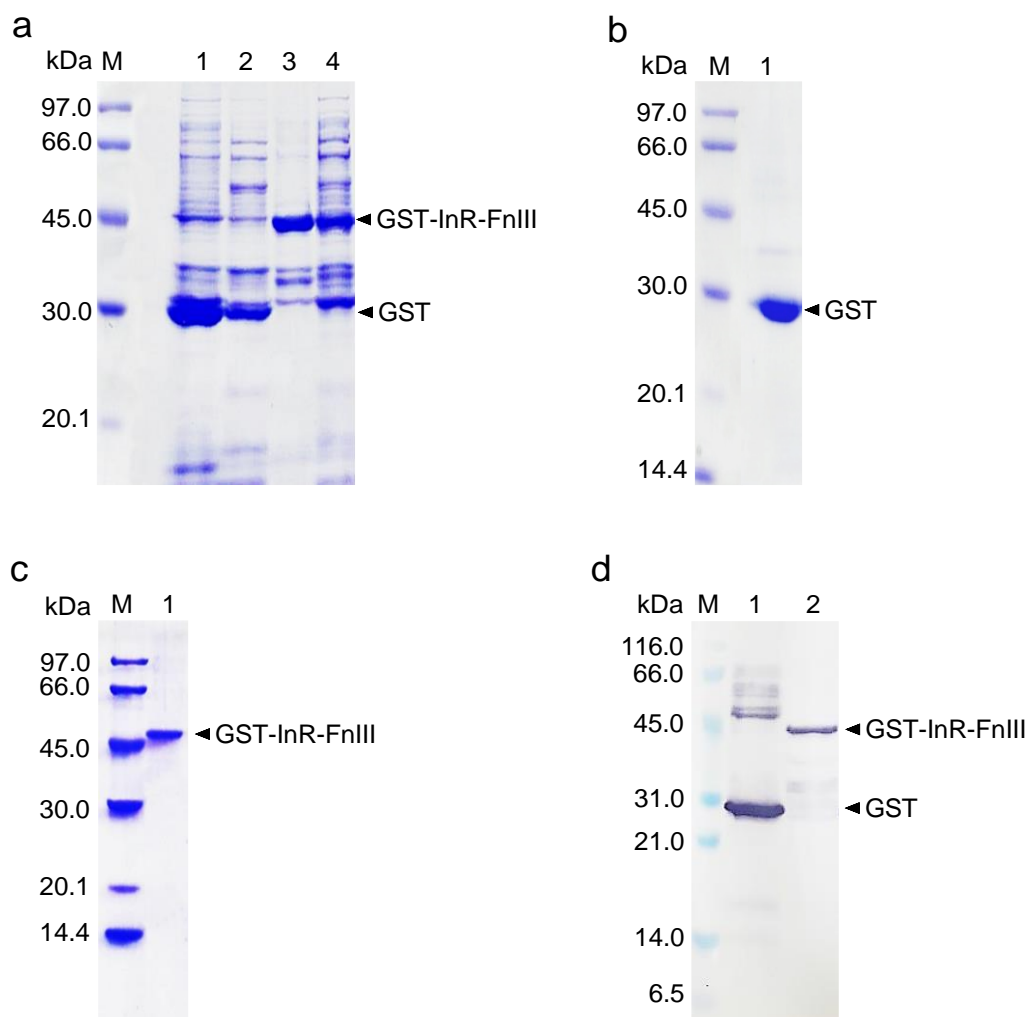


Figure 25. Expression and purification of the GST-InR-FnIII. (a) Coomassie blue staining of GST and GST-InR-FnIII protein expression. Lane 1–2: the extracted protein from bacterial clone 1 and clone 2 containing GST protein. Lane 3–4: the extracted protein from bacterial clone 1 and clone 2 containing GST-InR-FnIII protein. (b–c) Coomassie blue staining of purified GST and GST-InR-FnIII protein after affinity purification. (d) Western blot analysis confirmed the identity of the proteins by probing with the anti-GST antibody. The molecular mass of GST and GST-InR-FnIII showed around 28 and 44 kDa, respectively.

2.4. Expression, Purification, and Confirmation of the His-RpL10a protein

The pET-28a (+) expression vector harboring RpL10 was cloned (Wonglapsuan et al., 2010). His-RpL10a was expressed by induction with IPTG, and the lysate cell was separated through SDS-PAGE (Figure 26a). The molecular mass of the His-RpL10a protein is 29.2 kDa, which consists of the RpL10a (25.7 kDa) and His protein (3.5 kDa). The lysate was purified and examined the purity via SDS-PAGE (Figure 26b) and then was confirmed by western blot analysis probing with anti-His antibody (Figure 26c). The western blot result showed the His-RpL10a band with a molecular mass around 30 kDa

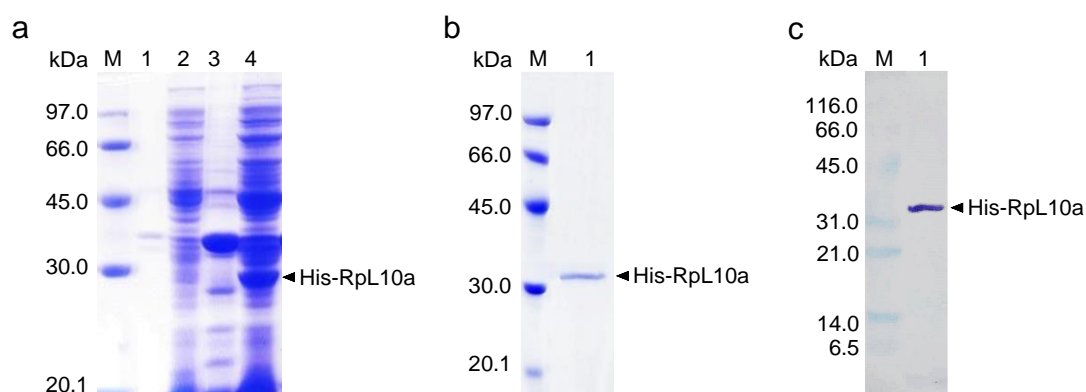


Figure 26. Expression and purification of the His-RpL10a, (a) Coomassie blue staining of His-RpL10a protein expression. Lane 1: non-induced pellet, lane 2: non-induced supernatant, lane 3: induced pellet, and lane 4: induced supernatant. (b) Coomassie blue staining of purified His-RpL10a protein after affinity purification. (c) Western blot analysis confirmed the identity of the proteins by probing with the anti-His antibody. The molecular mass of His-RpL10a showed around 30 kDa.

2.5. The binding of the GST-InR-FnIII and the His-RpL10a by GST pull-down (*In vitro*)

The interaction of the InR and the RpL10a was performed by GST pull-down assay. GST-InR-FnIII bound with His-RpL10a (Figure 27). Whereas the band of His-RpL10a was not found in the GST panel, indicating that there are no false-positive reaction between the His-RpL10a and the GST.

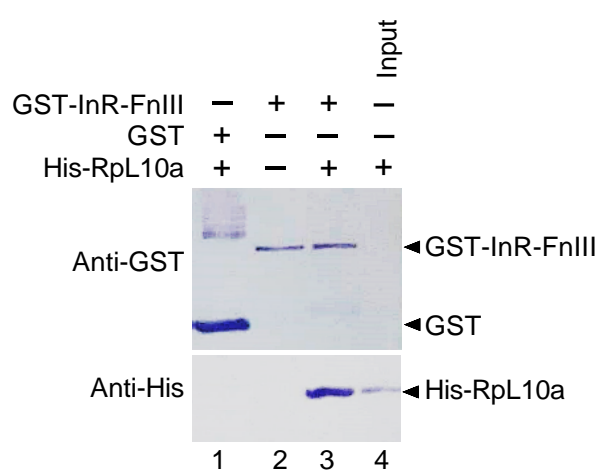


Figure 27. The interaction between His-RpL10a (prey) and GST-InR-FnIII (bait). Lane 1: the reaction mixture of GST incubated with His-RpL10a, lane 2: the reaction mixture of GST-InR-FnIII, lane 3: the reaction mixture of the GST-InR-FnIII incubated with the His-RpL10a, and lane 4: the His-RpL10a was used as a control. All reactions were pulled down with Glutathione Sepharose beads and examined with Western blotting probing with anti-His and anti-GST antibodies.

2.6. The binding of GST-InR-FnIII and His-RpL10a by immunofluorescence (*In vitro*)

The results gained from both the ClusPro program and the pull-down assay indicated that RpL10a could bind to InR at the FnIII domain position. In addition, the interaction of the InR and the RpL10a protein was also confirmed using an immunohistochemistry assay. CHO-S cells were incubated with His-RpL10a, and then the interaction between CHO InR and His-RpL10a protein was detected with anti-His and anti-InR antibodies (Figure 28). The fluorescence signal indicated the CHO InR expressed in the cellular membrane of the cells (red color), whereas His-RpL10a was located throughout the cells (green color), indicating that RpL10a could bind to the InR (merge color). In the control group, in which no antibody was used, a null fluorescence signal was observed (right panel).

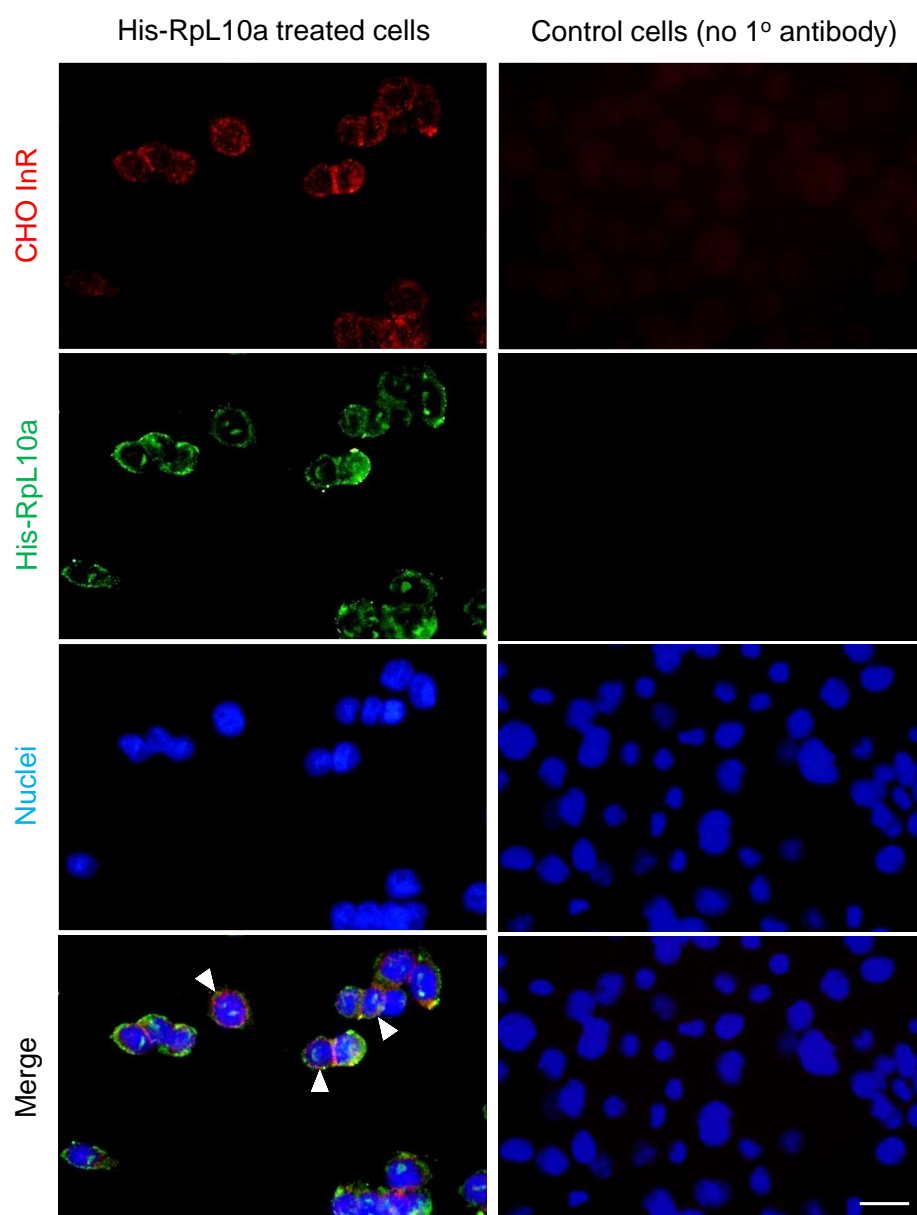


Figure 28. The interaction between insulin receptor (InR) and ribosomal protein L10a (RpL10a) was confirmed by using the immunofluorescence assay. Chinese hamster ovary (CHO-S) cells were incubated with 3 $\mu\text{g/ml}$ of His-RpL10a and incubated with anti-His and anti-InR antibodies. CHO InR protein was stained with rhodamine (Red color) and the additional His-RpL10a was stained with FITC (green color). The nuclei were stained with DAPI (blue) and the Merge image indicated the interaction of His-RpL10a and CHO InR (arrowheads). Right panels present the immunofluorescence signal in the control group, in which no primary antibody was incubated. The scale bar is 20 μm .

3. The effect after RpL10a and InR binding

3.1. RpL10a and InR binding induce phosphorylation of Akt

Normally, the phosphorylation cascade in the insulin signaling pathway was initiated after the binding of the InR and ligand. In this study, The RpL10a treated cells were collected after 24 h of RpL10a incubation to determine the phosphorylation level of Akt by western blot analysis with anti-p-Akt antibody. The graph showed the binding of RpL10a and InR could induce the phosphorylation of Akt compared with the control group (Figure 29).

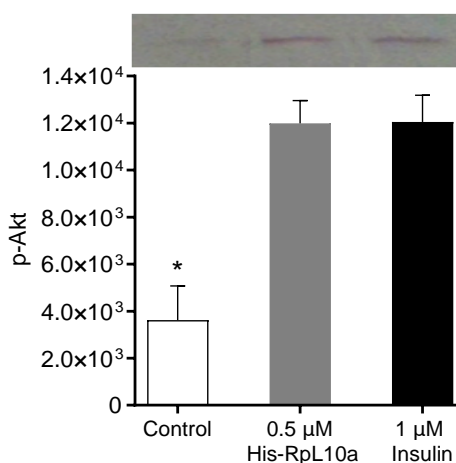


Figure 29. The binding of RpL10a and InR induced Akt phosphorylation in RpL10a treated cells. The protein expression of p-Akt was examined by western blot analysis. The histogram shows the p-Akt level. The asterisk indicated a significant difference during each group. ($p < 0.05$).

3.2. The effect of RpL10a and InR binding on sugar consumption

To investigate whether the carbohydrate metabolism was changed after binding of RpL10a and InR, the sugar consumption in CHO-S cells was also detected after incubating with RpL10a. CHO-S cells were incubated in various concentrations of RpL10a for 24 h, and the culture medium was collected at the indicated time point to

quantify the remaining sugar. The result showed that the medium sugar content in all groups of RpL10a treated cells tended to decrease especially in 1 μM RpL10a treated cells (Figure 30). Whereas the sugar content in the medium and in the dialysis treated cells remain unchanged.

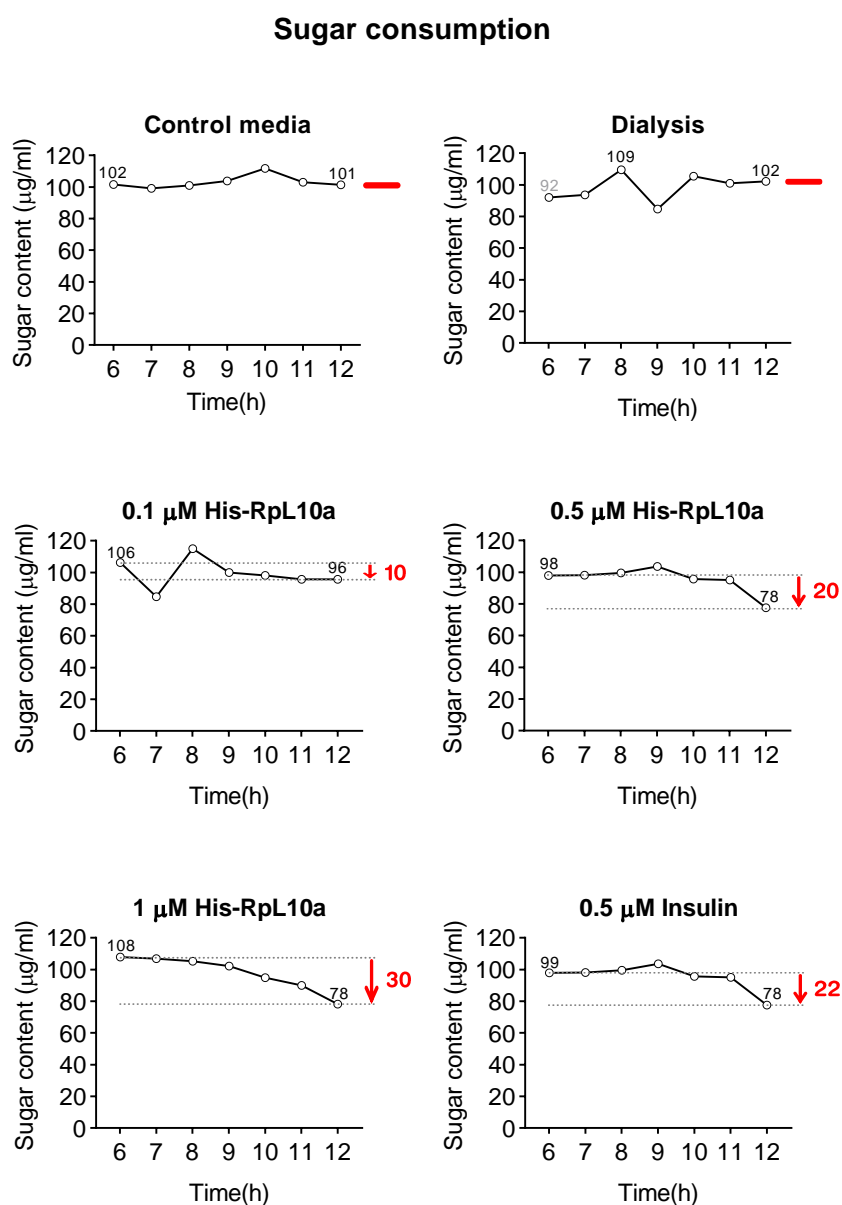


Figure 30. The binding of RpL10a and InR altered sugar metabolism in RpL10a treated cells. The sugar content was determined from the medium of cells incubated with 0 (Negative control), 0.1, 0.5, 1 μM RpL10a. Cells incubated with 0.5 μM insulin was used as a positive control, the medium was used as a control medium, and dialysis was used as a negative control.

3.3. RpL10a induces glucose uptake by CHO-S cells

To confirm that the RpL10a reduced the sugar in the culture medium by uptaking into the cells. The cells were starved before incubated with RpL10a. The RpL10a treated cells were then stimulated with 2-DG. After 2-DG uptaking by the cells, the content of 2-DG accumulated in the cells was detected. The result indicated that RpL10a could induce glucose uptake by the cells compared with the control group (Figure 31).

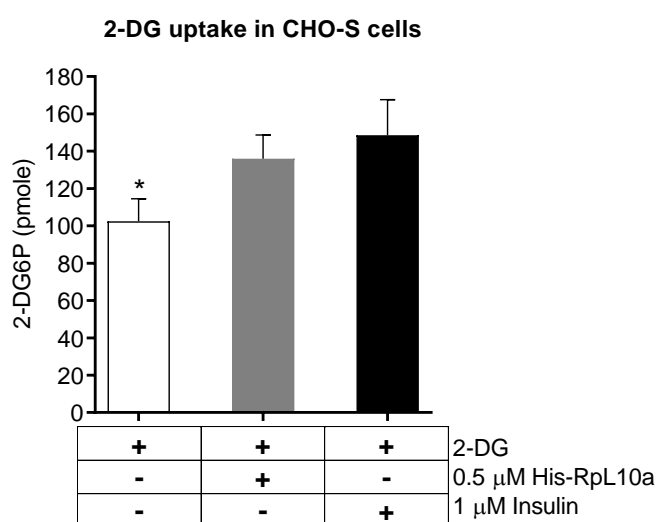


Figure 31. RpL10a induced glucose uptake in CHO-S cells. The glucose uptake was detected by a glucose uptake colorimetric assay kit. The histogram shows the level of 2DG6P accumulation in the cell. The cells incubated with only 2-DG was used as a negative control. The cells incubated with insulin, and 2-DG was used as a positive control. The asterisk indicated a significant difference during each group ($p < 0.05$).

These RpL10a and InR binding results and the effects that occurred after their binding suggest that the interaction can stimulate the insulin signaling pathway and then altered the carbohydrate metabolism. This stimulation of the signaling pathway could be the extra-ribosomal function of RpL10a. RpL10a bound to InR at a different site from insulin, so it may in the future be useful in treating insulin resistance in people with diabetes.

Part III: The effect of RpL10a in insulin resistance cells

1. Insulin resistance cells (IRCs) induction

To investigate whether RpL10a induces glucose uptake in IRCs. CHO-S cells were firstly induced to be the insulin resistance cells. Cells were induced in three induction conditions. After 24 h of induction, the result indicated that all induction conditions could reduce the glucose uptake by cells compared with the healthy cells group, which showing an insulin resistance condition (Figure 32). Besides, in 50 mM glucose induction condition reduced the glucose uptake level by CHO-S cells more than other conditions (Figure 32). At the same time, the cell numbers of each group were not different (Figure 33). Therefore the condition which induced cells with 50 mM glucose is suitable to induce IRCs.

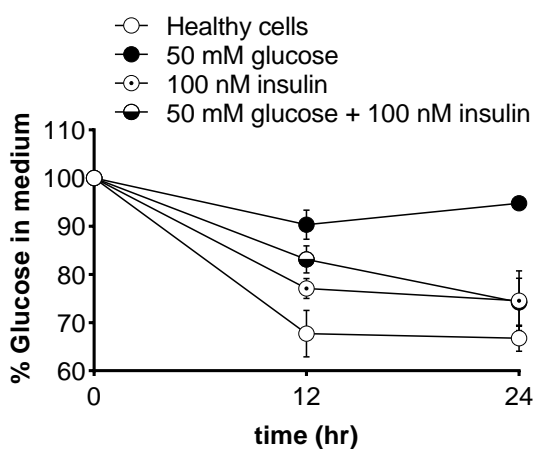


Figure 32. Induction of the Insulin resistance in Chinese hamster ovary (CHO-S) cells. Insulin resistance cells were induced under three induction conditions, including high (50 mM) glucose, high (100 nM) insulin, and both high glucose and high insulin. The rate of glucose utilization by CHO-S cells was detected after 12 and 24 h of induction.

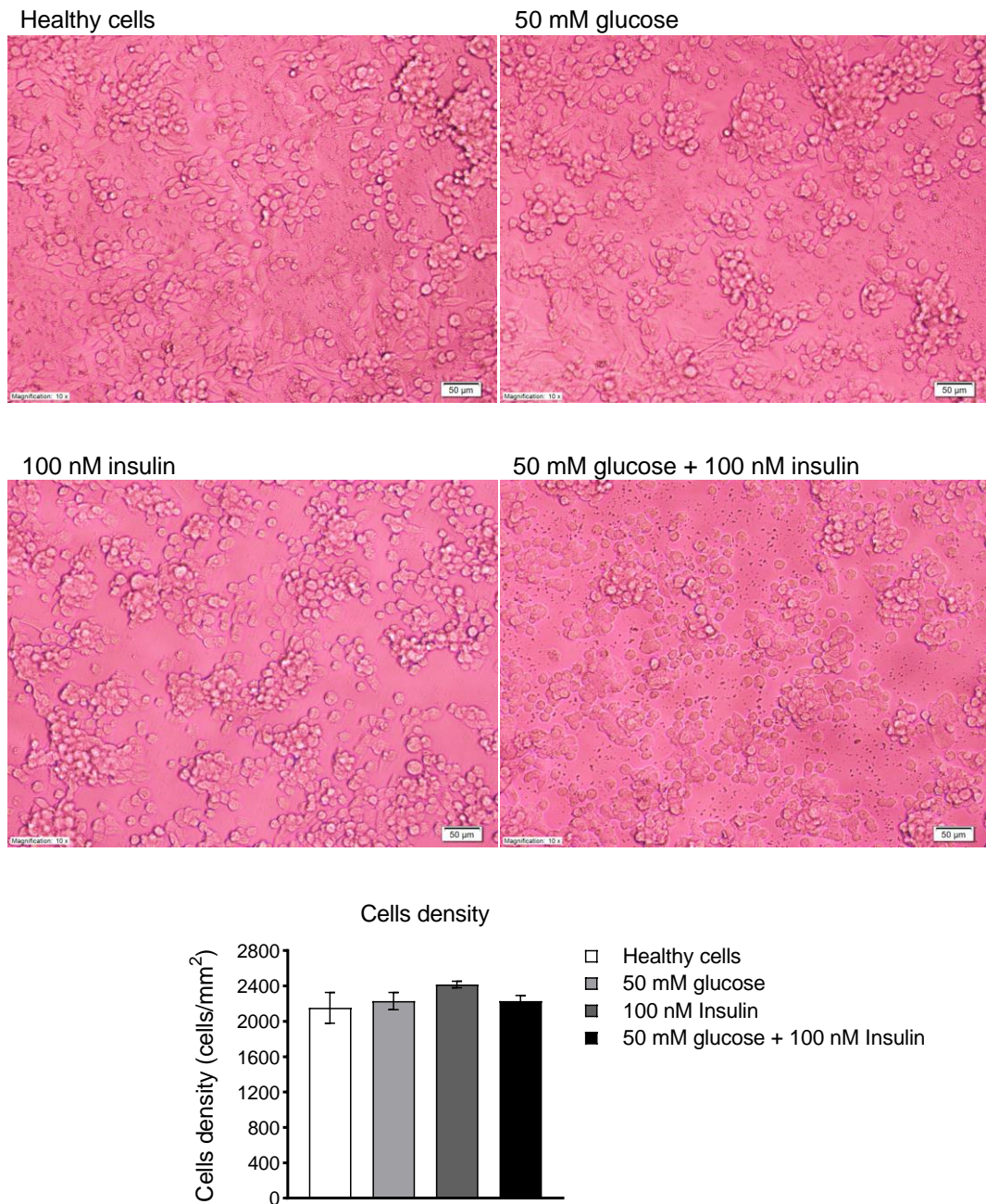


Figure 33. The cells density after 24 h of each induction condition. The scale bar is 50 µm. The histogram represents the density of cells after 24 h of induction. The number of cells in each induction condition was quantified using multi-point Tool in ImageJ software. The statistical data were analyzed using One-Way ANOVA with post-hoc Tukey HSD Test ($P < 0.05$).

The selected induction condition was confirmed by extending the induction to 48 h. The result showed that the culture medium's glucose content was reduced to approximately 70% of control levels (Figure 34). Thus, insulin resistance cells induced by 50 mM glucose for 48 h was used for the next experiment.

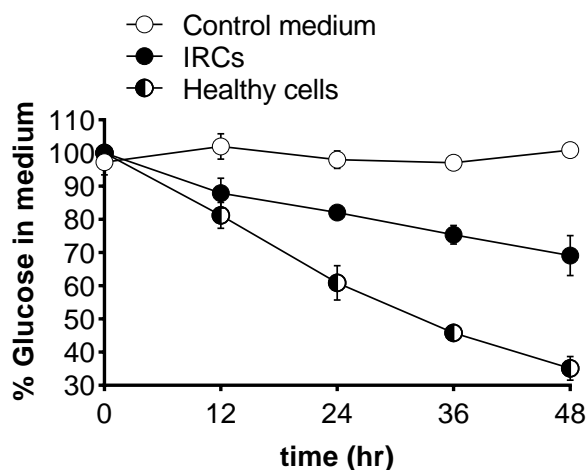


Figure 34. The Induction of Insulin resistance in Chinese hamster ovary (CHO-S) cells with 50 mM glucose for 48 h. The rate of glucose utilization by high glucose-induced insulin resistant cells (IRCs) compared with the healthy cells. The control medium was used as a control.

2. Effect of RpL10a on glucose consumption in IRCs

The healthy cells and IRCs were stimulated with three concentrations of His-RpL10a. The glucose level in the culture medium was evaluated after 24 h of stimulation. Both healthy cells and IRCs showed His-RpL10a stimulated cells increased the glucose uptake compared with the unstimulated cells (Figure 35a–b). The result showed 1 $\mu\text{g/ml}$ of His-RpL10a was sufficient to induce glucose uptake by IRCs compared with the unstimulated IRCs after 12 and 24 h of stimulation (Figure 35b). In comparison, the healthy cells were stimulated with ≥ 5 $\mu\text{g/ml}$ His-RpL10a to induce glucose uptake (Figure 35a). This result suggests that RpL10a induced glucose uptake by IRC better than healthy cells. However, the excess glucose also can cause the insulin-independent glucose uptake via the glucose transporter 1 (GLUT1) (Ebeling et

al., 1998) under high glucose conditions. Besides, insulin also activate the expression of insulin-like growth factor 1 receptor (IGF1R) and then promote cell proliferation, although this activation is less extent than the insulin-like growth factor 1 (IGF-1) (Boucher et al., 2010). As well as RpL10a that could induce cell proliferation by activating the InR and Shc expression. (Chaichanit et al., 2018; Wonglapsuwan et al., 2010). These evidence suggested that the proliferation of cells also affects glucose utilization.

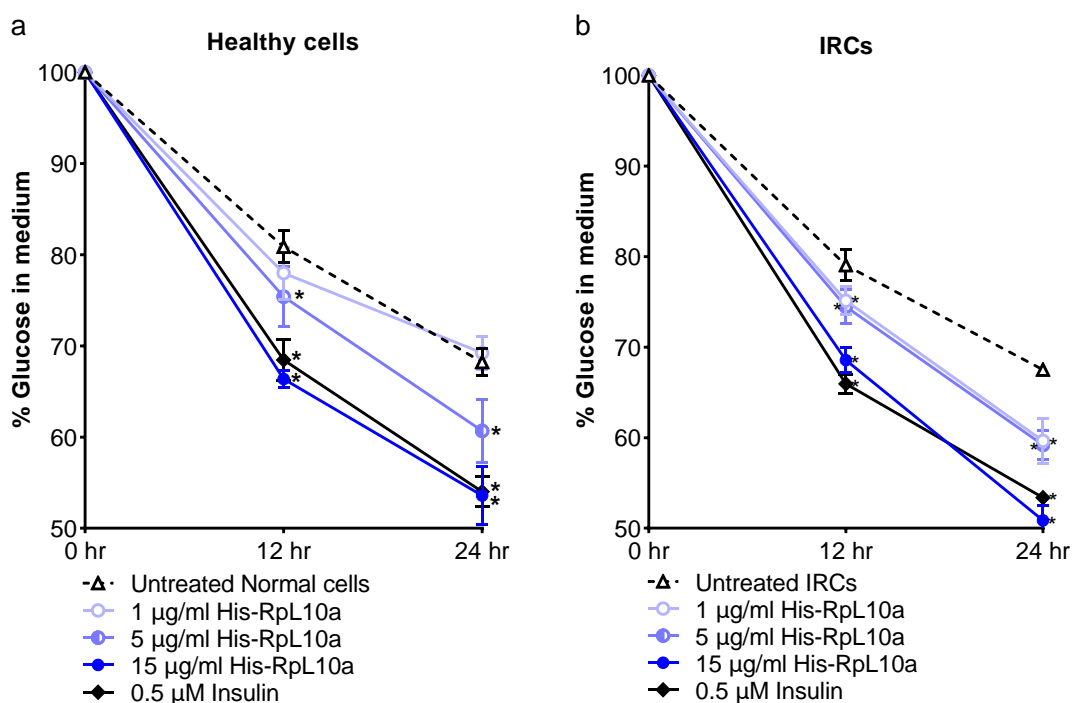


Figure 35. His-RpL10a increase the glucose uptake by healthy cells and insulin resistant cells (IRCs). The healthy cells and IRCs were incubated with various concentrations of His-RpL10a protein. The glucose utilization rates in (a) healthy cells and (b) IRCs were measured during His-RpL10a stimulation compared with the glucose utilization rates in untreated cells. The cells incubated with 0.5 µM insulin served as a control. The statistical data were analyzed using an independent-samples *t*-test. The asterisks indicate a significant differences compared with untreated cells ($P < 0.05$).

3. Effect of RpL10a on glucose metabolism-related gene expression in IRCs

Besides, the interesting genes involved in carbohydrate metabolism were evaluated, including *hexokinase*, the rate-limiting enzyme in glycolysis (Beutler, 1972; Robey and Hay, 2006) and *glucose 6-phosphatase*, last step enzymes play a role in glucose synthesis in the gluconeogenesis pathway (Nordlie, 1985). The expression of glycolysis and gluconeogenesis genes was changed after RpL10a treatment. The qPCR result showed the expression of the *hexokinase 1 (Hk1)* gene, which plays a role in converting glucose to glucose-6-phosphate (G6K) in the glycolysis pathway up-regulated. On the other hand, *Glucose-6-phosphatase 3 (G6pc3)* gene encoding glucose 6-phosphatase enzyme, which is the key enzyme in gluconeogenesis, was down-regulated (Figure 36). This result reveals that RpL10a alters the expression of these genes to increase the glycolysis and decrease the gluconeogenesis.

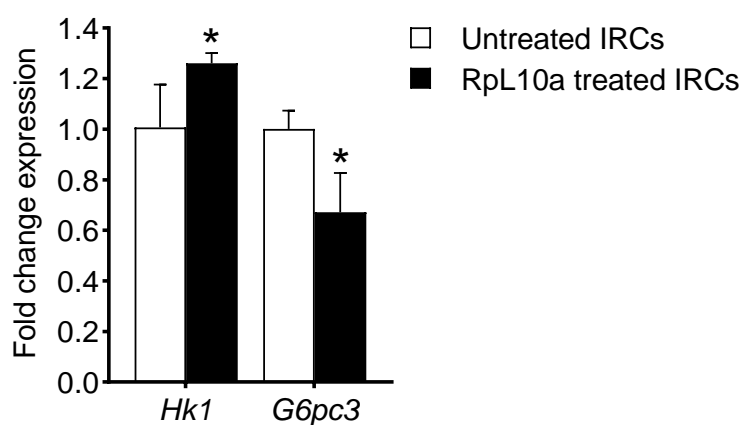


Figure 36. RpL10a changes the glucose metabolism-related genes expression. The fold changes expression of *Hk1* and *G6pc3* in IRCs incubated with 1 $\mu\text{g/ml}$ His-RpL10a was compared with their levels in untreated cells. The gene expression was normalised with the β -actin gene. The statistical significance were analyzed using an independent-samples *t*-test. The asterisks indicate significant differences ($P < 0.05$).

All these findings reveal that RpL10a could induce the cells to increase the glucose uptake level. And the glucose was then converted to G6P, which is the intermediate product in the glycolysis pathway. Therefore we suggest that the binding between RpL10a and InR can stimulate the insulin signaling pathway along with the glucose metabolism. However, the RpL10a should be tried in diabetic animals to confirm a potential application as an insulin-mimetic in the future.

CHAPTER 5

CONCLUSIONS

1. The excess of RpL10a induce insulin signaling pathway in RpL10a-overexpressed flies

The overexpression of RpL10a in the eyes of RpL10a-overexpressed flies (*GMR-GAL4; UAS-RpL10a*) induced the expression of InR in both mRNA and protein level and increased the phosphorylation level of some insulin signaling mediator, including Akt and dFOXO. This effect increased carbohydrate utilization and suppressed glycogenesis. RpL10a also induced the expression of the *Shc* gene involved in cell proliferation. This evidence indicating that RpL10a has a role in controlling the metabolism and cell proliferation via insulin signaling pathway which is supported by the eyes morphology of RpL10a-overexpressed flies showed the death of red pigment cells in the center of the eyes.

2. RpL10a could bind to the InR at a different binding site than insulin

The *in silico* binding result showed that the shrimp RpL10a protein could interact with the human InR protein at the FnIII domain of InR and the RpL10a-InR binding site located on the regions different from the insulin-InR binding site. RpL10a interacted with InR at amino acid residues 635–640 and 697–702 of the InR. While InR bound to the InR at residues 704–710. The binding of InR FnIII domain and RpL10a was confirmed by GST pull-down and the immunofluorescence result showed the His-RpL10a binding at the site where the InR exists. The RpL10a-InR binding at a different site from insulin may help treat insulin resistance people in the future.

3. The RpL10a induce the glucose uptake in CHO-S cells after binding with InR

After incubating CHO-S cells with His-RpL10a (1 μ M for 24 h). The His-RpL10a bound to CHO InR and induced the phosphorylation of Akt. This binding effect also increased the glucose utilization by cells after incubating with His-RpL10a (0.1–1 μ M). The glucose uptake assay suggested that the cells' induction to use glucose by RpL10a occurred by inducing the uptake of glucose by the cells.

4. RpL10a could alleviate the insulin resistance by stimulating the glucose uptake into the cells

A minimum dose of His-RpL10a (1 μ g/ml) was sufficient to induce glucose uptake by IRCs, the cells induced under high glucose (50 mM) condition. This dose of His-RpL10a could not induce the glucose uptake by healthy cells, but the cells require ≥ 5 μ g/ml of His-RpL10a to induce glucose uptake. The result indicated that RpL10a induced glucose uptake in IRCs better than in healthy cells. Moreover, RpL10a also increased glycolysis by inducing the expression of *Hk* and suppressed the glucose synthesis in the cells by suppressing the *G6pc* expression. This result revealed that RpL10a could alleviate insulin resistance by stimulating glucose utilization and suppressing glucose synthesis.

Future works

1. The extra-ribosomal function of RpL10a that acts as insulin-mimetic should be investigated in diabetes animal model (*in vivo*)
2. Investigate the effect of RpL10a on the expression profile of other insulin signaling mediators involved in carbohydrate metabolism and cell proliferation.
3. Study the effect of RpL10a on glucose transportation.

REFERENCES

- Accili, D., Arden, K.C., 2004. FoxOs at the crossroads of cellular metabolism, differentiation, and transformation. *Cell*. [https://doi.org/10.1016/S0092-8674\(04\)00452-0](https://doi.org/10.1016/S0092-8674(04)00452-0)
- Babu, S., Krishnan, M., Rajagopal, P., Periyasamy, V., Veeraraghavan, V., Govindan, R., Jayaraman, S., 2020. Beta-sitosterol attenuates insulin resistance in adipose tissue via IRS-1/Akt mediated insulin signaling in high fat diet and sucrose induced type-2 diabetic rats. *Eur. J. Pharmacol.* 873, 173004. <https://doi.org/10.1016/j.ejphar.2020.173004>
- Baik, I.H., Jo, G.H., Seo, D., Ko, M.J., Cho, C.H., Lee, M.G., Lee, Y.H., 2016. Knockdown of RPL9 expression inhibits colorectal carcinoma growth via the inactivation of Id-1/NF- κ B signaling axis. *Int. J. Oncol.* 49, 1953–1962. <https://doi.org/10.3892/ijo.2016.3688>
- Balcer-Kubiczek, E.K., Meltzer, S.J., Han, L.H., Zhang, X.F., Shi, Z.M., Harrison, G.H., Abraham, J.M., 1997. Csa-19, a radiation-responsive human gene, identified by an unbiased two-gel cDNA library screening method in human cancer cells. *Oncogene* 14, 3051–3057. <https://doi.org/10.1038/sj.onc.1201151>
- Belfiore, A., Frasca, F., Pandini, G., Sciacca, L., Vigneri, R., 2009. Insulin receptor isoforms and insulin receptor/insulin-like growth factor receptor hybrids in physiology and disease. *Endocr. Rev.* <https://doi.org/10.1210/er.2008-0047>
- Benkert, P., Biasini, M., Schwede, T., 2011. Toward the estimation of the absolute quality of individual protein structure models 27, 343–350. <https://doi.org/10.1093/bioinformatics/btq662>
- Beutler, E., 1972. Disorders due to enzyme defects in the red blood cell. *Adv. Metab. Disord.* <https://doi.org/10.1016/b978-0-12-027306-5.50010-3>
- Birnboim, H.C., Doly, J., 1979. A rapid alkaline extraction procedure for screening recombinant plasmid DNA, *Nucleic Acids Research*.
- Bloch-Damti, A., Bashan, N., 2005. Proposed mechanisms for the induction of insulin

- resistance by oxidative stress. *Antioxidants Redox Signal.*
<https://doi.org/10.1089/ars.2005.7.1553>
- Bluestone, J.A., Herold, K., Eisenbarth, G., 2010. Genetics, pathogenesis and clinical interventions in type 1 diabetes. *Nature.* <https://doi.org/10.1038/nature08933>
- Boucher, J., Tseng, Y.H., Kahn, C.R., 2010. Insulin and insulin-like growth factor-1 receptors act as ligand-specific amplitude modulators of a common pathway regulating gene transcription. *J. Biol. Chem.* 285, 17235–17245.
<https://doi.org/10.1074/jbc.M110.118620>
- Brand, H., Perrimon, N., 1993. Targeted gene expression as a means of altering cell fates and generating dominant phenotypes. *Development* 118, 401–415.
- Brogiolo, W., Stocker, H., Ikeya, T., Rintelen, F., Fernandez, R., Hafen, E., 2001. An evolutionarily conserved function of the *Drosophila* insulin receptor and insulin-like peptides in growth control. *Curr. Biol.* 11, 213–21.
[https://doi.org/10.1016/s0960-9822\(01\)00068-9](https://doi.org/10.1016/s0960-9822(01)00068-9)
- Brown, M.R., Clark, K.D., Gulia, M., Zhao, Z., Garczynski, S.F., Crim, J.W., Suderman, R.J., Strand, M.R., 2008. An insulin-like peptide regulates egg maturation and metabolism in the mosquito *Aedes aegypti*. *Proc. Natl. Acad. Sci. U. S. A.* 105, 5716–5721. <https://doi.org/10.1073/pnas.0800478105>
- Buranasin, P., Mizutani, K., Iwasaki, K., Pawaputanon Na Mahasarakham, C., Kido, D., Takeda, K., Izumi, Y., 2018. High glucose-induced oxidative stress impairs proliferation and migration of human gingival fibroblasts. *PLoS One* 13, e0201855. <https://doi.org/10.1371/journal.pone.0201855>
- Campbell, R.K., 2009. Type 2 diabetes: Where we are today: An overview of disease burden, current treatments, and treatment strategies. *J. Am. Pharm. Assoc.* 49, S3–S9. <https://doi.org/10.1331/JAPhA.2009.09077>
- Chaichanit, N., Wonglapsuwan, M., Chotigeat, W., 2018. Ribosomal protein L10A and signaling pathway. *Gene* 674, 170–177.
<https://doi.org/10.1016/J.GENE.2018.06.081>

- Chang, C.-I., Chou, C.-H., Liao, M.-H., Chen, T.-M., Cheng, C.-H., Anggriani, R., Tsai, C.-P., Tseng, H.-I., Cheng, H.-L., 2015. Bitter melon triterpenes work as insulin sensitizers and insulin substitutes in insulin-resistant cells. *J. Funct. Foods* 13, 214–224. <https://doi.org/10.1016/j.jff.2014.12.050>
- Chang, C.I., Hsu, C.M., Li, T.S., Huang, S. Da, Lin, C.C., Yen, C.H., Chou, C.H., Cheng, H.L., 2014. Constituents of the stem of *Cucurbita moschata* exhibit antidiabetic activities through multiple mechanisms. *J. Funct. Foods* 10, 260–273. <https://doi.org/10.1016/j.jff.2014.06.017>
- Chang, C.I., Tseng, H.I., Liao, Y.W., Yen, C.H., Chen, T.M., Lin, C.C., Cheng, H.L., 2011. *In vivo* and *in vitro* studies to identify the hypoglycaemic constituents of *Momordica charantia* wild variant WB24. *Food Chem.* 125, 521–528. <https://doi.org/10.1016/j.foodchem.2010.09.043>
- Chen, J., Kaitsuka, T., Fujino, R., Araki, K., Tomizawa, K., Yamamoto, T., 2016. Mutation of the key residue for extraribosomal function of ribosomal protein S19 cause increased grooming behaviors in mice. *Neurosci. Lett.* 629, 221–226. <https://doi.org/10.1016/j.neulet.2016.07.022>
- Chien, S., Reiter, L.T., Bier, E., Gribskov, M., 2002. Homophila: Human disease gene cognates in *Drosophila*. *Nucleic Acids Res.* 30, 149–151. <https://doi.org/10.1093/nar/30.1.149>
- Cho, K.S., Bang, S.M., Toh, A., 2014. Lipids and Lipid Signaling in *Drosophila* Models of Neurodegenerative Diseases, in: *Omega-3 Fatty Acids in Brain and Neurological Health*. Elsevier, pp. 327–336. <https://doi.org/10.1016/b978-0-12-410527-0.00026-0>
- Choismel, V., Bacqueville, D., Rouquette, J., Noaillac-Depeyre, J., Fribourg, S., Crétien, A., Leblanc, T., Tchernia, G., Da Costa, L., Gleizes, P.E., 2007. Impaired ribosome biogenesis in Diamond-Blackfan anemia. *Blood* 109, 1275–1283. <https://doi.org/10.1182/blood-2006-07-038372>
- Choismel, V., Fribourg, S., Aguisa-Touré, A.H., Pinaud, N., Legrand, P., Gazda, H.T., Gleizes, P.E., 2008. Mutation of ribosomal protein RPS24 in Diamond-Blackfan

- anemia results in a ribosome biogenesis disorder. *Hum. Mol. Genet.* 17, 1253–1263. <https://doi.org/10.1093/hmg/ddn015>
- Cohen, P., Frame, S., 2001. The renaissance of GSK3. *Nat. Rev. Mol. Cell Biol.* <https://doi.org/10.1038/35096075>
- Croll, T.I., Smith, B.J., Margetts, M.B., Whittaker, J., Weiss, M.A., Ward, C.W., Lawrence, M.C., 2016. Higher-Resolution Structure of the Human Insulin Receptor Ectodomain: Multi-Modal Inclusion of the Insert Domain. *Structure* 24, 469–476. <https://doi.org/10.1016/j.str.2015.12.014>
- de la Cruz, J., Karbstein, K., Woolford, J.L., 2015. Functions of ribosomal proteins in assembly of eukaryotic ribosomes *in vivo*. *Annu. Rev. Biochem.* 84, 93–129. <https://doi.org/10.1146/annurev-biochem-060614-033917>
- De Meyts, P., 2008. The insulin receptor: a prototype for dimeric, allosteric membrane receptors? *Trends Biochem. Sci.* <https://doi.org/10.1016/j.tibs.2008.06.003>
- De Meyts, P., 2000. *The Insulin Receptor and Its Signal Transduction Network*, Endotext.
- Dieci, G., Ruotolo, R., Braglia, P., Carles, C., Carpentieri, A., Amoresano, A., Ottonello, S., 2009. Positive modulation of RNA polymerase III transcription by ribosomal proteins. *Biochem. Biophys. Res. Commun.* 379, 489–493. <https://doi.org/10.1016/j.bbrc.2008.12.097>
- Drummond-Barbosa, D., Spradling, A.C., 2001. Stem cells and their progeny respond to nutritional changes during *Drosophila* oogenesis. *Dev. Biol.* 231, 265–278. <https://doi.org/10.1006/dbio.2000.0135>
- Duffy, J.B., 2002. GAL4 system in *Drosophila*: A fly geneticist's Swiss army knife. *Genesis.* <https://doi.org/10.1002/gene.10150>
- Ebeling, P., Koistinen, H.A., Koivisto, V.A., 1998. Insulin-independent glucose transport regulates insulin sensitivity. *FEBS Lett.* 436, 301–303. [https://doi.org/10.1016/S0014-5793\(98\)01149-1](https://doi.org/10.1016/S0014-5793(98)01149-1)
- Fischer, J.A., Giniger, E., Maniatis, T., Ptashne, M., 1988. GAL4 activates transcription

- in *Drosophila*. *Nature* 332, 853–856. <https://doi.org/10.1038/332853a0>
- Fisicaro, N., Katerelos, M., Williams, J., Power, D., D'Apice, A., Pearce, M., 1995. Identification of genes downregulated in the thymus by cyclosporin-A: Preliminary characterization of clone CSA-19. *Mol. Immunol.* 32, 565–572. [https://doi.org/10.1016/0161-5890\(95\)00032-A](https://doi.org/10.1016/0161-5890(95)00032-A)
- Flygare, J., Aspesi, A., Bailey, J.C., Miyake, K., Caffrey, J.M., Karlsson, S., Ellis, S.R., 2007. Human RPS19, the gene mutated in Diamond-Blackfan anemia, encodes a ribosomal protein required for the maturation of 40S ribosomal subunits. *Blood* 109, 980–986. <https://doi.org/10.1182/blood-2006-07-038232>
- GOLDFINE, I.D., 1987. The Insulin Receptor: Molecular Biology and Transmembrane Signaling*. *Endocr. Rev.* 8, 235–255. <https://doi.org/10.1210/edrv-8-3-235>
- Harris, T.E., Lawrence, J.C., 2003. TOR signaling. *Sci. STKE*. <https://doi.org/10.1126/stke.2122003re15>
- Heijnen, H.F., van Wijk, R., Pereboom, T.C., Goos, Y.J., Seinen, C.W., van Oirschot, B.A., van Dooren, R., Gastou, M., Giles, R.H., van Solinge, W., Kuijpers, T.W., Gazda, H.T., Bierings, M.B., Da Costa, L., MacInnes, A.W., 2014. Ribosomal Protein Mutations Induce Autophagy through S6 Kinase Inhibition of the Insulin Pathway. *PLoS Genet.* 10. <https://doi.org/10.1371/journal.pgen.1004371>
- Hermann-Le Denmat, S., Sipiczki, M., Thuriaux, P., 1994. Suppression of yeast RNA polymerase III mutations by the URP2 gene encoding a protein homologous to the mammalian ribosomal protein S20. *J. Mol. Biol.* <https://doi.org/10.1006/jmbi.1994.1412>
- Jager, J., Grémeaux, T., Cormont, M., Le Marchand-Brustel, Y., Tanti, J.F., 2007. Interleukin-1 β -induced insulin resistance in adipocytes through down-regulation of insulin receptor substrate-1 expression. *Endocrinology* 148, 241–251. <https://doi.org/10.1210/en.2006-0692>
- Johnson, A.M.F., Olefsky, J.M., 2013. The origins and drivers of insulin resistance. *Cell*. <https://doi.org/10.1016/j.cell.2013.01.041>

- Jung, S.O., Lee, J.Y., Kim, J., 2001. Yeast ribosomal protein S3 has an endonuclease activity on AP DNA. *Mol. Cells* 12, 84–90.
- Jünger, M.A., Rintelen, F., Stocker, H., Wasserman, J.D., Végh, M., Radimerski, T., Greenberg, M.E., Hafen, E., 2003. The *Drosophila* Forkhead transcription factor FOXO mediates the reduction in cell number associated with reduced insulin signaling. *J. Biol.* <https://doi.org/10.1186/1475-4924-2-20>
- Keith Campbell, R., 2009. Type 2 diabetes: Where we are today: An overview of disease burden, current treatments, and treatment strategies. *J. Am. Pharm. Assoc.* 49, S3–S9. <https://doi.org/10.1331/JAPhA.2009.09077>
- Kelly, S.M., Elchert, A., Kahl, M., 2017. Dissection and immunofluorescent staining of mushroom body and photoreceptor neurons in adult *Drosophila melanogaster* brains. *J. Vis. Exp.* 2017, 56174. <https://doi.org/10.3791/56174>
- Koga, M., Shichijo, S., Yamada, A., Ashihara, J., Sawamizu, H., Kusukawa, J., Itoh, K., 2003. Identification of ribosomal proteins S2 and L10a as tumor antigens recognized by HLA-A26-restricted CTL. *Tissue Antigens* 61, 136–145. <https://doi.org/10.1046/j.0001-2815.2002.00009.x>
- Laemmli, U.K., 1970. Cleavage of structural proteins during the assembly of the head of bacteriophage T4. *Nature* 227, 680–685. <https://doi.org/10.1038/227680a0>
- Li, Y., Kim, J., Li, J., Liu, F., Liu, X., Himmeldirk, K., Ren, Y., Wagner, T.E., Chen, X., 2005. Natural anti-diabetic compound 1,2,3,4,6-penta-O-galloyl-D-glucopyranose binds to insulin receptor and activates insulin-mediated glucose transport signaling pathway. *Biochem. Biophys. Res. Commun.* 336, 430–437. <https://doi.org/10.1016/j.bbrc.2005.08.103>
- Lo, K.A., Labadorf, A., Kennedy, N.J., Han, M.S., Yap, Y.S., Matthews, B., Xin, X., Sun, L., Davis, R.J., Lodish, H.F., Fraenkel, E., 2013. Analysis of *In Vitro* Insulin-Resistance Models and Their Physiological Relevance to *In Vivo* Diet-Induced Adipose Insulin Resistance. *Cell Rep.* 5, 259–270. <https://doi.org/10.1016/j.celrep.2013.08.039>
- Lovell, S.C., Davis, I.W., Arendall, W.B., De Bakker, P.I.W., Word, J.M., Prisant,

- M.G., Richardson, J.S., Richardson, D.C., 2003. Structure validation by $C\alpha$ geometry: ϕ, ψ and $C\beta$ deviation. *Proteins Struct. Funct. Genet.* 50, 437–450. <https://doi.org/10.1002/prot.10286>
- Lowry, O.H., Rosebrough, N.J., Farr, A.L., Randall, R.J., 1951. PROTEIN MEASUREMENT WITH THE FOLIN PHENOL REAGENT*. *J. Biol. Chem.* 193, 265–275.
- Lu, H., Zhu, Y.F., Xiong, J., Wang, R., Jia, Z., 2015. Potential extra-ribosomal functions of ribosomal proteins in *Saccharomyces cerevisiae*. *Microbiol. Res.* <https://doi.org/10.1016/j.micres.2015.05.004>
- Manchem, V.P., Goldfine, I.D., Kohanski, R.A., Cristobal, C.P., Lum, R.T., Schow, S.R., Shi, S., Spevak, W.R., Laborde, E., Toavs, D.K., Villar, H.O., Wick, M.M., Kozlowski, M.R., 2001. A novel small molecule that directly sensitizes the insulin receptor in vitro and in vivo. *Diabetes* 50, 824–830. <https://doi.org/10.2337/diabetes.50.4.824>
- Marygold, S.J., Roote, J., Reuter, G., Lambertsson, A., Ashburner, M., Millburn, G.H., Harrison, P.M., Yu, Z., Kenmochi, N., Kaufman, T.C., Leever, S.J., Cook, K.R., 2007. The ribosomal protein genes and Minute loci of *Drosophila melanogaster*. *Genome Biol.* 8, 216. <https://doi.org/10.1186/gb-2007-8-10-r216>
- McCall, K., 2004. Eggs over easy: Cell death in the *Drosophila* ovary. *Dev. Biol.* <https://doi.org/10.1016/j.ydbio.2004.07.017>
- Menting, J.G., Whittaker, J., Margetts, M.B., Whittaker, L.J., Kong, G.K.W., Smith, B.J., Watson, C.J., Žáková, L., Kletvíková, E., Jiráček, J., Chan, S.J., Steiner, D.F., Dodson, G.G., Brzozowski, A.M., Weiss, M.A., Ward, C.W., Lawrence, M.C., 2013. How insulin engages its primary binding site on the insulin receptor. *Nature* 493, 241–245. <https://doi.org/10.1038/nature11781>
- Millburn, G.H., Crosby, M.A., Gramates, L.S., Tweedie, S., Gelbart, W., Perrimon, N., Extavour, C., Broll, K., Dos Santos, G., Emmert, D., Falls, K., Matthews, B., Gelbart, S.R., Schroeder, A., Tabone, C., Zhou, P., Zytovicz, M., Brown, N., Antonazzo, G., Attrill, H., Costa, M., Marygold, S., Ponting, L., Rey, A., Staudt,

- N., Stefancsik, R., Urbano, J.M., Kaufman, T., Goodman, J., Grumbling, G., Strelets, V., Thurmond, J., Cripps, R., Werner-Washburne, M., Baker, P., 2016. Fly Base portals to human disease research using *Drosophila* Models. *DMM Dis. Model. Mech.* 9, 245–252. <https://doi.org/10.1242/dmm.023317>
- Mirzoyan, Z., Sollazzo, M., Allocca, M., Valenza, A.M., Grifoni, D., Bellosta, P., 2019. *Drosophila melanogaster*: A model organism to study cancer. *Front. Genet.* <https://doi.org/10.3389/fgene.2019.00051>
- Moura, L.F.W.G., da Silva Costa, H.P., da Silva Neto, J.X., Dias, L.P., Magalhães, F.E.A., van Tilburg, M.F., Florean, E.O.P.T., de Oliveira, J.T.A., Oliveira Bezerra de Sousa, D. de, Guedes, M.I.F., 2020. Orally hypoglycemic activity of an insulin mimetic glycoprotein isolated from *Cnidoscolus quercifolius* Pohl. (Euphorbiaceae) seeds, Cq-IMP. *Int. J. Biol. Macromol.* 159, 886–895. <https://doi.org/10.1016/j.ijbiomac.2020.05.033>
- Narla, A., Ebert, B.L., 2010. Ribosomopathies: Human disorders of ribosome dysfunction. *Blood.* <https://doi.org/10.1182/blood-2009-10-178129>
- Nelson, B.A., Robinson, K.A., Buse, M.G., 2000. High glucose and glucosamine induce insulin resistance via different mechanisms in 3T3-L1 adipocytes. *Diabetes* 49, 981–991. <https://doi.org/10.2337/diabetes.49.6.981>
- Nguyen, M.T.A., Satoh, H., Favelyukis, S., Babendure, J.L., Imamura, T., Sbodio, J.I., Zalevsky, J., Dahiyat, B.I., Chi, N.W., Olefsky, J.M., 2005. JNK and tumor necrosis factor- α mediate free fatty acid-induced insulin resistance in 3T3-L1 adipocytes. *J. Biol. Chem.* 280, 35361–35371. <https://doi.org/10.1074/jbc.M504611200>
- Nordlie, R.C., 1985. Fine tuning of blood glucose concentrations. *Trends Biochem. Sci.* [https://doi.org/10.1016/0968-0004\(85\)90236-1](https://doi.org/10.1016/0968-0004(85)90236-1)
- Olefsky, J.M., Glass, C.K., 2009. Macrophages, inflammation, and insulin resistance. *Annu. Rev. Physiol.* <https://doi.org/10.1146/annurev-physiol-021909-135846>
- Palasin, K., Makkapan, W., Thongnoi, T., Chotigeat, W., 2014. Stimulation of ovarian development in white shrimp, *Fenneropenaeus merguensis* De Man, with a

- recombinant ribosomal protein L10a. *Aquaculture* 432, 38–45.
<https://doi.org/10.1016/j.aquaculture.2014.04.025>
- Palasin, K., Makkapan, W., Wonglapsuwan, M., Chotigeat, W., 2019. Effect of a recombinant ribosomal protein L10a (rRpL10a) on mouse spermatogenesis. Discovery Service for Prince of Songkla University. *Songklanakarin J. Sci. Technol.* 41, 959–965.
- Pandey, U.B., Nichols, C.D., 2011. Human disease models in *Drosophila melanogaster* and the role of the fly in therapeutic drug discovery. *Pharmacol. Rev.* 63, 411–436. <https://doi.org/10.1124/pr.110.003293>
- Patti, M.E., Kahn, B.B., 2004. Nutrient sensor links obesity with diabetes risk. *Nat. Med.* <https://doi.org/10.1038/nm1004-1049>
- Pende, M., Kozma, S.C., Jaquet, M., Oorschot, V., Burcelin, R., Le Marchand-Brustel, Y., Klumperman, J., Thorens, B., Thomas, G., 2000. Hypoinsulinaemia, glucose intolerance and diminished β -cell size in S6K1-deficient mice. *Nature* 408, 994–997. <https://doi.org/10.1038/35050135>
- Peng, H., Zhao, Y., Chen, J., Huo, J., Zhang, Y., Xiao, T., 2019. Knockdown of ribosomal protein S3 causes preimplantation developmental arrest in mice. *Theriogenology* 129, 77–81.
<https://doi.org/10.1016/j.theriogenology.2019.02.022>
- Poloz, Y., Stambolic, V., 2015. Obesity and cancer, a case for insulin signaling. *Cell Death Dis.* <https://doi.org/10.1038/cddis.2015.381>
- Pritchett, T.L., McCall, K., 2012. Role of the insulin/Tor signaling network in starvation-induced programmed cell death in *Drosophila* oogenesis. *Cell Death Differ.* 19, 1069–1079. <https://doi.org/10.1038/cdd.2011.200>
- Qiang, G., Xue, S., Yang, J.J., Du, G., Pang, X., Li, X., Goswami, D., Griffin, P.R., Ortlund, E.A., Chan, C.B., Ye, K., 2014. Identification of a Small Molecular Insulin Receptor Agonist With Potent Antidiabetes Activity. *Diabetes* 63, 1394–1409. <https://doi.org/10.2337/db13-0334>

- Regazzetti, C., Peraldi, P., Grémeaux, T., Najem-Lendom, R., Ben-Sahra, I., Cormont, M., Bost, F., Marchand-Brustel, Y. Le, Tanti, J.F., Giorgetti-Peraldi, S., 2009. Hypoxia decreases insulin signaling pathways in adipocytes. *Diabetes* 58, 95–103. <https://doi.org/10.2337/db08-0457>
- Robey, R.B., Hay, N., 2006. Mitochondrial hexokinases, novel mediators of the antiapoptotic effects of growth factors and Akt. *Oncogene*. <https://doi.org/10.1038/sj.onc.1209595>
- Ross, S.A., Chen, X., Hope, H.R., Sun, S., McMahon, E.G., Broschat, K., Gulve, E.A., 2000. Development and Comparison of Two 3T3-L1 Adipocyte Models of Insulin Resistance: Increased Glucose Flux vs Glucosamine Treatment. *Biochem. Biophys. Res. Commun.* 273, 1033–1041. <https://doi.org/10.1006/bbrc.2000.3082>
- Rotter, V., Nagaev, I., Smith, U., 2003. Interleukin-6 (IL-6) Induces Insulin Resistance in 3T3-L1 Adipocytes and Is, Like IL-8 and Tumor Necrosis Factor- α , Overexpressed in Human Fat Cells from Insulin-resistant Subjects. *J. Biol. Chem.* 278, 45777–45784. <https://doi.org/10.1074/jbc.M301977200>
- Rujkijyanont, P., Adams, S.L., Beyene, J., Dror, Y., 2009. Bone marrow cells from patients with Shwachman-Diamond syndrome abnormally express genes involved in ribosome biogenesis and RNA processing. *Br. J. Haematol.* 145, 806–815. <https://doi.org/10.1111/j.1365-2141.2009.07692.x>
- Saetan, U., Sangket, U., Deachamag, P., Chotigeat, W., 2016. Ovarian Transcriptome Analysis of Vitellogenic and Non-Vitellogenic Female Banana Shrimp (*Fenneropenaeus merguensis*). *PLoS One* 11, e0164724. <https://doi.org/10.1371/journal.pone.0164724>
- Sakoda, H., Ogihara, T., Anai, M., Funaki, M., Inukai, K., Katagiri, H., Fukushima, Y., Onishi, Y., Ono, H., Fujishiro, M., Kikuchi, M., Oka, Y., Asano, T., 2000. Dexamethasone-induced insulin resistance in 3T3-L1 adipocytes is due to inhibition of glucose transport rather than insulin signal transduction. *Diabetes* 49, 1700–1708. <https://doi.org/10.2337/diabetes.49.10.1700>
- Samuel, V.T., Shulman, G.I., 2012. Mechanisms for insulin resistance: Common

- threads and missing links. *Cell*. <https://doi.org/10.1016/j.cell.2012.02.017>
- Sang, J.H., 2001. *Drosophila melanogaster*: The Fruit Fly. *Encycl. Genet. I*, 157.
- Schadt, E.E., Molony, C., Chudin, E., Hao, K., Yang, X., Lum, P.Y., Kasarskis, A., Zhang, B., Wang, S., Suver, C., Zhu, J., Millstein, J., Sieberts, S., Lamb, J., GuhaThakurta, D., Derry, J., Storey, J.D., Avila-Campillo, I., Kruger, M.J., Johnson, J.M., Rohl, C.A., van Nas, A., Mehrabian, M., Drake, T.A., Lusis, A.J., Smith, R.C., Guengerich, F.P., Strom, S.C., Schuetz, E., Rushmore, T.H., Ulrich, R., 2008. Mapping the Genetic Architecture of Gene Expression in Human Liver. *PLoS Biol.* 6, e107. <https://doi.org/10.1371/journal.pbio.0060107>
- Seino, S., Bell, G.I., 1989. Alternative splicing of human insulin receptor messenger RNA. *Biochem. Biophys. Res. Commun.* 159, 312–316. [https://doi.org/10.1016/0006-291X\(89\)92439-X](https://doi.org/10.1016/0006-291X(89)92439-X)
- Seong, K.M., Jung, S.O., Kim, H.D., Kim, H.J., Jung, Y.J., Choi, S.Y., Kim, J., 2012. Yeast ribosomal protein S3 possesses a β -lyase activity on damaged DNA. *FEBS Lett.* 586, 356–361. <https://doi.org/10.1016/j.febslet.2011.12.030>
- Shanik, M.H., Xu, Y., Krha, J.S., Dankner, R., Zick, Y., Roth, J., 2008. Insulin Resistance and Hyperinsulinemia Is hyperinsulinemia the cart or the horse? <https://doi.org/10.2337/dc08-s264>
- Shi, Z., Fujii, K., Kovary, K.M., Genuth, N.R., Röst, H.L., Teruel, M.N., Barna, M., 2017. Heterogeneous Ribosomes Preferentially Translate Distinct Subpools of mRNAs Genome-wide. *Mol. Cell* 67, 71–83.e7. <https://doi.org/10.1016/j.molcel.2017.05.021>
- Smith, B.J., Huang, K., Kong, G., Chan, S.J., Nakagawa, S., Menting, J.G., Hu, S.Q., Whittaker, J., Steiner, D.F., Katsoyannis, P.G., Ward, C.W., Weiss, M.A., Lawrence, M.C., 2010. Structural resolution of a tandem hormone-binding element in the insulin receptor and its implications for design of peptide agonists. *Proc. Natl. Acad. Sci. U. S. A.* 107, 6771–6776. <https://doi.org/10.1073/pnas.1001813107>
- Smith, T.R., Elmendorf, J.S., David, T.S., Turinsky, J., 1997. Growth hormone-induced

- insulin resistance: Role of the insulin receptor, IRS-1, GLUT-1, and GLUT-4. *Am. J. Physiol. - Endocrinol. Metab.* 272. <https://doi.org/10.1152/ajpendo.1997.272.6.e1071>
- Sun, L.L., Sun, Z.Y., Zhang, P., Zhai, X.W., Tang, J., Pan, Q.J., Shi, Q.H., Shen, W., 2010. Effect of insulin on oogenesis from mouse fetal germ cells in a serum-free 3D culture system. *Reprod. Biomed. Online* 20, 11–25. <https://doi.org/10.1016/j.rbmo.2009.11.001>
- Taniguchi, C.M., Emanuelli, B., Kahn, C.R., 2006. Critical nodes in signalling pathways: Insights into insulin action. *Nat. Rev. Mol. Cell Biol.* <https://doi.org/10.1038/nrm1837>
- Tremblay, F., Krebs, M., Dombrowski, L., Brehm, A., Bernroider, E., Roth, E., Nowotny, P., Waldhäusl, W., Marette, A., Roden, M., 2005. Overactivation of S6 kinase 1 as a cause of human insulin resistance during increased amino acid availability. *Diabetes* 54, 2674–2684. <https://doi.org/10.2337/diabetes.54.9.2674>
- Turtoi, A., Brown, I., Oskamp, D., Schneeweiss, F.H.A., 2008. Early gene expression in human lymphocytes after γ -irradiation - A genetic pattern with potential for biodosimetry. *Int. J. Radiat. Biol.* 84, 375–387. <https://doi.org/10.1080/09553000802029886>
- Ugur, B., Chen, K., Bellen, H.J., 2016. *Drosophila* tools and assays for the study of human diseases. *DMM Dis. Model. Mech.* <https://doi.org/10.1242/dmm.023762>
- Um, S.H., Frigerio, F., Watanabe, M., Picard, F., Joaquin, M., Sticker, M., Fumagalli, S., Allegrini, P.R., Kozma, S.C., Auwerx, J., Thomas, G., 2004. Absence of S6K1 protects against age- and diet-induced obesity while enhancing insulin sensitivity. *Nature* 431, 200–205. <https://doi.org/10.1038/nature02866>
- Van Handel, E., 1985a. Rapid determination of glycogen and sugars in mosquitoes. *J. Am. Mosq. Control Assoc.* 1, 299–301.
- Van Handel, E., 1985b. Rapid determination of total lipids in mosquitoes. *J. Am. Mosq. Control Assoc.* 1, 302–304.

- Wang, X., Gu, C., He, W., Ye, X., Chen, H., Zhang, X., Hai, C., 2012. Glucose oxidase induces insulin resistance via influencing multiple targets *in vitro* and *in vivo*: The central role of oxidative stress. *Biochimie* 94, 1705–1717. <https://doi.org/10.1016/j.biochi.2012.03.024>
- Ward, C.W., Lawrence, M.C., 2009. Ligand-induced activation of the insulin receptor: a multi-step process involving structural changes in both the ligand and the receptor. *BioEssays* 31, 422–434. <https://doi.org/10.1002/bies.200800210>
- Warner, J.R., McIntosh, K.B., 2009. How Common Are Extraribosomal Functions of Ribosomal Proteins? *Mol. Cell* 34, 3–11. <https://doi.org/10.1016/J.MOLCEL.2009.03.006>
- Waterhouse, A., Bertoni, M., Bienert, S., Studer, G., Tauriello, G., Gumienny, R., Heer, F.T., De Beer, T.A.P., Rempfer, C., Bordoli, L., Lepore, R., Schwede, T., 2018. SWISS-MODEL: homology modelling of protein structures and complexes. *Nucleic Acids Res.* 46, W296–W303. <https://doi.org/10.1093/nar/gky427>
- Wonglapsuwan, M., Chotigeat, W., Timmons, A., McCall, K., 2011. RpL10A regulates oogenesis progression in the banana prawn *Fenneropenaeus merguensis* and *Drosophila melanogaster*. *Gen. Comp. Endocrinol.* 173, 356–363. <https://doi.org/10.1016/j.ygcen.2011.06.012>
- Wonglapsuwan, M., Miyazaki, T., Loongyai, W., Chotigeat, W., 2010. Characterization and Biological Activity of the Ribosomal Protein L10a of the White Shrimp: *Fenneropenaeus merguensis* De Man During Vitellogenesis. *Mar. Biotechnol.* 12, 230–240. <https://doi.org/10.1007/s10126-009-9220-3>
- Wool, I.G., 1996. Extraribosomal functions of ribosomal proteins. *Trends Biochem. Sci.* 21, 164–165. [https://doi.org/10.1016/S0968-0004\(96\)20011-8](https://doi.org/10.1016/S0968-0004(96)20011-8)
- Xie, J., Wang, S., Ma, P., Ma, F., Li, J., Wang, W., Lu, F., Xiong, H., Gu, Y., Zhang, S., Xu, H., Yang, G., Lerner, R.A., 2020. Selection of Small Molecules that Bind to and Activate the Insulin Receptor from a DNA-Encoded Library of Natural Products. *iScience* 23, 101197. <https://doi.org/10.1016/j.isci.2020.101197>
- Xu, T., Kumar, S., Denton, D., 2017. Characterization of Autophagic Responses in

Drosophila melanogaster, in: Methods in Enzymology. Academic Press Inc., pp. 445–465. <https://doi.org/10.1016/bs.mie.2016.09.089>

Yamamoto, S., Jaiswal, M., Charng, W.L., Gambin, T., Karaca, E., Mirzaa, G., Wiszniewski, W., Sandoval, H., Haelterman, N.A., Xiong, B., Zhang, K., Bayat, V., David, G., Li, T., Chen, K., Gala, U., Harel, T., Pehlivan, D., Penney, S., Vissers, L.E.L.M., De Ligt, J., Jhangiani, S.N., Xie, Y., Tsang, S.H., Parman, Y., Sivaci, M., Battaloglu, E., Muzny, D., Wan, Y.W., Liu, Z., Lin-Moore, A.T., Clark, R.D., Curry, C.J., Link, N., Schulze, K.L., Boerwinkle, E., Dobyns, W.B., Allikmets, R., Gibbs, R.A., Chen, R., Lupski, J.R., Wangler, M.F., Bellen, H.J., 2014. A *Drosophila* genetic resource of mutants to study mechanisms underlying human genetic diseases. *Cell* 159, 200–214. <https://doi.org/10.1016/j.cell.2014.09.002>

Yoon, M.S., 2017. The role of mammalian target of rapamycin (mTOR) in insulin signaling. *Nutrients*. <https://doi.org/10.3390/nu9111176>

Zhang, B., Salituro, G., Szalkowski, D., Li, Z., Zhang, Y., Royo, I., Vilella, D., Díez, M.T., Pelaez, F., Ruby, C., Kendall, R.L., Mao, X., Griffin, P., Calaycay, J., Zierath, J.R., Heck, J. V., Smith, R.G., Moller, D.E., 1999. Discovery of a small molecule insulin mimetic with antidiabetic activity in mice. *Science* (80-.). 284, 974–977. <https://doi.org/10.1126/science.284.5416.974>

Zhang, Y., O’Leary, M.N., Peri, S., Wang, M., Zha, J., Melov, S., Kappes, D.J., Feng, Q., Rhodes, J., Amieux, P.S., Morris, D.R., Kennedy, B.K., Wiest, D.L., 2017. Ribosomal Proteins Rpl22 and Rpl2211 Control Morphogenesis by Regulating Pre-mRNA Splicing. *Cell Rep.* 18, 545–556. <https://doi.org/10.1016/j.celrep.2016.12.034>

Zick, Y., 2004. Uncoupling insulin signalling by serine/threonine phosphorylation: A molecular basis for insulin resistance, in: *Biochemical Society Transactions*. pp. 812–816. <https://doi.org/10.1042/BST0320812>

APPENDIX

APPENDIX A

1. Protein measurement with Lowry's method (Lowry et al., 1951)

Bovine serum albumin (BSA) was used as a protein standard for protein measurement. The stock BSA solution (100 mg/ml) was diluted to 1 mg/ml. The working standard BSA was prepared to a concentration of 6.25, 12.5, 25, 50, 100, and 200 µg/ml. Each concentration of BSA was made in duplicates with a final volume of 1 ml. The protein sample was diluted to a range of 1: 100–1: 1,000 in a final volume of 1 ml. The standard and sample solution were mixed with 1 ml of reagent A and stored at room temperature for 10 min. Then, 0.5 ml of reagent B was added and mixed rapidly before placing again at room temperature for 30 min. After 30 min, the standard and sample were read the protein content by determining the optical density at 750 nm. The concentration of protein sample was calculated from a standard curve of BSA.

2. SDS-polyacrylamide gel electrophoresis (SDS-PAGE) (Laemmli, 1970)

To Make the SDS-PAGE gel, the cleaned and dried glass plates, combs, clamp, and silicone spacer were prepared before assembling the gel cassette. Then, the separating gel with a 12% acrylamide was prepared in 5 ml, swirled, and quickly poured into the gel cassette between the glass plates and fill up to about 0.7 cm below the bottom of the comb position. A small layer of water was laid to the top of the gel prior to polymerization to straighten the level of the gel. The Separating gel was stored at room temperature for 30 min to form polymerization. This can be observed by a line between the water and stacking gel. Then, the water layer was completely poured off from the gel cassette before adding 3 ml of prepared stacking gel with a 5% acrylamide and putting the comb.

Table 11. Composition of 12% SDS-PAGE gel

Solution	Separating Gel (5 ml)	Stacking Gel (3 ml)
Water	1.7	2.1
30% Acrylamide mix ^a	2.0	0.5
1.5 M Tris (pH 8.8)	1.3	-
1.0 M Tris (pH 6.8)	-	0.38
10% SDS ^b	0.05	0.03
10% APS ^c	0.05	0.03
TEMED ^d	0.002	0.003

^a30% Acrylamide = acrylamide: N, N'-Methylenebisacrylamide, 29:1

^bSDS = sodium dodecyl sulfate

^cAPS = ammonium persulfate

^dTEMED = N,N,N',N' – tetramethylethylenediamine

After 30 min of polymerization, the gel cassette was removed from the casting stand and washed with running buffer before placing it in the electrophoresis tank. The running buffer was filled into the tank between the gel cassettes to fill the wells of the gel and filled in the region outside of the gel cassettes. The protein sample determined by Lowry's method was mixed with SDS gel loading buffer and boiled for 5 min before loading onto the prepared gel. The electrophoresis was carried out in the descending direction with Tris-glycine buffer (25 mM Tris-HCl, pH 6.8, 192 mM glycine and 0.1% (w/v) SDS) using a constant 100 V for 150 min or until the tracking dye reached the edge of the gel. The protein patterns were visualized by Coomassie blue staining.

3. Preparation of *E. coli* competent cells

A single colony of *E. coli* was inoculated into 10 ml of LB broth containing 10 µg/ml of tetracycline and incubated at 37°C overnight with 180 rpm. This culture, then, was inoculated in 90 ml of fresh LB medium (1:100 dilutions) and incubated at 37°C until the OD₅₉₀ reached 0.3–0.5. After that, the culture was placed on ice for 10 min. The cell pellet was harvested by centrifugation at 4,000 rpm for 10 min at 4°C and washed with 30 ml of cold 50 mM MgCl₂, 10 mM Tris-HCl, pH 8.0, and then incubated on ice for 30 min to establish competency. The cell suspension was centrifuged at 4,000 rpm for 10 min at 4°C. The pellets were suspended in 4 ml of cold 50 mM MgCl₂, 10 mM Tris-HCl, pH 8.0. A volume of 0.85 ml of glycerol was added into the 1.5 ml of cell suspension to give a 15% (w/v) final concentration. 200 µl aliquots of the cell suspension were dispensed per tube and stored at –80°C.

4. Agarose gel electrophoresis

For the gel, a 1.2% (w/v) of agarose gel in 0.5x TAE buffer (20 mM Tris-acetate, 0.5 mM EDTA) was melted and poured on a plastic tray, a comb was placed in the gel. After the agarose gel was completely set, the comb was carefully removed and the gel was installed on the electrophoresis tank containing 0.5x TAE buffer. The DNA or RNA samples were mixed with gel-loading dye and slowly loaded into the well of the gel. The electrophoresis was carried out at a constant 100 V for 15–30 min depending on the size and type of sample. Then, the gel was stained with 2.5 µg/ml of ethidium bromide solution for 5 min and destained with water for 15 min. After that the DNA or RNA patterns was observed with UVITEC Cambridge Gel Documentation System (BIO-RAD, USA).

APPENDIX B

1. Chemical stock solution and buffer

0.5 M EDTA (pH 8.0)

EDTA 93.06 g

Dissolve EDTA in 350 ml of distilled water. Adjust the pH to 8.0 with HCl. Adjust the volume of the solution to 500 ml with distilled water and sterilize by autoclaving.

100 mM PMSF

PMSF 0.174 g

Dissolve PMSF in 10 ml of isopropanol. Sterilize by filtration and store at -20°C .

2 M NaCl

NaCl 58.44 g

Dissolve NaCl in 400 ml of distilled water and adjust the volume to 500 ml with distilled water. Sterilize by autoclaving and store the solution at room temperature.

2 M Tris-HCl (pH 9.5)

Tris-HCl 121.14 g

Dissolve 121.1 g of Tris base in 400 ml of distilled water. Adjust the pH to 9.5 with HCl. Adjust the volume of the solution to 500 ml with distilled water and sterilize by autoclaving.

10% (w/v) SDS

SDS 50 g

Dissolve SDS in 400 ml of distilled water and adjust the volume to 500 ml with distilled water. Store at room temperature. Sterilization is not necessary.

1 N NaOH

NaOH 20 g

Dissolve NaOH in 400 ml of distilled water and adjust the volume to 500 ml with distilled water. Sterilize by autoclaving and store at room temperature.

1N HCl

Concentrated HCl (36–38% w/v) 7.3 ml

Slowly pour Concentrated HCl into 160 ml of distilled water and adjust the volume to 200 ml with distilled water. Store at room temperature.

100 mg/ml Bovine serum albumin (BSA)

BSA 1 g

Dissolve BSA in 8 ml of distilled water and adjust the volume to 10 ml with distilled water. Store at -20°C . Sterilization is not necessary.

DEPC-treated water

DEPC (Sigma) 0.5 ml

Distilled water 500 ml

Leave solution at room temperature for overnight and sterilize by autoclaving.

RNase A (10 mg/ml)

RNase A	10 mg
---------	-------

Dissolve and bring up to 1 ml with sterile distilled water. Boil in water for 5 min and store at -20°C.

2. Medium for *Drosophila melanogaster***Cornmeal, Molasses and Yeast Medium (Bloomington *Drosophila* Stock Center)**

Water	266 ml
Yeast	3.3 g
Yellow cornmeal	16.3 g
Agar	1.6 g
Molasses	20 ml
10% p-Hydroxy-benzoic acid methyl ester in 95% ethanol	3.8 ml

Dissolve the agar into 80% of the water before boiling until agar are completely dissolved. And dissolve the yeast in the remaining water (or save a bit for rinsing) at the same time, then mix with the cornmeal. Add the yeast/cornmeal/water mix into the boiled agar, stir, and add the molasses into the the yeast/cornmeal/agar/water mix. Use the remaining water to rinse the dregs into the cooking pot and then simmer for 5 to 10 minutes. Cool the medium for 5 minutes or more and carefully add p-Hydroxy-benzoic acid methyl ester into the medium. Then, pour the food into the culture tube.

3. Solution for ommatidia dissection and immuno staining

Phosphate-buffered saline (PBS, pH 7.4)

NaCl	8 g
KCl	0.2 g
Na ₂ HPO ₄	1.14 g
KH ₂ PO ₄	0.22 g

Dissolve the ingredients in 800 ml of distilled water. Adjust the pH to 7.4 with HCl. Adjust the volume to 1000 ml with distilled water. Sterilize the buffer by autoclaving and store at room temperature.

Fixative buffer

Graces medium	300 µl
16% Formaldehyde	100 µl
Heptane	200 µl

Washing buffer (PBST)

PBS	1000 ml
Tween 20	5 g

Mix the solution well and store at 4°C.

Blocking buffer (PBAF)

PBS	100 ml
Bovine serum albumin	0.5 g
Fetal calf serum	5 g

Mix the solution well and store at 4°C.

4. Lysis buffer for fly eyes

Tris-HCl	0.23 g
SDS	0.6 g
0.5 M EDTA	0.02 ml
100 mM PMSF	0.1 ml

Dissolve the ingredients in 8 ml of distilled water and adjust the volume to 10 ml with distilled water. Sterilize the buffer by filtration and store at 4°C.

5. Solution for Lowry's method**Copper tartrate carbonate solution (CTC solution)**

NaCO ₃	20 g
CuSO ₄ .5H ₂ O	1 g
Na-tartrate	2 g

Dissolve the ingredients in 800 ml of distilled water. Adjust the volume of the solution to 1000 ml with distilled water. Sterilization is not necessary.

Reagent A (CTC solution: 5% SDS: 0.8 N NaOH = 1: 2: 1 in volume)

CTC solution	10 ml
10% SDS	10 ml
1 N NaOH	8 ml

Mix the solutions and adjust the volume of the solution to 40 ml with distilled water and store at 4°C. Sterilization is not necessary.

Reagent B (2 N Folin-Ciocalteu phenol: H₂O = 1:5)

2 N Folin-Ciocalteu phenol	10 ml
H ₂ O	50 ml

Mix the solutions and store at 4°C. Sterilization is not necessary.

6. Solution for SDS-PAGE

30% Acrylamide solution

Acrylamide	29 g
N, N'-Methylenebisacrylamide	1 g

Dissolved acrylamide in 80 ml of distilled water and N, N' Methylene-bisacrylamide. Add distilled water to 100 ml.

1.5 M Tris-HCl (pH 8.8)

Tris-HCl	90.83 g
----------	---------

Dissolve Tris base in 400 ml of distilled water. Adjust the pH to 8.8 with concentrated HCl. Adjust the volume of the solution to 500 ml with distilled water and sterilize by autoclaving.

1 M Tris-HCl (pH 6.8)

Tris-HCl	60.6 g
----------	--------

Dissolve Tris base in 400 ml of distilled water. Adjust the pH to 6.8 with concentrated HCl. Adjust the volume of the solution to 500 ml with distilled water and sterilize by autoclaving.

10% Ammonium persulphate solution (APS)

APS	0.1 g
H ₂ O	1 ml

Mix APS in 1 ml of distilled water and Store at 4°C. Sterilization is not necessary.

10X Running buffer

Tris base	30 g
Glycine	144 g
SDS	10 g

Dissolve in 800 ml of distilled water and adjust the volume of the solution to 1000 ml with distilled water. The pH of the buffer should be 8.3 and no pH adjustment is required. Store at room temperature and dilute to 1X before use.

SDS gel-loading buffer (2X)

1 M Tris-HCl (pH 6.8)	1 ml
10% SDS	4 ml
Glycerol	2 ml
β -mercaptoethanol	0.14 ml
Bromophenol blue	0.02 g

Adjust the volume of the solution to 10 ml with distilled water and store at 4°C.

SDS gel-loading buffer (4X)

1 M Tris-HCl (pH 6.8)	2 ml
SDS	0.8 g
Glycerol	4 ml
β -mercaptoethanol	0.28 ml
Bromophenol blue	0.04 g

Adjust the volume of the solution to 10 ml with distilled water and store at 4°C.

7. Solution for SDS-PAGE gel staining

Coomassie Brilliant Blue staining solution

Coomassie Brilliant Blue R	1 g
Methanol	212.5 ml
Acetic acid	37.5 ml
Distilled water	250 ml

Mix the ingredients. Store at room temperature and protect from light.

Destaining I

Methanol	500 ml
Acetic acid	75 ml
Distilled water	425 ml

Mix the ingredients and store at room temperature.

Destaining II

Methanol	50 ml
Acetic acid	75 ml
Distilled water	875 ml

Mix the ingredients and store at room temperature.

8. Solution for Western blot analysis

Transfer buffer

Tris-HCl	0.605 g
Glycine	2.88 g
Methanol	40 ml

Dissolve Tris-HCl and Glycine in 100 ml of distilled water. Add methanol and adjust the volume to 200 ml with distilled water.

Tris-Buffered Saline (TBS, pH 7.5) for p-Akt and p-FOXO

Tris-HCl	3.029 g
KCl	0.186 g
NaCl	8.182 g

Dissolve the ingredients in 800 ml of distilled water. Adjust the pH to 7.4 with HCl. Adjust the volume to 1000 ml with distilled water. Sterilize the buffer by autoclaving and store at 4°C.

Washing buffer (TBST) for p-Akt and p-FOXO

TBS	999 ml
Tween 20	1 ml

Mix the solution well and store at 4°C.

Blocking buffer for p-Akt and p-dFOXO

TBST	20 ml
BSA	1 g

Mix the solution before using.

Blocking buffer for recombinant protein

PBS pH 7.4	20 ml
Tween 20	0.02 ml
Skim milk	1 g

Mix the solution before using.

Detection buffer (Alkaline phosphatase buffer)

2 M NaCl	500 μ l
2 M Tris-HCl pH 9.5	500 μ l
MgCl ₂	0.238 g

Mix the ingredients in 40 ml of distilled water and adjust the volume to 50 ml with distilled water.

Stop solution

Glacial acetic acid	1 ml
---------------------	------

Mix glacial acetic acid in 99 ml of distilled water to adjust the concentration to 1% v/v

9. Solution for agarose gel electrophoresis**50X TAE, Electrophoresis buffer**

Tris-base	242 g
Glacial acetic acid	57.1 ml
0.5 M EDTA, pH 8.0	100 ml

Dissolve the ingredients in distilled water and bring up to volume 1000 ml. Working solution in the gel and the buffer is 0.5X.

6X DNA loading dye

Glycerol	3 ml
0.5 M EDTA	1.2 ml
Bromophenol blue	25 mg

Mix the ingredients in 10 ml of distilled water and store at 4°C.

Ethidium bromide (10 mg/ml)

Ethidium bromide	1 g
Distilled water	100 ml

Stir on a magnetic stirrer for several hours to ensure that the dye has dissolved. Wrap the container in aluminum foil or transfer the solution to a dark bottle and store at room temperature.

10. Solution for carbohydrate determination**Glucose stock 1mg/ml**

Glucose	20 mg
25% Ethanol	20 ml

Mix the ingredients in 20 ml of 25% Ethanol and store at 4°C.

Trehalose stock 1mg/ml

Glucose	20 mg
25% Ethanol	20 ml

Mix the ingredients in 20 ml of 25% Ethanol and store at 4°C.

0.2% sodium sulfate (Na₂SO₄) solution

Na ₂ SO ₄	20 mg
Distilled water	10 ml

Mix the ingredients in 10 ml of distilled water and store at room temperature.

Anthrone reagent

Concentrated H ₂ SO ₄	380 ml
Anthrone	750 mg
Distilled water	150 ml

Carfully pour 380 ml of concentrated H₂SO₄ in 150 ml of cool distilled water. Dissolve 750 mg anthrone in this diluted sulfuric acid. Store at 4°C in dark.

11. Solution for lipid determination**Chloroform : Methanol 1:1**

Chloroform	20 ml
Methanol	20 ml

Mix the solution and store at 4°C.

Lipid stock 1 mg/ml

Commercial vegetable oil (e.g., soy bean oil)	20 mg
Chloroform	20 ml

Mix the solution and store at 4°C.

Vanillin-phosphoric acid reagent

Vanillin	600 mg
Distilled water	100 ml
85% phosphoric acid (H ₃ PO ₄)	400 ml

Dissolve 600 mg of vanillin in 100 ml hot water. Add 400 ml 85% phosphoric acid into diluted vanillin and store at 4°C in dark. The reagent is stable for several months, but should be discarded when it darkens.

12. Media and antibiotics for bacterial**Ampicillin (50 mg/ml)**

Ampicillin 50 mg

Dissolve in 1 ml of sterile distilled water. Store at -20°C .

Kanamycin (30 mg/ml)

Kanamycin 30 mg

Dissolve in 1 ml of sterile distilled water. Store at -20°C .

LB (Luria-Bertani) broth

Tryptone 10 g

Yeast extract 5 g

NaCl 5 g

Adjust the volume of the solution to 1000 ml with distilled water and sterilize by autoclaving for 20 min at 15 psi. Store at 4°C .

LB broth (supplement with 80 $\mu\text{g/ml}$ ampicillin)

Sterilized LB broth 100 ml

50 mg/ml Ampicillin stock 160 μl

Mix the ingredients well and store at 4°C .

LB agar (supplement with 80 µg/ml ampicillin)

Tryptone	2 g
Yeast extract	1 g
NaCl	1 g
Agar	3 g
50 mg/ml Ampicillin stock	320 µl

Adjust the volume of the solution to 200 ml with distilled water and sterilize by autoclaving for 20 min at 15 psi. Add 320 µl of ampicillin (50 mg/ml) into warm medium (50°C). The medium was poured into glass plate.

LB broth (supplement with 100 µg/ml ampicillin)

Sterilized LB broth	100 ml
50 mg/ml Ampicillin stock	200 µl

Mix the ingredients well and store at 4°C.

LB agar (supplement with 100 µg/ml ampicillin)

Tryptone	2 g
Yeast extract	1 g
NaCl	1 g
Agar	3 g
50 mg/ml Ampicillin stock	400 µl

Adjust the volume of the solution to 200 ml with distilled water and sterilize by autoclaving for 20 min at 15 psi. Add 400 µl of ampicillin (50 mg/ml) into warm medium (50°C). The medium was poured into glass plate.

LB broth (supplement with 30 µg/ml kanamycin)

Sterilized LB broth	1000 ml
30 mg/ml Kanamycin stock	1 ml

Mix the ingredients well and store at 4°C.

LB agar (supplement with 30 µg/ml kanamycin)

Tryptone	2 g
Yeast extract	1 g
NaCl	1 g
Agar	3 g
30 mg/ml Kanamycin stock	200 µl

Adjust the volume of the solution to 200 ml with distilled water and sterilize by autoclaving for 20 min at 15 psi. Add 200 µl of kanamycin (30 mg/ml) into warm medium (50°C). The medium was poured into glass plate.

13. Solution for plasmid DNA extraction**Solution I**

Glucose	0.9 g
Tris-HCl	0.3 g
EDTA	0.372 g

Dissolve the ingredients in 80 ml of distilled water. Add distilled water to 100 ml. Sterilize the buffer by autoclaving and store at 4°C.

Solution II

1 N NaOH	20 ml
10% SDS	10 ml
Distilled water	70 ml

Prepare the solution before use.

Solution III

Potassium acetate	29.44 g
Glacial acetic acid	11.8 ml

Dissolve potassium acetate in 88.5 ml of distilled water and sterilize the buffer by autoclaving. Add glacial acetic acid and store at room temperature.

14. Solution for protein expression

1 M IPTG stock

IPTG	2.38 g
------	--------

Dissolve in 10 ml with distilled water and sterilize by filtration.

PBS (pH 7.3) for GST-InR-FnIII

NaCl	1.64 g
------	--------

KCl	0.04 g
-----	--------

Na ₂ HPO ₄	0.28 g
----------------------------------	--------

KH ₂ PO ₄	0.049 g
---------------------------------	---------

Dissolve the ingredients in 150 ml of distilled water. Adjust the pH to 7.3 with HCl. Adjust the volume to 200 ml with distilled water. Sterilize the buffer by autoclaving and store at 4°C.

Lysis buffer (pH 8.0) for His-RpL10a

Na ₂ H ₂ PO ₄ ·2H ₂ O	7.8 g
---	-------

NaCl	17.54 g
------	---------

Imidazole	0.68 g
-----------	--------

Dissolve the ingredients in 800 ml of distilled water. Adjust the pH to 8.0 by adding 1 M NaOH. Adjust the volume of the solution to 1000 ml with distilled water. Sterilize by autoclaving and store at 4°C.

30 mg/ml Lysozyme stock

Lysozyme	0.3 g
----------	-------

Distilled water	70 ml
-----------------	-------

Mix the ingredients well and store at -20°C.

15. Solution for protein purification

Binding buffer (pH 8.0) for His-RpL10a

Na ₂ H ₂ PO ₄ ·2H ₂ O	7.8 g
NaCl	17.54 g
Imidazole	0.68 g

Dissolve the ingredients in 800 ml of distilled water. Adjust the pH to 8.0 by adding 1 M NaOH. Adjust the volume of the solution to 1000 ml with distilled water. Sterilize by autoclaving and store at 4°C.

Washing buffer (pH 8.0) for His-RpL10a

Na ₂ H ₂ PO ₄ ·2H ₂ O	7.8 g
NaCl	17.54 g
Imidazole	2.72 g
β-mercaptoethanol	0.7 ml

Dissolve the ingredients in 800 ml of distilled water. Adjust the pH to 8.0 by adding 1 M NaOH. Adjust the volume of the solution to 1000 ml with distilled water. Sterilize by autoclaving and store at 4°C.

Elution buffer (pH 8.0) for His-RpL10a

Na ₂ H ₂ PO ₄ ·2H ₂ O	7.8 g
NaCl	17.5 g
Imidazole	34 g

Dissolve the ingredients in 800 ml of distilled water. Adjust the pH to 8.0 by adding 1 M NaOH. Adjust the volume of the solution to 1000 ml with distilled water. Sterilize by autoclaving and store at 4°C.

Dialysis buffer (pH 7.4) for His-RpL10a

NaCl	17.54 g
Na ₂ H ₂ PO ₄ ·2H ₂ O	7.8 g

Dissolve the ingredients in 800 ml of distilled water. Adjust the pH to 7.4 by adding 1 M NaOH. Adjust the volume of solution to 1000 ml. Sterilize by autoclaving and store at 4°C.

Elution buffer (pH 8.0) for GST-InR-FnIII

Tris-HCl	0.606 g
Reduced glutathione	0.307 g

Dissolve the ingredients in 80 ml of distilled water. Adjust the pH to 8.0 by adding 1 N HCl. Adjust the volume of the solution to 100 ml with distilled water. Sterilize by filtration and store at 4°C.

16. Solution for immunofluorescence assay**Blocking buffer**

PBS pH 7.4	100 ml
Triton X-100	0.1 ml
BSA	1 g
Glycine	2.252 g

Dissolve the ingredients in 80 ml of PBS pH 7.4. Adjust the volume of the solution to 100 ml with PBS pH 7.4. Sterilize by filtration and store at 4°C.

17. Amino acids

Table 12. Code of amino acids

Amino acid	Three-letter code	One-letter code
Alanine	Ala	A
Arginine	Arg	R
Asparagine	Asn	N
Aspartic acid	Asp	D
Aspsragine or Aspartic acid	Asx	B
Cysteine	Cys	C
Glutamine	Gln	Q
Glutamic acid	Glu	E
Glutamine or Glutamic acid	Glx	Z
Glycine	Gly	G
Histidine	His	H
Isoleucine	Ile	I
Leucine	Leu	L
Lysine	Lys	K
Methionine	Met	M
Phenylalanine	Phe	F
Proline	Pro	P
Threonine	Thr	T
Serine	Ser	S
Tryptophan	Try	W
Tyrosine	Tyr	Y
Valine	Val	V

VITAE

Name Miss Netnapa Chaichanit

Student ID 5610230011

Educational Attainment

Degree	Name of Institution	Year of Graduation
Bachelor of Science (Biotechnology)	Prince of Songkla University	2012

Scholarship Awards during Enrolment

2012-2013	PSU-Ph.D. Scholarship
2013	Research Grant for Thesis
2013-Present	The Royal Golden Jubilee Ph.D. Program (RGJ-Ph.D. Program)

List of Publication and Proceeding

Chaichanit, N., Wonglapsuwan, M., Chotigeat, W., 2018. Ribosomal protein L10A and signaling pathway. *Gene* 674, 170–177.

Chaichanit, N., Saetan, U., Wonglapsuwan, M., Chotigeat, W., 2020. Effect of the interaction between ribosomal protein L10a and insulin receptor on carbohydrate metabolism. *Heliyon* 6, e05714.